Experimental and Computational Sonic Boom Assessment of Boeing N+2 Low Boom Models

Donald A. Durston[1]
NASA Ames Research Center, Moffett Field, California 94035

Alaa A. Elmiligui[2]
NASA Langley Research Center, Hampton, Virginia 23681

Susan E. Cliff[3]
NASA Ames Research Center, Moffett Field, California 94035

Courtney S. Winski,[4] Melissa B. Carter,[5] and Eric L. Walker[6]
NASA Langley Research Center, Hampton, Virginia 23681

Near-field pressure signatures were measured and computational predictions made for several sonic boom models representing Boeing's Quiet Experimental Validation Concept (QEVC) supersonic transport, as well as for three axisymmetric calibration models. The concept was designed under a NASA Research Announcement (NRA) contract to address environmental and performance goals, specifically for low sonic boom loudness levels and high cruise efficiency, for an aircraft anticipated to enter service in the 2020-timeframe. Wind tunnel tests were conducted on the aircraft and calibration models during Phases I and II of the NRA contract from 2011 to 2013 in the NASA Ames 9- by 7-Foot and NASA Glenn 8- by 6-Foot Supersonic Wind Tunnels. Sonic boom pressure signatures were acquired primarily at Mach 1.6 and 1.8, and force and moment data were acquired from Mach 0.8 to 1.8. The sonic boom test data were obtained using a 2-in. flat-top pressure rail and a 14-in. tapered "reflection factor 1" (RF1) pressure rail. Both rails capture an entire pressure signature in one data point, and successive signatures at varying positions along or above the rail were used to improve data quality through spatial averaging. The sonic boom data obtained by the rails were validated with high-fidelity numerical simulations of off-body pressures. The test results showed good agreement between the computational and experimental data when a variety of testing techniques including spatial averaging of a series of pressure signatures were employed. The two wind tunnels generally produced comparable data.

Nomenclature

CAD	=	computer-aided design
CoR	=	center of rotation
h, h_nose	=	model altitude at model nose, in.
h/L, h_nose_L	=	model altitude non-dimensionalized by model length
HumidAvg	=	average humidity from wind tunnel sensors, ppm by weight
L	=	model reference length, in.
M	=	Mach number

[1] Aerospace Engineer, Experimental Aero-Physics Branch, NASA Ames, AIAA Senior Member
[2] Research Aerospace Engineer, Configuration Aerodynamics Branch, NASA Langley, AIAA Senior Member
[3] Aerospace Engineer, Applied Modeling and Simulations Branch, NASA Ames, AIAA Associate Fellow
[4] Research Aerospace Engineer, Configuration Aerodynamics Branch, NASA Langley, AIAA Senior Member
[5] Research Aerospace Engineer, Configuration Aerodynamics Branch, NASA Langley, AIAA Senior Member
[6] Research Aerospace Engineer, Configuration Aerodynamics Branch, NASA Langley, AIAA Senior Member

MAC	=	mean aerodynamic chord
P, P_{Rail}	=	rail static pressure, psfa
P_∞	=	free stream static pressure, psfa
P_T	=	free stream total pressure, psfa
$psfa$	=	pounds/square foot absolute
q	=	dynamic pressure, psf
$QEVC$	=	Quiet Experimental Validation Concept
Re	=	Reynolds number, non-dimensional, $\rho VL/\mu$
Re_L	=	Reynolds number per unit length, 1/foot
$RF1$	=	reflection factor 1, name of 14-in. pressure rail
$RBOS$	=	retro-reflective background-oriented Schlieren
S_{REF}	=	model reference area, sq ft
SWT	=	supersonic wind tunnel
X	=	longitudinal coordinate, positive aft, in.
X_{Ram}	=	longitudinal extension of linear actuator ram, in.
Z	=	coordinate in tunnel angle-of-attack plane: lateral in 9x7, vertical in 8x6, positive "above" rail, in.
α	=	angle of attack, degrees
β	=	angle of sideslip, degrees
$\Delta P/P$	=	overpressure coefficient, $(P - P_\infty)/P_\infty$
ϕ	=	off-track angle, or model roll angle relative to the rail, degrees
Subscripts		
$Data$	=	Data run, where model pressure signature was measured on the rail
Ref	=	Reference run "empty" tunnel measurement, where model pressure signature was *not* on the rail; also a reference parameter for model geometry

I. Introduction

Flight at speeds greater than the speed of sound is currently not permitted over land primarily because of the sonic boom annoyance and potential structural damage caused by large pressure waves generated by supersonic aircraft. Mitigation of the sonic boom is a key focus area of the High Speed Project under NASA's Fundamental Aeronautics Program. The project is focusing on technologies to enable future civilian aircraft to fly efficiently with reduced sonic boom, engine and aircraft noise, and emissions. One major objective is the improvement of both computational and experimental capabilities for design of low boom aircraft. NASA and industry partners are developing improved wind tunnel testing techniques and new pressure instrumentation to measure the weak sonic boom pressure signatures of modern vehicle concepts. In parallel, computational methods are being developed to provide rapid design and analysis of supersonic aircraft with improved meshing techniques that provide efficient, robust, and accurate off-body pressures at several body lengths from vehicles with very low sonic boom overpressures. The maturity of these critical parallel efforts is necessary before low-boom flight can be demonstrated and commercial supersonic flight can be realized.

The measurement of the sonic boom pressure signatures of modern low-boom supersonic vehicles in wind tunnels is challenging. Historically, these signatures were measured in a wind tunnel using needle-like conical probes that measure static pressure at a single point in the flow-field. This technique requires axial translation of the model past the probe to obtain a complete pressure signature of the model (or translation of the probe past the model). Traditional methods used a move-pause data acquisition technique requiring between 40-60 minutes per signature, although a recent effort has shown that near continuous model translation with environmentally-controlled pressure transducers and shortened pressure lines can significantly speed up data acquisition time using a probe.[1] However, the single-probe technique is still prone to reduced data accuracy because of small changes in tunnel flow conditions even over short data acquisition times. Humidity, turbulence, ambient pressure variations and stream angle changes during model translation all contribute to reduced data quality.

Unlike single-point conical probes, pressure rails with hundreds of closely-spaced pressure orifices measure a model's entire sonic boom pressure signature at one location of the model in the tunnel. Rails offer significant gains in efficiency and precision compared with conventional conical probe testing. Several rails with different cross-sectional shapes have been investigated in the 9- by 7-Foot Supersonic Wind Tunnel at NASA Ames Research Center since 2008.[1,2] Initial rail concepts had flat or large-diameter rounded tips that resulted in unknown and inconsistent reflection (or amplification) of the model's pressure signature and unknown rail boundary layer

influence on the signature. A pressure rail that effectively eliminates shock reflection and boundary layer growth effects on the tip of rail was designed in 2010 using CFD analyses.[2] This rail, designated the "reflection factor 1" (RF1) rail, is 14 in. tall and tapered toward the tip to a 0.05-in. radius, and was used in some of the tests discussed in this report. Another rail used in these tests was a 2-in. tall flat-top rail, but reflection of the model shocks off the surface of this rail caused some parts of the model signature to be amplified.

When the pressure rails were first used in NASA sonic boom testing in 2008, it was envisioned that model translation would be unnecessary since the rails capture an entire model signature at once. However, further testing with rails showed that spatially averaging a series of pressure signatures from a number of model positions significantly improved measurement accuracy.[3] Small ambient pressure oscillations and disturbances caused by small shocks emanating from the tunnel structure are nearly eliminated by spatial averaging techniques.

In 2009, NASA published a NASA Research Announcement (NRA) requesting proposals for "System-Level Experimental Validations for Supersonic Commercial Transport Aircraft Entering Service in the 2020 Time Period." The aircraft concepts were to be designed to second generation "N+2" supersonic vehicle technology with a focus on providing system-level solutions capable of overcoming the efficiency, environmental, and performance barriers to practical supersonic flight. The N+2 environmental and performance goals are given in Table 1.

Table 1. N+2 Supersonic Transport (2020) Goals

Environmental Goals	
Sonic Boom	85 PLdB up to 20° off-track
Airport Noise (cumulative below stage 3)	10–20 EPNdB
Cruise Emissions	< 10 EIN Ox
Performance Goals	
Cruise Speed	Mach 1.6–1.8 low-boom flight
Range	4000 nm
Payload (passengers)	35–70 passengers
Fuel Efficiency (passenger-nm per lb of fuel)	3.0

The NRA contractors were to independently design N+2 concepts to meet these goals, and then build and test wind tunnel models to validate the sonic boom and aerodynamic performance estimates. Two companies were awarded the NRA contracts: Lockheed-Martin Aeronautics Company (LMAC) and The Boeing Company (TBC). This paper covers the experimental measurements and CFD predictions for the concepts developed by Boeing.[4]

The contracts with both companies were executed in two phases, each concluding with wind tunnel test validation of the sonic boom characteristics of their design efforts. The first phase of Boeing's efforts was focused on design of a low boom airliner (Fig. 1), the reduction of sonic boom signatures under-track, and assessment of aerodynamic performance in light of the environmental and performance goals specified in the NRA. The second phase focused on nacelle integration with the airframe in terms of its effects on the boom signatures and aerodynamic performance, as well as inlet performance.

Figure 1. Artist's concept of Boeing N+2 QEVC supersonic transport

Predicting accurate sonic boom

pressure signatures has historically been difficult, but significant improvements in the accuracy of these predictions have been realized in the work of the High Speed Project. Accurate CFD simulations can be obtained in many ways. One is by providing dense meshes within the sonic boom pressure disturbance along with mesh rotation techniques[5] to align the mesh with the Mach angle, or alternatively by using solution-adaptive techniques.[6-15] Also, structured overset grid methods,[16] or hybrid methods[16-20] that utilize unstructured flow solutions in the near-field and a structured grid solutions in the far-field can also provide accurate on-track calculations. Grid generation tools that allow stretching of the mesh in addition to alignment to the Mach angle[21-23] offer smaller meshes that maintain density in the axial direction and reduce the effects of dissipation along characteristic lines. The CFD computations provided here use Mach cone aligned prism meshes.[23] Some solution-adaptive (Cartesian and tetrahedral)[9-12] results, and overset-grid computations will also be shown.

II. Test Objectives and Overview

There were three primary objectives for conducting the tests in this experimental validations program:

1. Obtain data to evaluate sonic boom and aerodynamic performance of the Boeing configurations, including the effects of nacelle changes and varying mass flows
2. Improve wind tunnel test techniques for acquiring such data
3. Provide a large, high-quality experimental validation database for CFD tool development and improvement of low-boom design methods

Boeing designed their N+2 transport to meet the NRA goals, and then conducted the series of wind tunnel tests below with NASA to meet the above objectives:

Phase I:

1. TBC1: Ames 9x7-ft wind tunnel, April 2011, Test 97-0229
2. TBC2: Ames 11x11-ft wind tunnel, June 2012, Test 97-0249
3. TBC3: Glenn 8x6-ft wind tunnel, September 2012, Test 86-12-002

Phase II:

4. TBC4: Ames 9x7-ft wind tunnel, April 2013, Test 97-0259
5. TBC5: Glenn 8x6-ft wind tunnel, March 2013, Test 86-13-001

This report will cover data only from the TBC3 and TBC4 tests and where the data were spatially averaged, and also from a 9x7 "parametric" test (April 2012, Test 97-0250, also referred to herein as "97p"). This was the first test in which Boeing models were run in multiple-position X or Z sweeps to permit spatially averaging the data. Various combinations of the Boeing N+2 "Boom" models, a "Performance" model, and axisymmetric calibration models were run in the above tests, which will be described in detail in the Models section below. Boeing has reported on the design of their QEVC aircraft and on the wind tunnel test results from Phase I and II in Ref. 4 and 24, respectively.

III. Facilities

Wind tunnel tests for the data presented herein were conducted at the NASA Ames 9- by 7-Foot and the NASA Glenn 8- by 6-Foot Supersonic Wind Tunnels. Brief descriptions of the wind tunnel facilities are presented in this section.

A. Ames 9- by 7-Foot Supersonic Wind Tunnel

The Ames 9- by 7-Foot Supersonic Wind Tunnel[25] is part of the Unitary Plan Wind Tunnel complex at NASA Ames Research Center at Moffett Field, California. It is a continuous flow, closed circuit, variable-density tunnel equipped with an asymmetric sliding-block nozzle for setting Mach number. The floor of the wind tunnel test section is part of the nozzle block. It translates axially (streamwise) to vary the nozzle throat area while the contoured tunnel ceiling remains stationary. This combination provides a Mach number range from 1.55 to 2.5. The sidewalls are flat and parallel through the nozzle and test section. The asymmetric nozzle results in slightly larger stream angle variations in the vertical plane, on the order of 0.25 to 0.5 degrees, whereas stream angle in the horizontal plane is generally less than 0.2 degrees. The angle-of-attack plane is therefore horizontal, and the model support strut at the rear of the test section is horizontal as well. Models are thus normally mounted wings vertical,

and the strut's side-to-side heave compensation keeps the model in the center of the tunnel as the pitch angle is changed. The forward end of the strut centerbody pivots by means of a mechanical joint (knuckle-sleeve system) to achieve any combination of angle of attack or sideslip within a 15° cone angle. Throughout this report, the model distance from the rail on the sidewall of the tunnel is referred to as "height," even though in reality it is a horizontal distance in the 9x7 wind tunnel.

The tunnel is driven by an 11-stage axial compressor powered by four wound-rotor motors totaling 216,000 hp. The tunnel operates at total pressures between 634 and 3600 psfa with corresponding unit Reynolds numbers between 0.8 and 5.7 million per foot. For the subject series of sonic boom tests, the Mach number and total pressure have been prescribed rather than Mach and Reynolds number because small changes in Reynolds number do not affect the boom data, and it is more productive to run in constant-pressure mode.

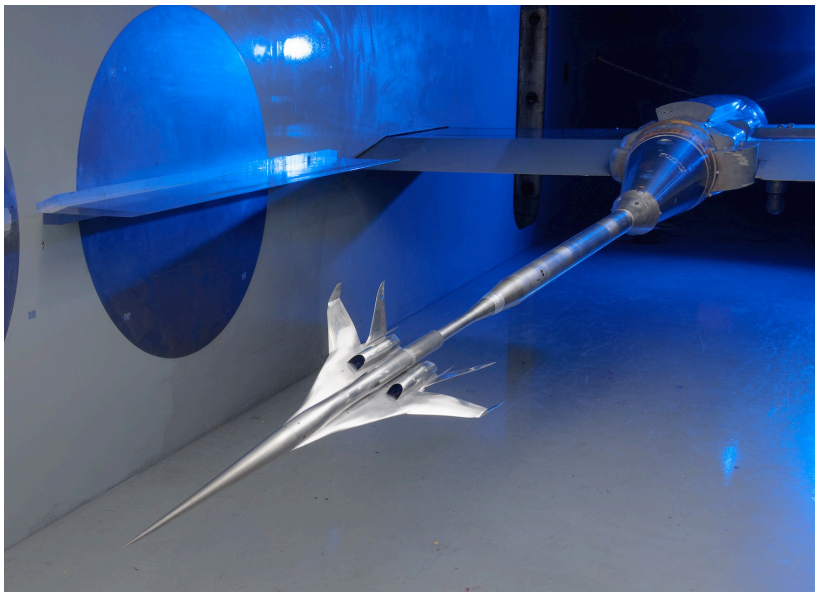

Figure 2. Performance model installed in Ames 9x7-ft wind tunnel

Most types of testing in the 9x7 wind tunnel do not require very low humidity and fine control of it, but sonic boom testing is an exception because static pressure measurements are sensitive to humidity. Humidity is normally brought down to operational levels (less than 500 ppm by weight, depending on the test requirements) by purging the tunnel of wet air and pumping back up with dry air, but for best data quality in sonic boom testing, this purging is supplemented by continuously injecting dry, high-pressure air to keep the humidity below ~300 ppm. Modulation of this dry-air injection has proven capable of maintaining humidity within ±5 ppm, which has allowed more consistent static pressure measurements relative to earlier tests where humidity was not so tightly controlled.

An installation photograph of the Boeing Performance model in the 9x7 tunnel is shown in Fig. 2. The model, RF1 pressure rail, strut and centerbody are visible in the photograph (the model is shown rolled approximately 60° from its normal wings-vertical orientation to better show the model's upper surface features). The RF1 pressure rail is mounted on the north sidewall of the test section to measure the pressure signatures below the model. The wind tunnel strut movement controls the distance from the model to the top of the rail.

B. Glenn 8- by 6-Foot Supersonic Wind Tunnel

The Glenn 8- by 6-Foot Supersonic Wind Tunnel[26] is an atmospheric facility with a test section Mach number range from 0.25 to 2.0 (at discrete Mach numbers). It has dual-cycle operation in that it can operate closed-loop in an aerodynamic cycle, or open-loop in a propulsion cycle when combustion products are being introduced into the air stream. The tunnel is driven by a 7-stage axial compressor powered by three wound-rotor motors totaling 87,000 hp. Total pressure in the tunnel is a function of Mach number and temperature since the tunnel is not pressurized. High temperatures from the heat of compression are cooled by a heat exchanger on the leg of the tunnel opposite to the compressor and 8x6 test section, but with the test section being immediately downstream of the compressor, temperatures in the 8x6 typically reach 200° F at speeds of Mach 1.8 and higher. The range of total pressure from minimum to maximum Mach number is roughly 2150 to 3625 psfa, with corresponding unit Reynolds numbers between 1.7 to 5.1 million per foot. A balance chamber surrounds the test section and is used to provide boundary layer and Mach number control of the airflow in the test section through perforations in the walls.

Humidity is controlled by an air dryer in the tunnel circuit that consists of activated alumina in multiple beds. Each bed is two feet thick, through which all the wind tunnel air is continuously passed when not in bypass mode. On days when the outside humidity is high, the dryer beds can reach saturation during or by the end of an operating shift in the tunnel. At this point, they can no longer maintain a low dew point (upper limit is typically -15° F, an approximate humidity of 320 ppm by weight) to continue running without sacrificing data quality. The time it takes

to reach saturation is dependent on the humidity of the outside air, as the tunnel is an atmospheric tunnel. During multiple-day test operations, the dryer beds are put through a heating and cooling cycle on a non-running shift to remove the excess moisture; there is no active humidity control other than the dryer beds.

The test section of this facility is 8 ft high by 6 ft wide and 23.5 ft long. The nozzle upstream of the test section consists of flexible walls that are moved inward by hydraulic jacks for supersonic flow, and the floor and ceiling of the tunnel through the nozzle and test section areas are flat and parallel. The test section is divided into two sections: a supersonic section, 9.08 ft long starting from the end of the nozzle, and a transonic section 14.42 ft long from the end of the supersonic section. The walls around the supersonic section are solid, and around the transonic section they are porous with 1-in. diameter holes at 60° angles through the walls.

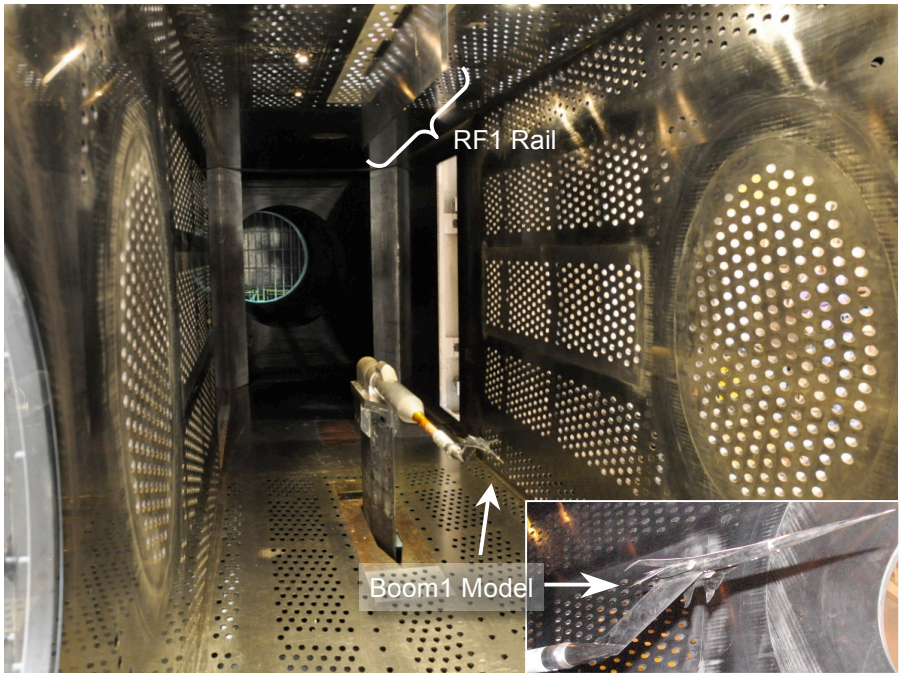

Figure 3. Boom1 model installed in Glenn 8x6-ft wind tunnel

Several different strut arrangements are available for the tunnel; in sonic boom testing, a supersonic strut that raises and lowers through the tunnel floor with a pitch capability of -5° to 20° is used. Models are mounted wings-horizontal since the angle-of-attack plane is vertical.

For the TBC3 test, the RF1 pressure rail was mounted on the top wall of the test section to measure the pressure signatures of the models, which were thus required to be mounted upside-down on the strut so the rail would see the model lower-surface pressures. The distance from the model to the tip of the rail was controlled by the wind tunnel strut. A view of the Boeing Boom1 model in the 8x6 tunnel with the RF1 rail on the ceiling is shown in Fig. 3.

A short table summarizing the operational characteristics of the Ames 9x7 and the Glenn 8x6 wind tunnels is given in Table 2. Throughout this report, data from the 9x7 are presented at Mach numbers of 1.6 and 1.8, but the Mach numbers obtained in the 8x6 were 1.56 and 1.78 because of their discrete Mach number capability. These slight differences are believed to be not significant for the comparisons made in this report.

Table 2. Tunnel Operational Characteristics

	Ames 9x7-Ft Supersonic Wind Tunnel	Glenn 8x6-Ft Supersonic Wind Tunnel
Mach Range	1.55 – 2.5, continuously variable	0.36 – 2, discrete
Pressure Control	Range of 634 to 3600 psf	Atmospheric; P_T varies with Mach
Temperature Control	Heat exchanger removes most heat of compression	Heat exchanger partially effective, T_T dependent on Mach number
Humidity Control	Humidity control continuously available by make-up air and high-pressure air	Humidity controlled by dryer beds, run time dependent on weather
Nozzle Design	Asymmetric sliding block (floor) nozzle	Symmetric vertical flex walls

IV. Full Scale Configuration and Wind Tunnel Models

A. Quiet Experimental Validation Concept (QEVC)

The Boeing Quiet Experimental Validation Concept (QEVC) supersonic transport configuration was developed during Phase I of the Supersonic Experimental Validations NRA contract with Boeing. It was designed to the NASA N+2 goals (Table 1) for low sonic boom loudness levels and high cruise efficiency as an airliner feasible for entry into service in the 2020 timeframe. It was designated by Boeing as their 6007 configuration after an extensive design study, and its design flight conditions were Mach 1.8, C_L = 0.104, and an angle of attack of 3.28 degrees.

The flight vehicle attributes are given in Table 3, and a three-view drawing of the configuration is shown in Fig. 4. It is a twin-engine design with the nacelles on top of the wing, and V-tails mounted outboard of the nacelles. The nacelles were placed on the upper surface to minimize their effect on the sonic boom signature, but this location creates potential problems with inlet recovery and distortion. The inlet performance, the effects of nacelles on the sonic boom, and the aerodynamic performance were investigated in Phase II.

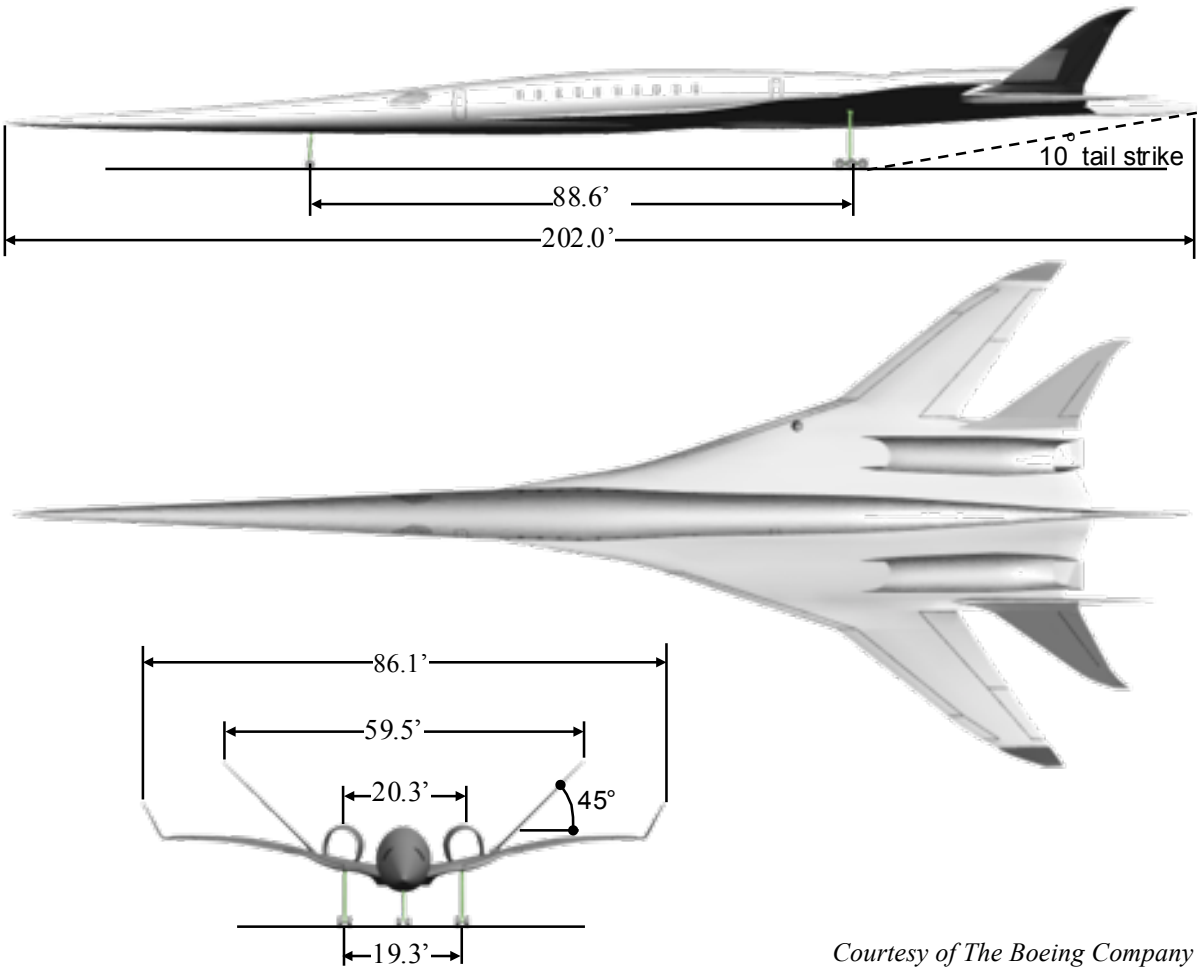

Courtesy of The Boeing Company

Figure 4. Boeing QEVC transport three-view drawing

Table 3. Flight Vehicle Attributes

	QEVC N+2 Configuration
Length (ft)	202
Span (ft)	86.1
Reference area (sq ft)	2,592
Flight altitude (ft)	47,500
Cruise Mach number	1.8
Cruise L/D	11.6
Aspect ratio	2.86
Taper ratio	0.17
LE sweep angles (inbd/mid/outbd)	80°/71°/52°
MAC (ft)	34.1

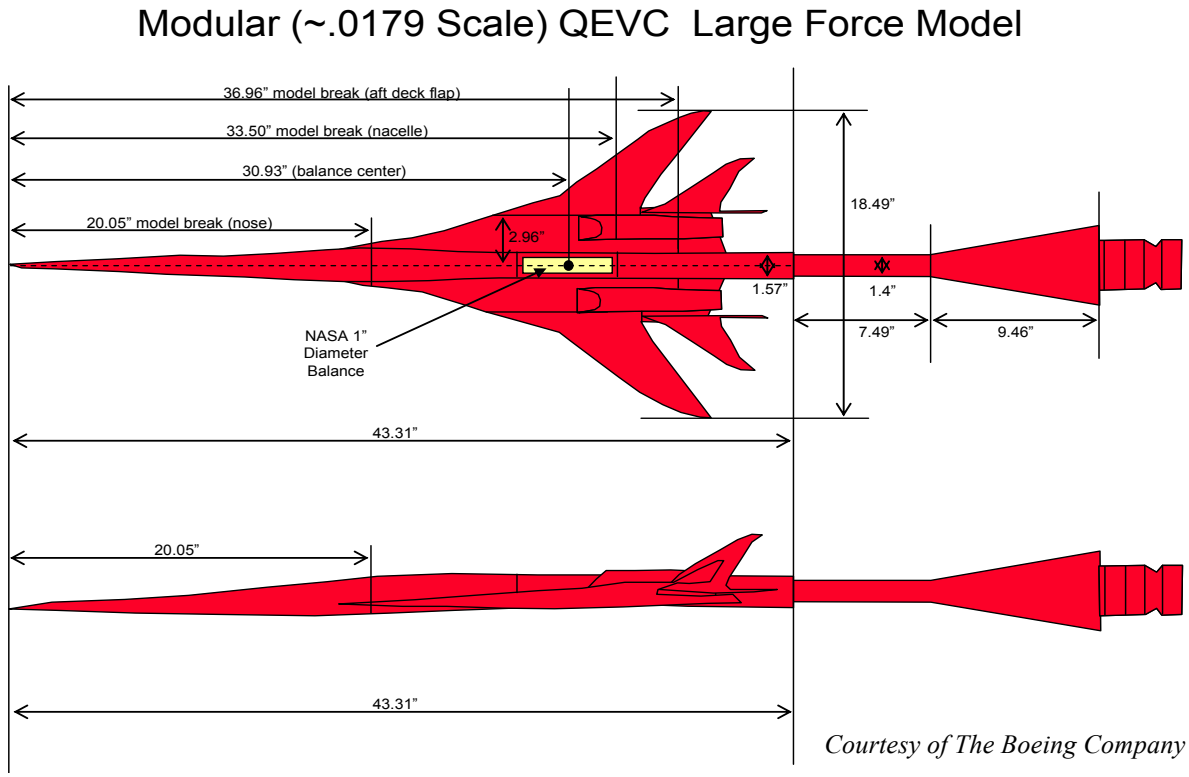

Figure 5. Performance model top- and side-view drawings

B. Wind Tunnel Models

1. Performance Model

The Performance model is a 43.31-in.-long, 1.79%-scale model of the QEVC. This model was sized primarily for good resolution in measuring aerodynamic performance, with some reduced capability to measure off-body sonic boom pressure signatures as its length sometimes prevented fitting the entire signature on the rail, depending on position. It is sting-mounted, with a 1-in. diameter six-component balance located in the center of the model. To accommodate the sting and the balance, the aft body of the model had to be made with a constant cross section, thus unavoidably compromising the boom signature from this part of the model. In addition, the edges of the wings, V-

Figure 6. Rear view of Performance model in Ames 9x7 tunnel

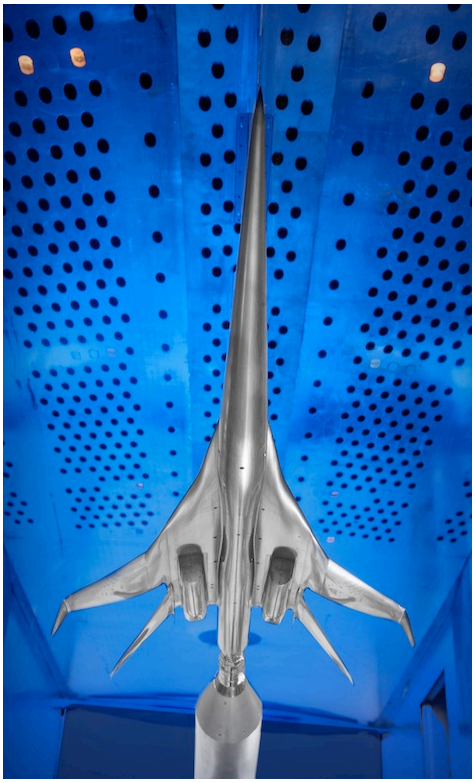

Figure 7. Performance model installed in Glenn 8x6 wind tunnel

tails, and nacelle inlets and nozzles were thickened to a minimum of 0.004 in. at model scale for manufacturability and durability. Other changes from the full-scale configuration necessitated by model manufacturing requirements were that the nacelles had to be moved inboard 5 in. (full scale), the support pod thickness needed to be increased by 50%, and the V-tail wing tips and winglet thicknesses needed to be increased from an original t/c = 3% to 4.5%.

Top- and side-view drawings of the model with sting are shown in Fig. 5, and photographs of the model installed in the 9x7 and 8x6 wind tunnels are provided in Fig's. 6 and 7, respectively. The model is shown in these views with a "sting can" at the rear of the model, which extends the cylindrical body 6-in. aft to minimize the influence of the sting on the sonic boom pressures and the aerodynamic performance. It was found during the TBC1 and TBC3 tests, however, that the aft-facing cavity area between the sting can and the sting was adversely affecting the aft part of the pressure signature, so sting covers (two clamshell halves) were made to replace the sting can and continue the cylindrical cross section of the aft body as far back as possible along the sting, to the point where it tapers up in size to meet strength requirements. The assembly of these sting covers on the sting is referred to as the "tailored dummy sting," and this, along with the sting can (in a split view), are shown in the exploded CAD views in Fig. 8. A lock plug was inserted into the back end of the model just ahead of the dummy sting to prevent the model from rotating about the balance and causing steps and gaps when deflecting under aerodynamic loads. Note that this plug and the attachment of the dummy sting to the model bridge the balance, thus rendering the balance readings invalid. During the TBC4 test, the Performance model was run with the tailored dummy sting for all boom signature measurements, and with the sting can for force and moment measurements. All of the experimental signature data for this model presented in this paper were acquired with the tailored dummy sting.

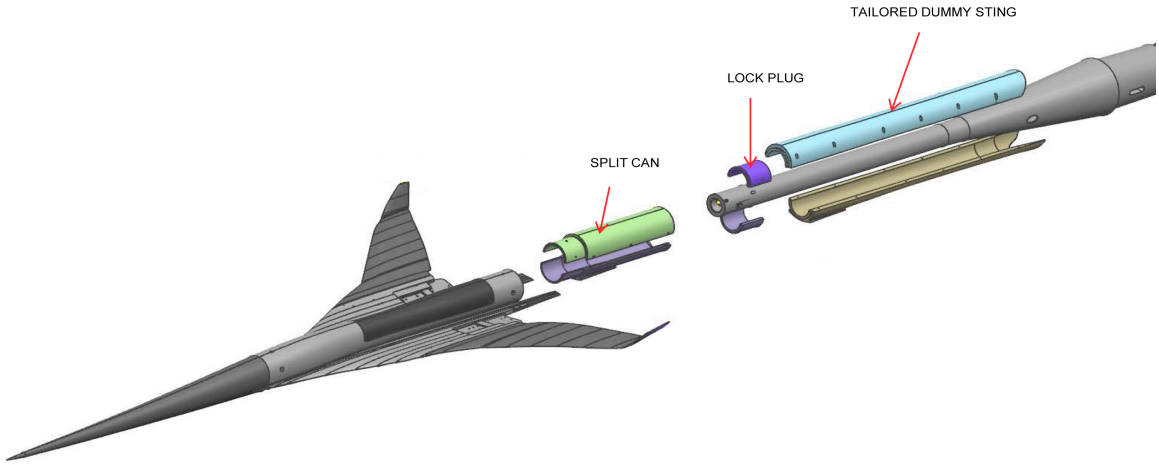

Figure 8. Exploded CAD views of the sting can and tailored dummy sting for the Performance model

2. Boom1 Model

The Boom1 model is a 15.748-in.-long model of the QEVC at 0.65% scale. It has the same aerodynamic lines as the Performance model aside from the differences for the mounting provisions. Boeing sized the Boom1 model to provide the best compromise of model fidelity and the ability to measure off-body sonic boom pressure signatures in a large wind tunnel. The small size was selected to measure the full signature of model on the pressure rail with room to spare for various sting or strut mounting configurations at various positions and sweeps relative to the rail. As with the Performance model, the sharp edges of the wings, V-tails, and nacelle inlets and nozzles had to be thickened relative to their true scaled-down thicknesses to a minimum of 0.004 in.

Drawings of the model are shown in Fig. 9, which show that the model was attached to the balance by a swept blade strut and a balance adapter. The same 1-in. diameter six-component balance that was used for the Performance model was also used for this and all the other Boeing models. Two blade struts were made in Phase I of the NRA study for this model and the Boom2 model (discussed in next section): a short one, VS1 (10.03 in. long, shown in Fig's. 9 and 11), and a long one, VS2 (11.65 in., shown in Fig's. 10 and 11). They both attach to the model at the same mounting location, and the longer length of VS2 places the model nose 1.625 in. further forward in the tunnel than VS1. The longer strut was preferred for minimizing effects on the model signature, but the shorter one was tested first to determine whether the cantilevered model would have high lateral dynamics in the wind tunnel. After this was determined to be a non-issue, VS2 was run with the Boom1 model from then on. Two views of the Boom1 model with the VS2 strut installed in the 9x7 wind tunnel are shown in Fig. 10.

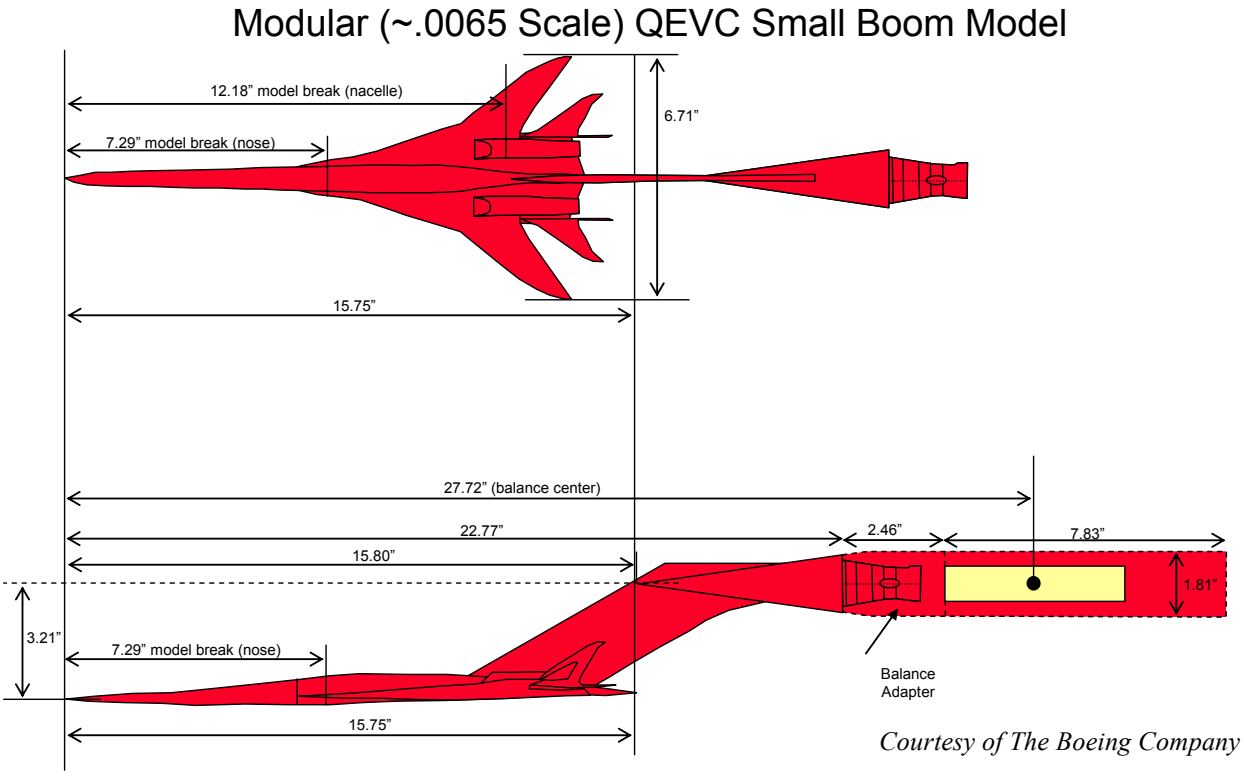

Figure 9. Boom1 model top and side view drawings with VS1 strut and balance adapter

3. Boom2 Model

The Boom2 model is an alternate low-boom design with the same general features as the Boom1 model. However, it was designed for a Mach number of 1.6 and $C_L = 0.14$, with a focus more on drag and pitching moment reduction than on the near-field signature shape. It did result in significantly lower drag than Boom1 and a lower pitching moment, with an under-track signature comparable to Boom1. The off-track signatures were somewhat worse for Boom2, however. Aside from minor wing contour changes, the underside of the Boom2 model is noticeably flatter than on Boom1, and this accounts for part of the drag and pitching moment changes. Data plots for this model are not included in this paper since the model was only run in the TBC1 test, which was conducted before spatial averaging became a standard procedure in NASA's sonic boom tests.

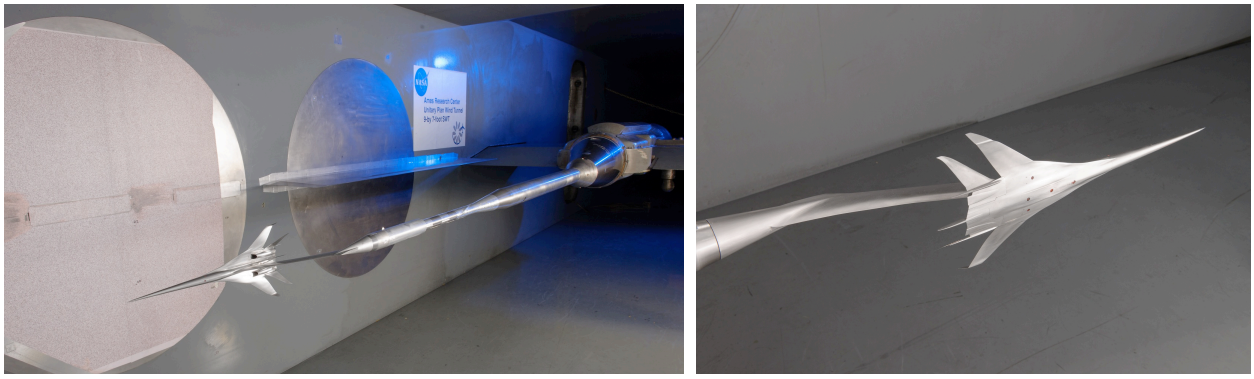

Figure 10. Boom1 model installed in Ames 9x7-ft wind tunnel

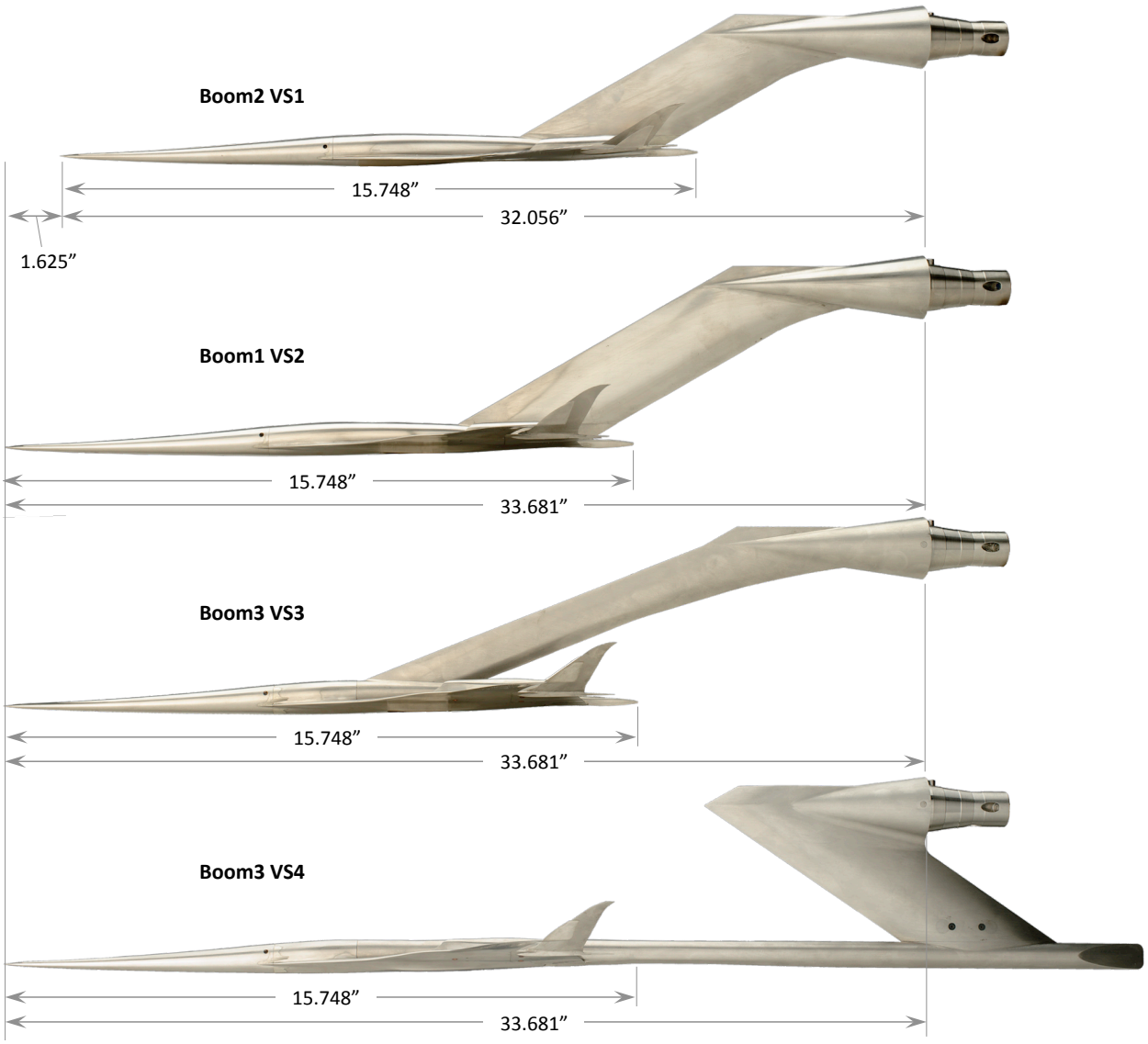

Figure 11. Photographs of Boom1, Boom2, and Boom3 models with VS1, VS2, VS3, and VS4 struts

4. Boom3 Model

The Boom3 model was made during Phase II of the NRA contract, and has the same aerodynamic lines as the Boom1 model aside for provisions for mounting on the new VS3 and VS4 struts. VS3 is a forward-swept strut similar to VS1 and VS2, but it is significantly longer than VS2 (14.37 vs. 11.65 in.), though its attachment location is closer to the center of the model so that the nose remains the same distance from the balance center as with VS2. VS4 is an aft-swept strut that supports a straight, rear-entry sting for the Boom3 model. As with VS3, it too is designed to place the model nose at the same station as the VS2 strut.

Photographs of the Boom1, Boom2, and Boom3 models mounted on the VS1 through VS4 struts are provided in Fig. 11.

5. AS1, AS2, AS3 Axisymmetric Models

Three axisymmetric calibration models were tested to calibrate the pressure rail signature and provide data for CFD validation. The three models were designated AS1, AS2, and AS3. Boom results will only be presented for the AS2 model in this report because it was used as the common calibration body in the various Boeing tests, and data from AS1 and AS3 are not pertinent to this report. The attributes of the AS2 model are provided in Table 4 (with all the other models), where the diameter listed is that of the cylindrical portion of the model. A photograph of the isolated AS2 model is given in Fig. 12, and a photograph of it mounted in the 9x7 tunnel is shown in Fig. 13. The AS-2 model is a "Seeb" configuration designed after the work of George and Seebass.[27] It was designed without alteration of the aft signature and was designed to produce a sonic boom pressure signature with a small 2-in. flat pressure region behind the nose shock.

Table 4. Wind Tunnel Model Geometry

Model	***AS2****	***Boom† Models on VS1***	***Boom† Models on VS2,3,4***	***Performance***
Scale	—	0.65%	0.65%	1.79%
L_{Ref} (in)	18.611	15.748	15.748	43.307
S_{Ref} (sq in)	—	15.322	15.322	115.891
C_{Ref} (in)	—	2.6714	2.6714	7.3465
b_{Ref} or Dia. (in)	0.965	6.7111	6.7111	18.4555
X_{Ref} (in)	—	11.4706	11.4706	31.5441
Z_{Ref} (in)	—	0	0	0
X_{Nose} to BMC (in)	24.024	26.854	28.478	31.345
Z_{Nose} to BMC (in)	0	3.201	4.139	1.053

** Reference parameters for AS models were set equal to those for Boom models for consistency in test data reduction; actual AS2 model dimensions are given here.*

† All Boom models have the same reference dimensions.

Figure 12. Close-up photograph of AS2 model

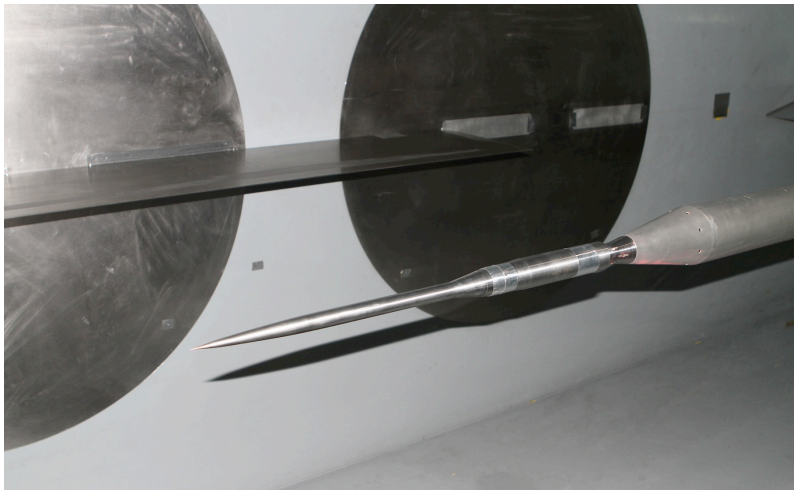

Figure 13. AS2 model installed in 9x7 wind tunnel with RF1 rail

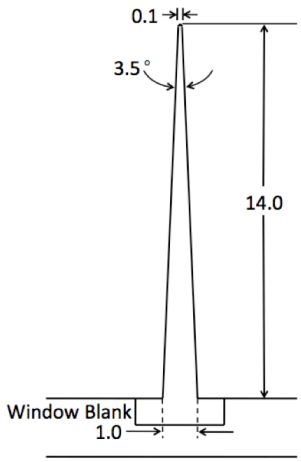

Figure 14. Cross section of the RF1 rail (dimensions in inches)

V. Instrumentation and Model Positioning

Sonic boom pressure signatures in the various tests were measured using either the tapered RF1 (14-in.) pressure rail or the flat-top 2-in. pressure rail, and a few selected signatures were measured on both rails (one at a time) in a given test for direct comparisons.

A. RF1 (14-in.) Pressure Rail

The RF1 rail has a small rounded tip and is blade-like with a small 3.5-degree angle from the tip to the base. A cross sectional cut through the pressure measuring center section of the rail is shown in Fig. 14 and a CAD drawing of the design is shown in Fig. 15. The rail is shown attached to two window blanks (54-in. diameter steel plates that replace the windows in the 9x7 wind tunnel) in the drawing. The rail stands off the wall 14 in., has a 0.05-in. radius tip, and a 1-in. base width, and is 90-in. long with an instrumented section 66-in. long. The rail height was selected to prevent contamination of the aft part of a model's signature measured on the rail by reflections off the tunnel wall of model shock waves from the forward part of the model. The height of 14 in. provides reflection-free data for model lengths of 35 and 43 in. at Mach 1.6 and 1.8, respectively. The design of this rail is discussed in detail in Ref. 2.

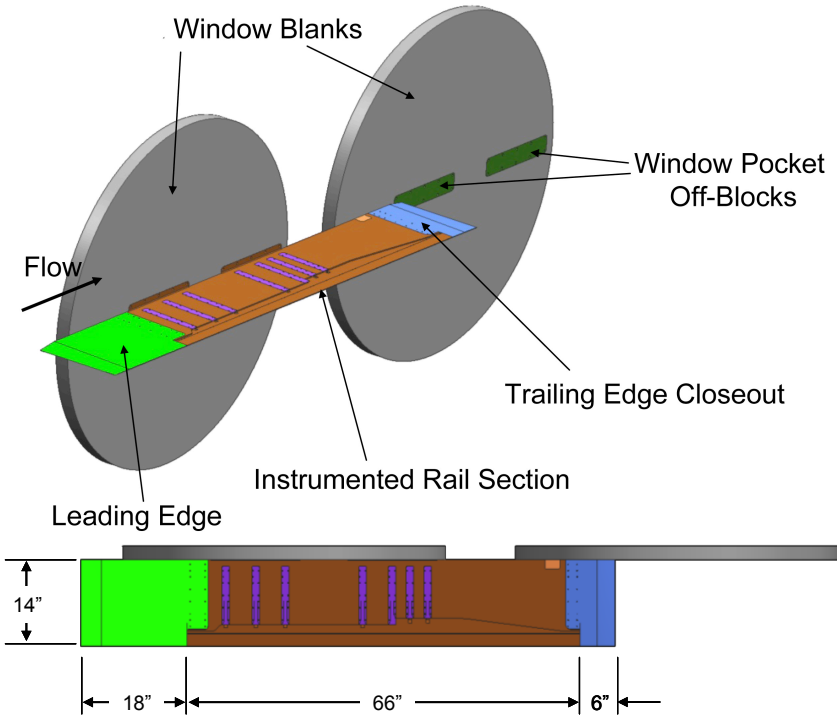

Figure 15. CAD views of RF1 rail mounted on forward window blank of 9x7 wind tunnel

The rail has 420 pressure orifices of 0.015-in. diameter, spaced 4 mm (approximately 0.1575 in.) apart along its tip. Prefabricated ferrules were used to accommodate the small orifice size, and were connected to metal pressure tubes that were routed through seven machined grooves on one side of the rail. Covers over these grooves are shown in purple in the CAD images of Fig. 15, which lead the tubes through the rail footpads mounted in the 9x7 window

blanks. The mounting location of the rail in this figure is referred to as the forward location, since most of the pressure orifices are over the forward window blank, and all the pressure tubing runs through this blank. The rail can also be mounted on the aft window blank, where the aft end of the rail is secured to the tunnel wall downstream of the aft blank. In the 8x6 tunnel, the rail was just mounted in one position in the tunnel ceiling.

The RF1 rail was used in conjunction with the 2-in. rail during the TBC3 and 9x7 parametric tests and exclusively during the TBC4 test.

B. 2-in. Pressure Rail

The RF1 rail was used in the Lockheed Phase I test before the first Boeing test in the 9x7 wind tunnel, but it was desired to build and test a more "conventional" flat-top 2-in. pressure rail for the Boeing TBC1 test. Instead of a tapered cross-section like the RF1 rail, it has a rectangular cross-section, being 1.5 in. wide and 2 in. tall. The flat surface of the rail caused shock reflections that were known to amplify some parts of the model signatures. The rail is 96 in. long with a 72-in. instrumented section used for boom signature measurement. The leading- and trailing-edge sections, 18 in. and 6 in. long, respectively, are wedge-shaped as shown in the CAD view of the rail on the aft window blank in Fig. 16. The rail consists of 458 pressure orifices spaced 4 mm (approximately 0.1575 in.) apart, each with an internal diameter of 0.015 in. Pressure tubes from the orifices were routed from the rail through the rail foot pads and tunnel window blank to the 64-port PSI modules located just outside of the test section. A photograph of the rail installation in the 9x7 test section is shown in Fig. 167

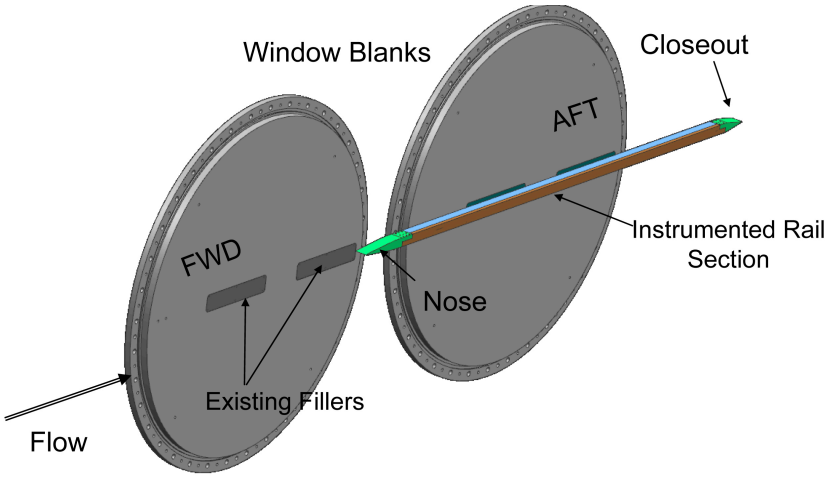

Figure 16. CAD view of 2" rail mounted on aft window blank of 9x7 wind tunnel

The 2-in. rail was used exclusively during the TBC1 test, and in conjunction with the RF1 rail during the TBC3 and 9x7 parametric tests. More details about the rail design and validation can be found in Ref. 3.

Figure 17. Photograph of 2-in. rail mounted on 9x7 WT aft window blank

C. Balance and Pressure Instrumentation

All the Boeing models in the Phase I and II tests used the Ames 1.0-in. Task Mk XIV-C six-component force balance. In the Performance model the balance was located close to the center of the model, but for the Boom and axisymmetric models the balance was located in a balance adapter with one of the VS1 through VS4 struts in between. The axisymmetric models were directly attached to the balance adapter. The use of the adapter was required because there was insufficient room for a balance inside the smaller models without compromising the outer mold lines, but the downstream location of the balance meant that the resolution of the model forces was not as good. The recorded force data were not adjusted for aerodynamic tares from the blade strut or balance adapter.

The 14-in. rail pressures were measured using seven 64-port, 5-psid ESP electronic pressure scanners deranged to 1.67 psid. Eight such scanners were used for the 2-in. rail since it has 6-in. more length of pressure orifices. The accuracy of these scanners was determined to be 0.08% of the deranged value, which equates to about 0.0013 psi or 0.187 psf.

D. Roll Mechanism

The Ames small model roll mechanism (SMRM) was used for enabling off-ground-track boom signature measurements in the 9x7 parametric and TBC4 tests, but not at the 8x6 in the TBC3 test. The roll mechanism has a fixed 7.5° bend in it to accommodate extended angle-of-attack or -sideslip ranges desired by other tests. This bend has been useful in sonic boom tests in that it allows a model to be moved closer to the rail (mounted on the north wall) or further from the rail (toward the south wall) than would be possible without it.

E. Linear Actuator

A linear actuator was used in the 9x7 parametric and TBC3 tests to translate the model longitudinally in the wind tunnel. This allowed acquisition of multiple pressure signatures at small increments in the *X* direction over a specified distance, such as 26 positions spaced 0.63 in. apart (~4 rail orifices) in a typical *X* sweep conducted in the 9x7 parametric test. In the TBC4 test, the linear actuator was not installed, so the only sweeps were in the *Z* direction, accomplished by translating the tunnel strut. Both *X* and *Z* sweeps in the various tests were successfully used in improving the quality of the signatures through spatial averaging.

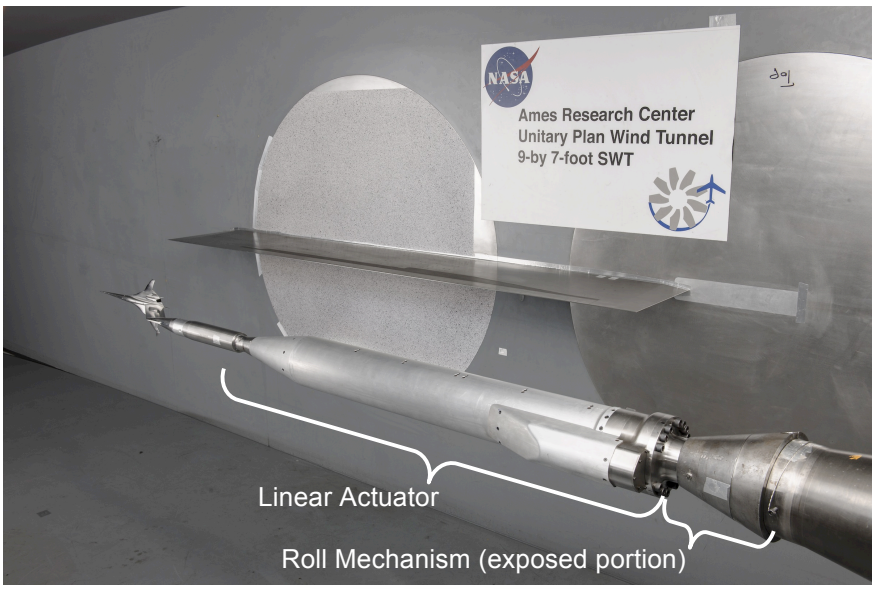

Figure 18. View of linear actuator and roll mechanism in 9x7 wind tunnel

The linear actuator is remotely controlled and its ram translates forward and aft at a rate of 0.7 in. per second over a 24-in. traverse distance. The minimum and maximum (retracted and extended) lengths of the linear actuator plus ram are 44 in. and 68 in., respectively. The linear actuator mounts into the roll mechanism with a 2.875 in. diameter male taper, and accommodates the model sting in the linear actuator with a 1.05-in. diameter female taper.

A photograph showing the linear actuator and exposed portion of the roll mechanism in the 9x7 wind tunnel is provided in Fig. 18. The ram of the actuator is shown in its retracted position, where the minimum of 2.625 in. of it is exposed at the front end of the actuator. The tilted-cone-shaped head of the roll mechanism is visible between the primary adapter (at right, partially hidden) and the rear of the linear actuator. The non-rotating cylindrical body of the roll mechanism is secured in the forward end of the primary adapter.

VI. Wind Tunnel Flow Quality and Test Techniques

A. Wind Tunnel Flow Quality

Ideally, a wind tunnel flow field surrounding a model would be completely uniform and steady for all model positions in the tunnel. However, this is rarely the case in supersonic wind tunnels, and in the 9x7 wind tunnel, there are spatial variations in terms of undesired flow angularity and Mach number variation throughout the test section, as well as temporal variations. These variations are caused in large part by the asymmetric sliding-block nozzle, and the fixed nozzle contours of the floor and ceiling, which result in a design that is optimized for one Mach number and not ideal for the others. Therefore, it is not surprising that unsteady characteristic waves emanate from the nozzle through the test section, affecting flow angles, Mach number, and steadiness of the flow. It is not possible to completely correct for these issues, but spatial and temporal averaging have been used to minimize their effects on the sonic boom signatures. To illustrate some of these flow features in the tunnel, Schlieren and shadowgraph images of the flow in the 9x7 will be presented.

1. Schlieren and Shadowgraph Imaging

Undesired facility-generated shock waves within a wind tunnel become significant in a sonic boom test when the shock waves from a low-sonic-boom design are generally weaker than those from the facility. This is evident in

viewing shadowgraph and retro-reflective background-oriented Schlieren (RBOS)[28] images in Fig. 19 that reveal both the ambient tunnel pressure waves and the model shock waves. RBOS is an alternative technique that is used when optical access is limited, such as in sonic boom tests where window blanks are installed on one side of the tunnel to accommodate the pressure rail. For the tests of the Boeing models in the 9x7, cameras and lights were placed on the south side of the tunnel, and a highly reflective material (3M Scotchlite brand film 900X) was placed on the north side window blanks behind the model. This was then speckled with ink in order to provide a background against which image-processing techniques would highlight density gradients in the field of view, due to the apparent movement of the speckles between wind-on and wind-off images.

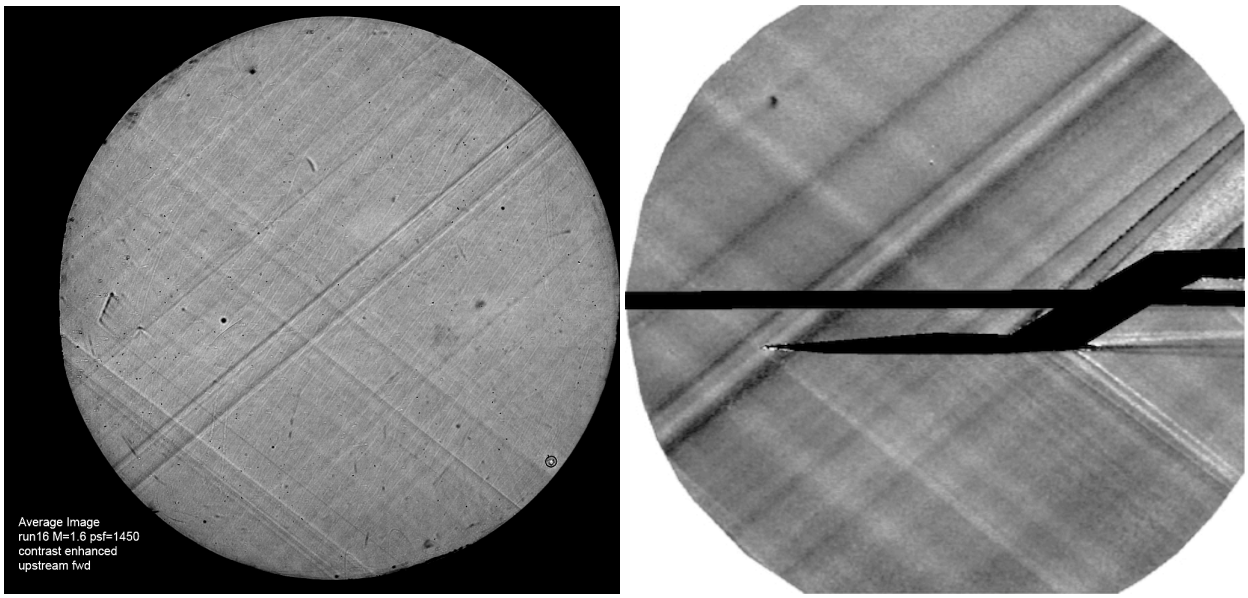

(a) Shadowgraph image, empty tunnel **(b) RBOS image, Boom1 VS2 model**

Figure 19. Shadowgraph and RBOS images of Mach 1.6 flow in 9x7 wind tunnel, taken through the forward Schlieren windows

A shadowgraph image through the forward windows of the 9x7 shown in Fig. 19(a) taken with the tunnel empty shows a pair of strong shock waves running from the lower left to upper right, along with quite a few weaker shocks and Mach lines throughout the window view. An RBOS view in Fig. 19(b) through the same window of the Boeing Boom1 model mounted with the wings horizontal in the tunnel also shows what appear to be the same pair of strong shocks and various weaker ones. Many of the model shocks are clearly visible, such as from the region around the model support strut, nacelles, and tails, but the weaker ones among these and the nose shocks are very difficult to distinguish from the facility shock waves. Note that the shocks from the model appear as dark bands going upward and light bands going downward; this is because the density gradients resolved by the RBOS technique are measured by the vertical deflection of the light path, equivalent to a horizontal knife edge in conventional Schlieren.

The Schlieren and shadowgraph images show the shock wave patterns in the tunnel at an instant in time, but time-resolved video (not shown herein) using Schlieren, shadowgraph, and RBOS reveals that the tunnel ambient pressure waves randomly shift positions by small amounts. This shifting covers distances on the order of one-quarter of an inch on the average, and occurs both in short-term temporal variations (at frequencies on the order of 100 Hz or more) and in long-term variations (several seconds or more). The short-term variations are averaged out in the data samples, but the long-term variations cause differences to be seen in the force and pressure data for the short data samples (~2 second durations). The source of the strong facility shock waves was not able to be determined during the test as no steps or bumps could be found on the tunnel floor or side walls in line with these waves; it is possible that some are characteristic waves from the nozzle bouncing between the floor and ceiling.

2. Stream Angle Variations

The Ames 9x7 and the Glenn 8x6 wind tunnels have stream angle variations throughout the test sections which result in variations in the model forces, moments, and angles when the model is moved in the *X* or *Z* direction to acquire multiple signatures. These stream angle variations in the 9x7 tunnel can be up to about a third of a degree over typical model translation distances, and about half this amount in the 8x6 tunnel. For the Boeing models run in

the two tunnels, the magnitude of the variations through typical X or Z sweeps was generally up to 0.02 in lift coefficient, 0.07° in angle of attack, and 0.07 in pitching moment. These changing model conditions throughout a sweep result in a somewhat incorrect averaging of the signature data. The data could be reprocessed using only those X positions where the model conditions are fairly constant, but that has not been done as of the writing of this report, and it would reduce the number of signatures used in the average, which could reduce data quality more so than any improvement due to consistent model conditions.

B. Corrections for Reference Runs

The standard technique for acquiring sonic boom data using a pressure rail is to subtract a reference run from a data run, so that the difference yields only the model's signature and not the ambient freestream signature from the tunnel flow. The reference run is taken in a "clean" tunnel, where the model shocks (if the model is present) are either off the rail or behind where they will be in the data run. Truly clean-tunnel runs can also be used, where the model and support components are physically out of the tunnel, but this is usually not necessary as long as the model shocks from the reference run do not overlap with those from the data run.

Model locations for example reference and data runs are illustrated in Fig. 20, where the Boom1 VS2 model and test set up is shown in the 9x7 wind tunnel. The red model is in the reference run position (nose 52 in. above rail, alpha 3.4°, ram retracted), and its shocks (dashed lines drawn at the Mach line angle as an approximation) pass just behind the rail at the 14-in. height of the rail orifices above the wall. For the data run, the blue model (at 8- and 24-in. ram positions) is 30 in. above the rail at an angle of attack of 3.4°. Note that the model shocks for this data run fall on the instrumented section of the rail—from tunnel station -84 to -106 in. It is clear from this figure that the data run model shocks are far enough ahead of those from the reference run to produce valid measurements, given that in supersonic flow there is no appreciable influence ahead of a model leading shock wave, aside from miniscule influences that might feed forward through the thin boundary layer of the rail tip.

Pressure signatures measured on the RF1 rail for the reference and data runs of the layout in Fig. 20 are shown in Fig. 21. In the top of figure, the reference and data runs are plotted as $\Delta P/P$, where $\Delta P = P_{Rail} - P_{\infty}$, and the P in the denominator is P_{∞}. The red curve is the reference run, which is the tunnel's ambient pressure signature on the rail. The variance of the pressures over the length of the rail is due to the non-uniformity of the tunnel flow (including various facility shocks as discussed above) and the influence of the rail on the ambient flow as it passes over the 18-in. leading-edge section and establishes itself over the instrumented section. The black curve is the data run, visible mostly in the region where the model shocks fall on the rail at tunnel stations approximately from -84 to -106 in. Where the black curve appears slightly separated from the red curve *ahead* of the model shocks is indicative of small temporal variations in the tunnel flow between the reference and data runs. The corrected pressure signature of the model is shown in the figure as the blue curve (offset by -0.04 in $\Delta P/P$ for clarity), obtained by subtracting the reference signature from the data signature.

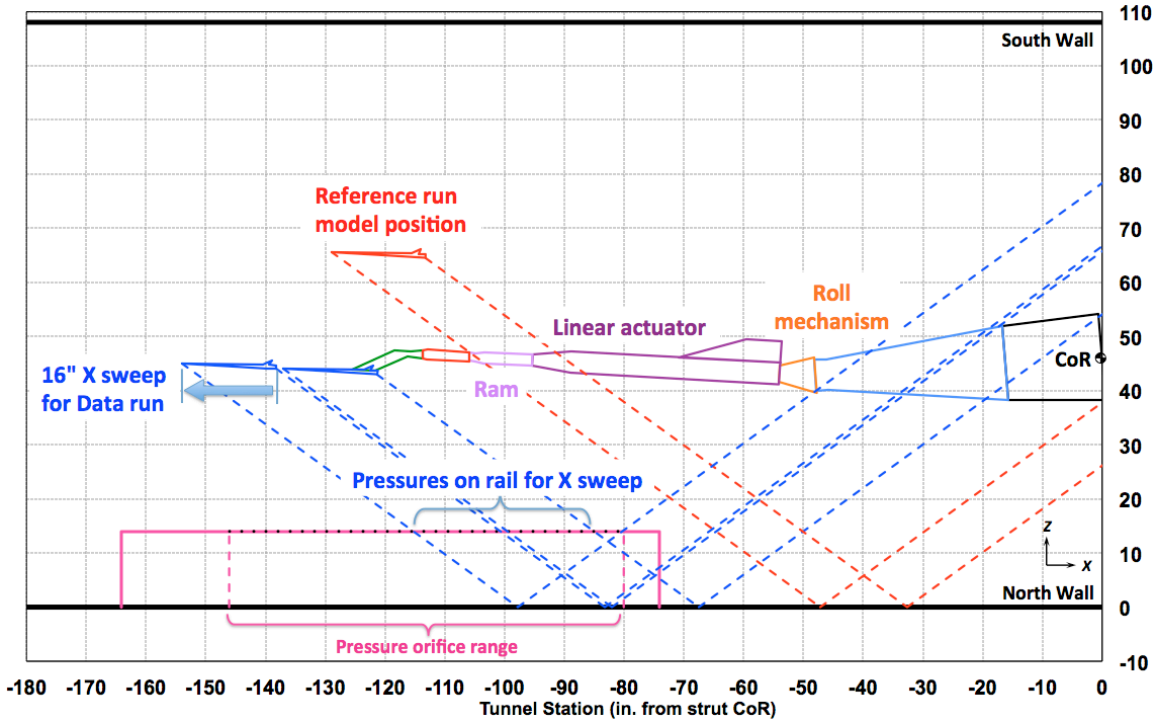

Figure 20. Layout of reference and data runs in 9x7 wind tunnel (view from floor of tunnel looking up)

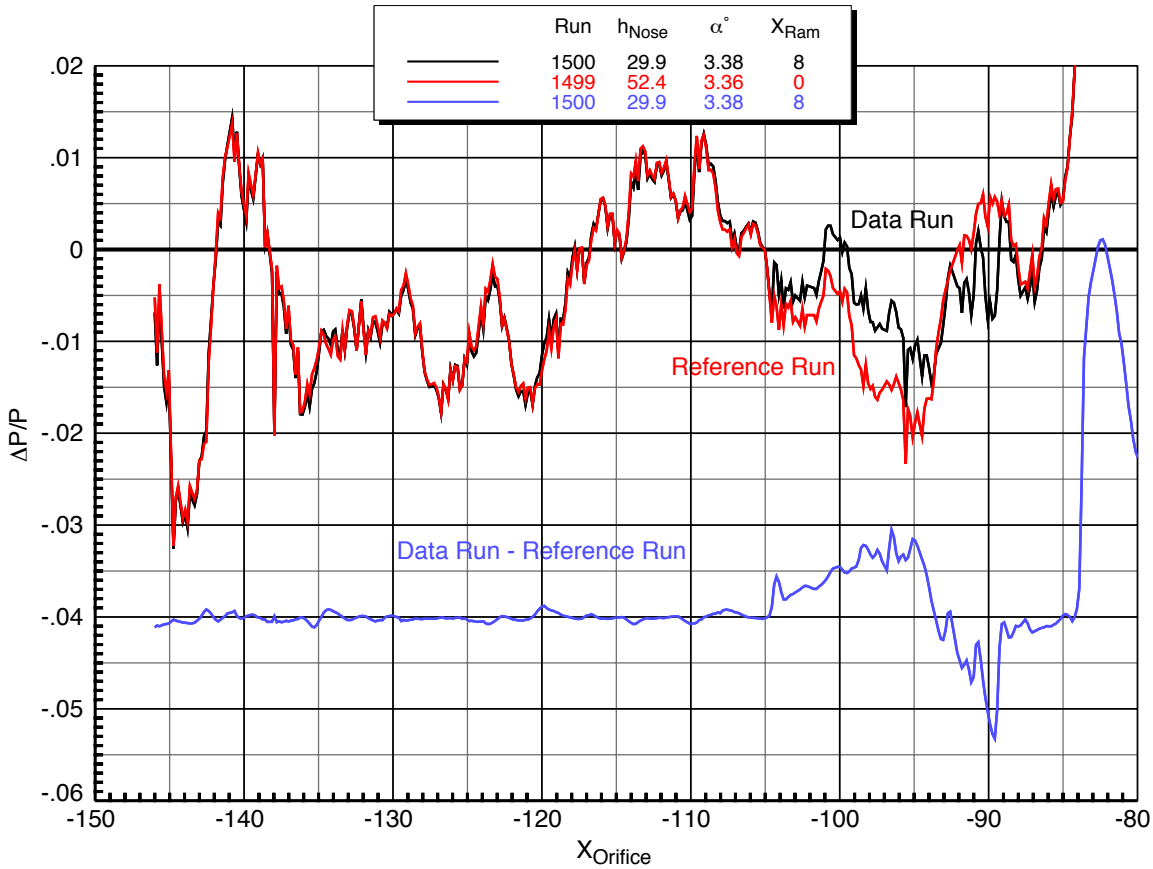

Figure 21. Differencing technique to isolate model pressure signature with rail
9x7 Parametric Test, Boom1 VS2 Model, M = 1.60, P_T = 2292 psf, *HumidAvg* = 314 ppm

C. Test Technique Improvements

NASA and its NRA contract partners found that some changes employed in the current tests to some former test techniques resulted in improved accuracy and repeatability of the sonic boom pressure data. A brief overview of spatial averaging is discussed here, and the reader is referred to Ref. 29 for the other test technique improvements, which included:

- Spatially average the data over limited model movements in the *X* or *Z* direction
- Operate the 9x7 tunnel at a higher total pressure (2300 psf) than in previous sonic boom tests
- Reduce the freestream humidity to less than 250 ppm and maintain within 4 ppm
- Position the model upstream of the leading edge shocks from the rails
- Optimize the sampling duration of the reference and data runs

The spatial averaging technique was developed to reduce the effect of tunnel flow field spatial distortions on the data at single model positions during supersonic wind tunnel testing.[2,3,30] In sonic boom testing in the 9x7 wind tunnel, the non-uniform flow field causes pressure signatures on the rail to be different for different model positions in the test section. To enable the spatial averaging technique, the model is typically translated a short distance longitudinally (*X* direction) or vertically (*Z* direction, away from the rail), and a number of sonic boom signatures are acquired at multiple positions as shown in the waterfall plot in Fig. 22(a). The *X* locations at each point on the individual signatures need to be aligned in order to enable the averaging. For an *X* sweep, the *X* values of the rail orifice locations are aligned by simply adding the ram position, as shown in Fig. 22(b):

$$X_{Aligned} = X_{Orif} + X_{Ram}$$

For a *Z* sweep, the *X* values of the rail orifice locations are adjusted by subtracting the height of the model nose at each *Z* position multiplied by the Mach number beta parameter:

$$X_{Aligned} = X_{Orif} - h_{Nose}\sqrt{M^2 - 1}$$

Plots that further illustrate this aligning and averaging procedure are given in the next section.

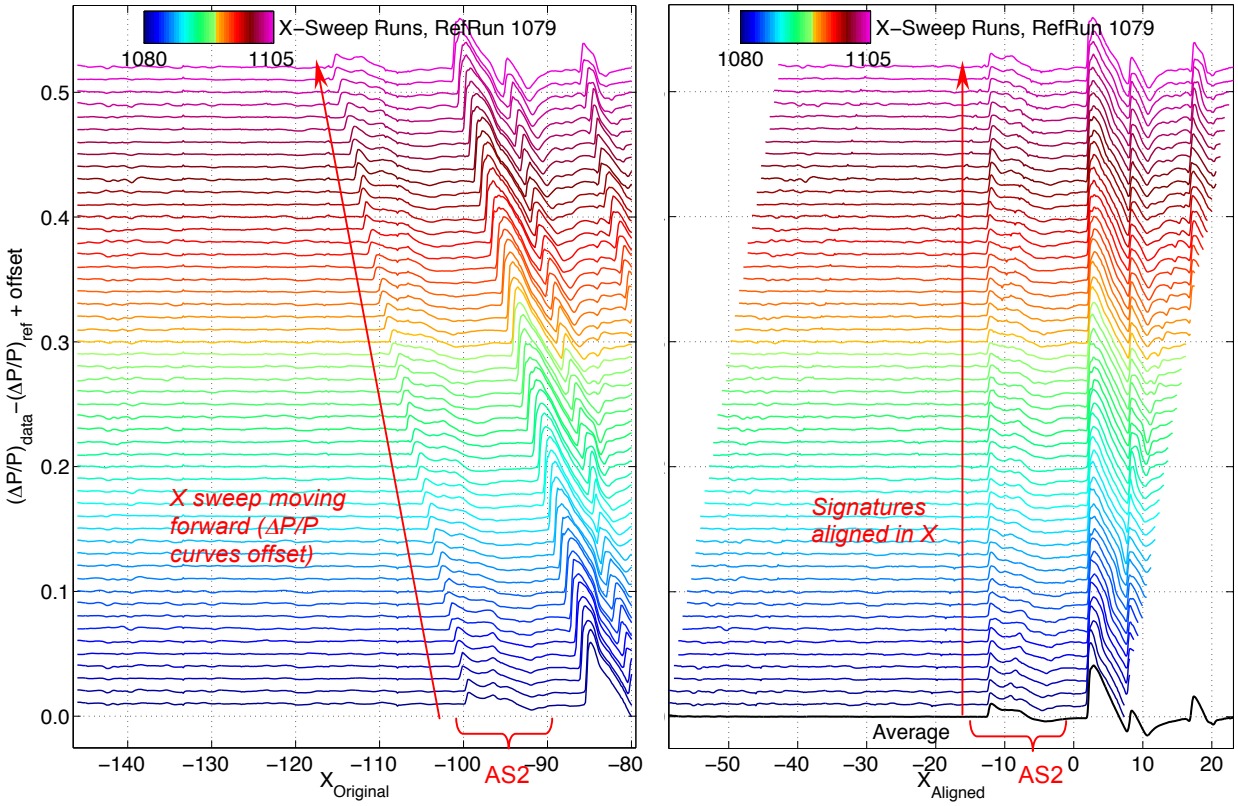

(a) Model signatures not aligned **(b) Model signatures aligned**

Figure 22. Non-aligned and aligned waterfall plots for 9x7 parametric test *X* sweep runs for AS2 model

VII. Experimental Results

Selected experimental data from the Boeing AS2, Boom1, Boom3, and Performance models run in the 9x7 wind tunnel parametric and TBC4 tests and in the 8x6 wind tunnel TBC3 test are presented in this section. Sample composite plots of individual pressure signatures taken during *X* or *Z* sweeps and their resulting averages are given first to illustrate the averaging procedure. Then the remainder of the plots consisting only of the averaged signatures will be shown to isolate various comparisons among the data, such as repeat runs, rail comparisons, *X* vs. *Z* sweeps, model variations, angle-of-attack effects, etc. Note that a "sig set" (signature set) number is included in the legends of the plots—this is a sequential count of the *X* or *Z* sweeps (referring to a run range) within a test, and the sig set numbers were restarted at 1 for each test.

A. Composite Plots of *X*- and *Z*-Sweep Individual and Averaged Signatures

Sample composite plots of a *Z* sweep for the Boeing AS2 model and an *X* sweep for the Boeing Boom1 model are shown in Fig's. 23 and 24. Each composite plot consists of four plots: an aligned waterfall plot (upper left) showing individual pressure signatures (offset in small $\Delta P/P$ increments, in various colors) obtained within a sweep, along with the spatially-averaged signature (in black, at the bottom); a similar plot of the individual and averaged signatures but collapsed to the same $\Delta P/P$ scale (lower left); a zoomed-in plot of just the average model signature (lower right); and a small layout diagram showing the reference and sweep positions for the model (middle right). Average values and ranges of the model parameters for the sweep represented by the plots are given in the table at the top of each plot.

The waterfall plots are shown after alignment of the signatures. Prior to alignment, the edges of the signatures are vertical in the waterfall plot (as in Fig. 22(a); representing the first and last orifices on the rail at their fixed *X* positions in the tunnel), and the locations of the model shocks vary throughout the sweep. The alignment allows the signatures to be averaged together, but note that the ends of the averaged signature do not use all of the individual signatures in computing the average because of the forward-sweeping (in viewing from bottom to top) signature edges in the aligned waterfall plot. The goal in the testing was to keep the model shocks far enough from the ends of the rail orifices so that as many as possible, if not all, of the signatures in the sweep could be used in the average. This was generally easy to do for the smaller models, but the large 43-in.-long Performance model required careful planning to make sure its signature was sufficiently centered on the rail. The layout diagram shown on these composite plots and in Fig. 20 was created by the author in Excel to permit the researchers to estimate shock locations on the rail for any given model and position in the tunnel.

The variation of the corrected pressures from one model position to the next can be seen in the waterfall plot (albeit at a very compressed vertical scale). These variations are seen at their normal scale in the plot below the waterfall plot. The ambient flow upstream of the wind tunnel model should produce a pressure signature of exactly zero as a result of subtracting the reference run from the data run. The cause of these corrected pressures not being zero is due to temporal variations in the wind tunnel flow between the reference and data runs. The flatness of these "leading zero" pressures upstream of the model are a good indication of the quality of the pressure signature of the model—if the tunnel flow variations are small enough that these leading zero pressures are close to zero, then the temporal effects on the model signature will be slight. Other contributors to errors in the model signature measurements are tunnel turbulence (temporal variations that are short term and small scale) and model vibration. Also, the discrete spacing (4 mm) of the pressure taps on the rail can lead to rounding of the model signatures if the shock peaks mostly fell between the rail orifices during the sweeps.

Fig. 23 shows the experimental pressures for the AS2 model from the 9x7 parametric test 97-0250 for the run series 1010–1043. A *Z* sweep was conducted in this series, consisting of an 8-in. vertical traverse with 0.25-in. spacing in the *Z* direction (roughly equivalent to 2-orifice, 0.31-in., spacing in *X*). Within the whole range of rail pressures shown, the AS2 model pressure signature runs from the first shock wave at approximately $X = -12$, followed by a short flat region, then a recovery at negative $\Delta P/P$ and back to ambient pressure at $X = 2$, before the large shock wave from the balance adapter aft of that point. The signatures show slight pressure variations at each *Z* position in the tunnel due to non-uniformities in the tunnel flow, and some of these can be identified by small bumps or spikes in the signatures at constant orifice locations on the rail.

A composite signature plot for the Boom1 model in the 97p test is shown in Fig. 24. Note that with this *X* sweep, the ends of the signatures in the waterfall plot sweep *aft* from the bottom to the top, in contrast to the *forward*-swept edges of the *Z* sweep in the previous figure. Keep in mind that as model height above the rail is increased, the model shocks move *aft* on the rail, whereas in an *X* sweep, the model shocks move *forward* on the rail, and the alignment process shifts the edges of the signatures on the waterfall plots in the opposite direction to get the model shocks to line up at constant *X* values.

X_{ram}, in	h, in	h/L
16.00 (16.00–16.00)	30.02 (26.02–34.01)	1.61 (1.40–1.83)
α, deg	β, deg	ϕ, deg
0.04 (0.04–0.04)	0.01 (0.01–0.01)	–0.15 (–0.18– –0.13)
C_L	C_D	C_M
0.006 (–0.003–0.010)	0.04470 (0.04180–0.04972)	–0.021 (–0.052–0.047)

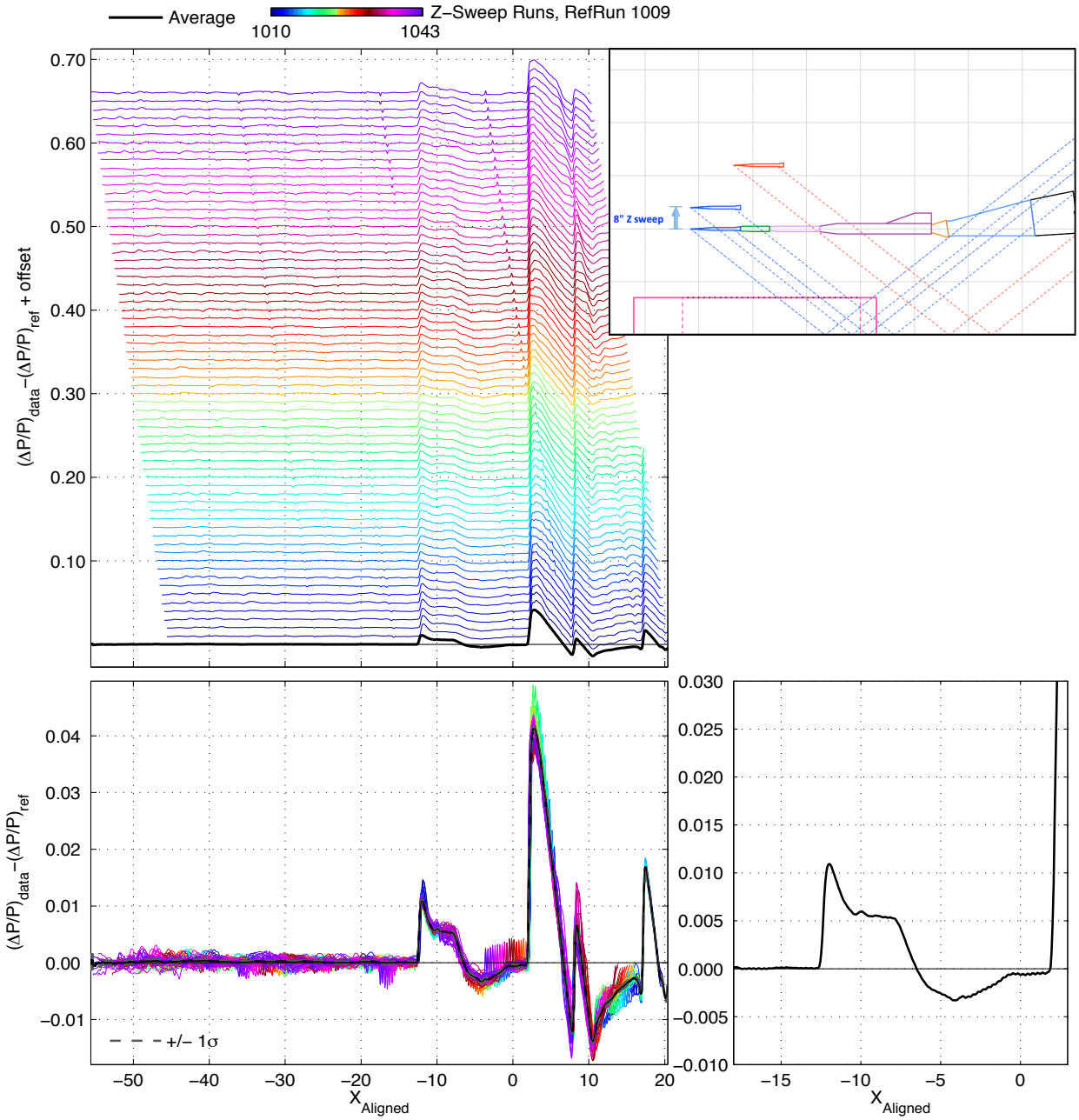

Figure 23. AS2 model aligned waterfall plot and averaged signature plots for *Z* sweep from 26" to 34" at X_{Ram} = 16," *M* = 1.6, 14" forward rail, 97p test

X_{ram}, in	h, in	h/L
7.87 (–0.00–15.75)	59.59 (59.10–60.08)	3.78 (3.75–3.82)
α, deg	β, deg	ϕ, deg
3.40 (3.38–3.42)	0.21 (0.20–0.22)	0.39 (0.34–0.43)
C_L	C_D	C_M
0.100 (0.090–0.104)	0.07165 (0.06711–0.07379)	–0.019 (–0.028–0.000)

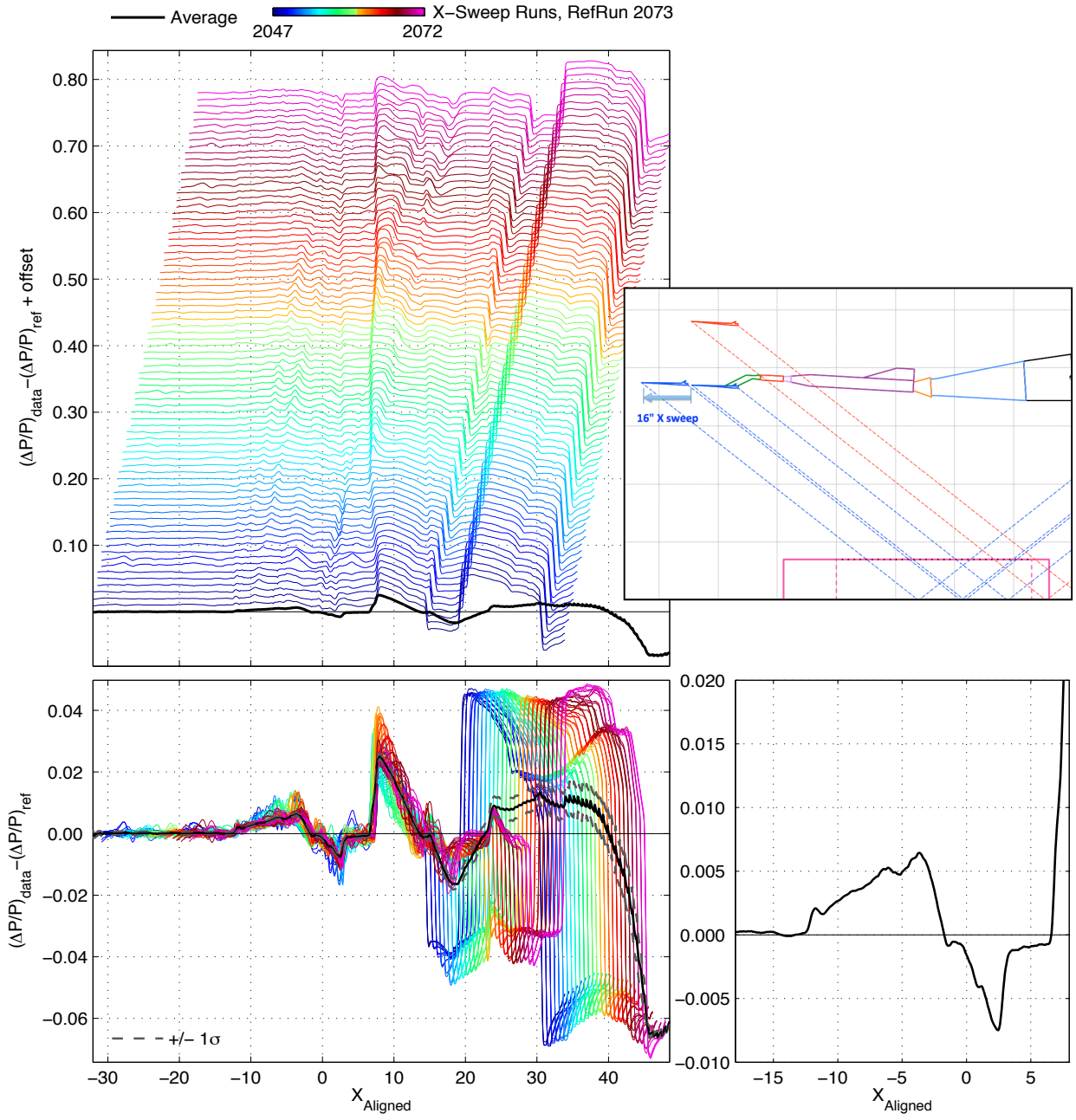

Figure 24. Boom1 VS2 model aligned waterfall plot and averaged signature plots for *X* sweep from 0" to 16" at h_{Nose} = 60," *M* = 1.6, 14" forward rail, 97p test

B. Repeatability

The plots in the remainder of the report showing experimental data will now consist only of the *spatially averaged* pressure signatures, as opposed to those of the previous subsection which included the individual signatures that were used to generate the average. It should be noted that the Mach, total pressure, and humidity values in the second title lines of each of the following plots are the *average* values of those parameters for all of the runs shown in the plots. On plots where these parameters vary among the runs, the plot legends will show those values for each set of runs.

Short-term repeatability of signature measurements for three models in the 9x7 tests are shown in Fig's. 25 and 26. (Long-term repeat runs in the 9x7 tests were not acquired because of limitations on test time, nor were *any* repeat runs acquired in the 8x6 test.) Back-to-back *Z* sweeps followed by an *X* sweep from the 9x7 parametric test for the AS2 model (offset by 0.02 in $\Delta P/P$) at heights of 30 and 31.8 in. are shown in Fig. 25, where the three signatures are almost identical except for a roughly 10% difference in the $\Delta P/P$ levels in the flat part of the signatures behind the nose shock. This difference could be due to the slight differences in model height or due to the type of sweep (more on these effects later), but considering the variation in individual signatures seen in Fig's. 22 and 23, it could also be considered within the scatter of the data. Boom1 VS2 model signatures in the lower part of Fig. 25 at a model height of 60 in. also show very good repeatability.

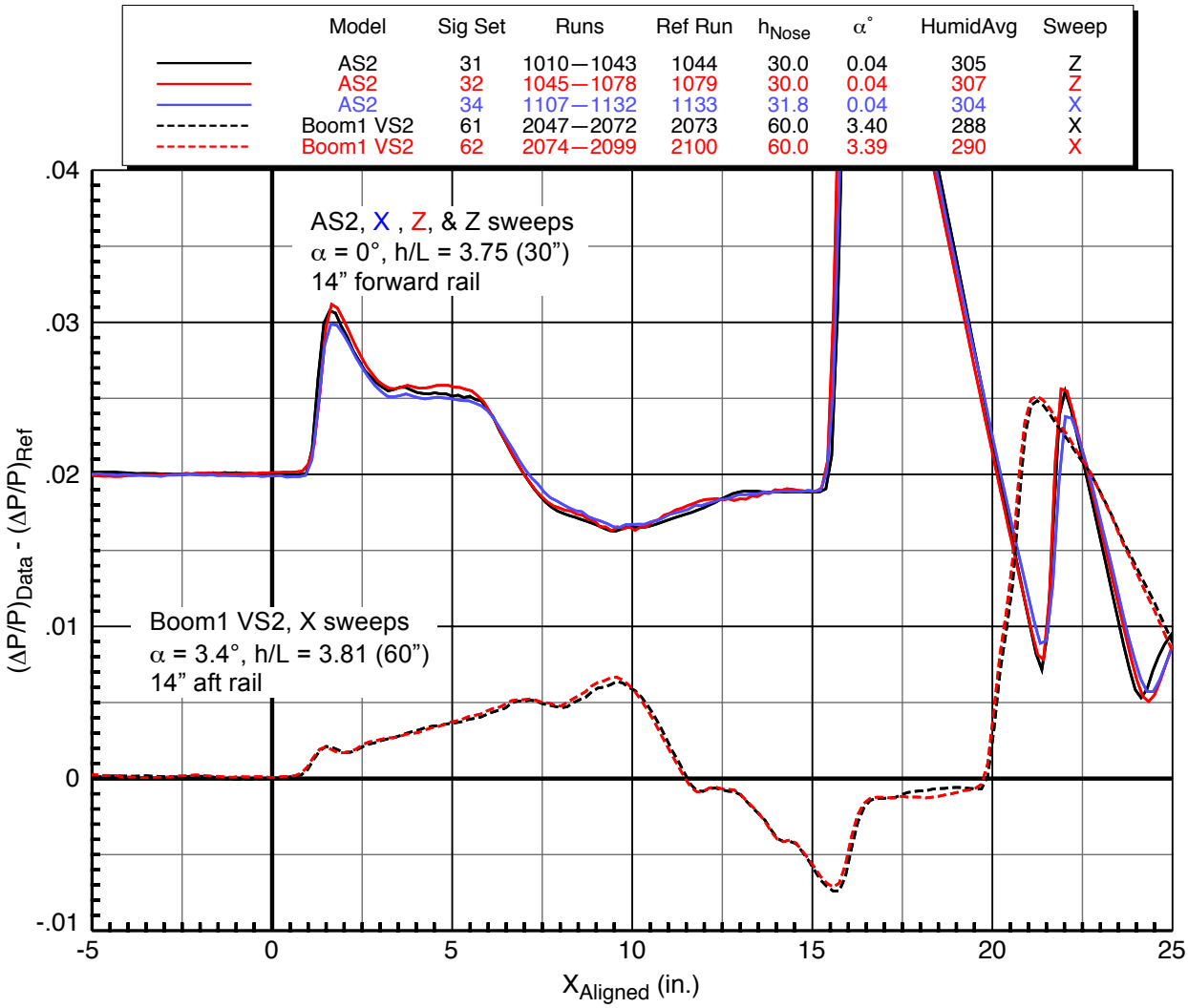

Figure 25. Repeatability for AS2 model with 14-in. fwd rail and Boom1 VS2 model with 14-in. aft rail 9x7 Parametric Test, $M = 1.60$, $P_T = 2291$ psf

Repeatability between two *Z* sweeps for the Performance model in the TBC4 test are shown in Fig. 26. Overall, the comparison is fairly good, though there are several places where the differences are up to ~0.0020 in *ΔP/P*, and the repeatability is not as good as it is for the Boom1 model at the same nominal height of 60 in. The deviations here and in the previous plots are probably a fair representation of the repeatability that can be expected for sonic boom measurements in the 9x7, and are most likely due to model fluctuations or variations in tunnel flow conditions over time.

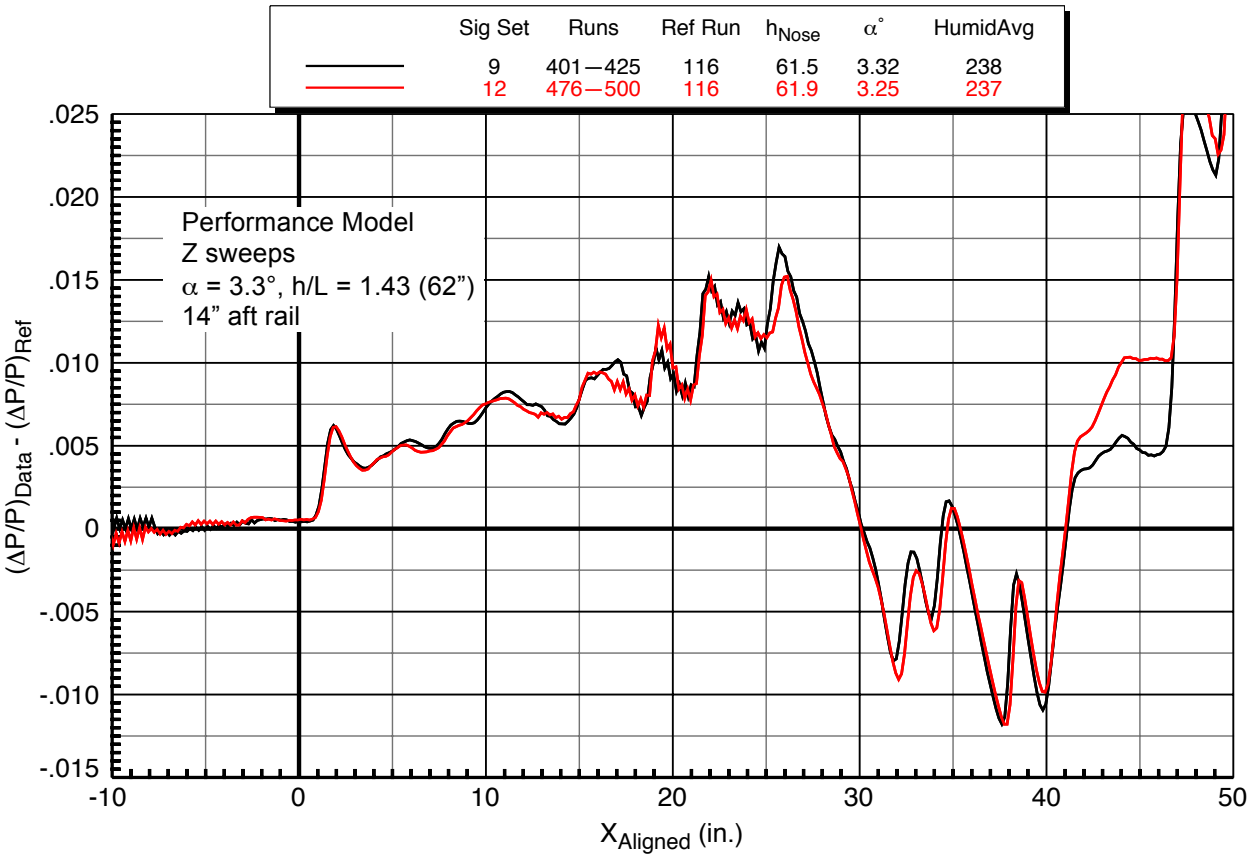

Figure 26. Repeatability for Performance model, *Z* sweeps (59" to 64")
9x7 TBC4 Test, 14-in Aft Rail, $M = 1.80$, $P_T = 2301$ psf

C. Effects of Model Height

For a given rail and mounting position on the wall of the 9x7 tunnel, there are allowable ranges of model *X* and *Z* positions where the model shocks stay within the instrumented section of the rail (refer to Fig. 20 for the general layout). For the Boom1 model with the VS2 strut at Mach 1.6, $\alpha = 3.4°$ in the 9x7 tunnel, with the rail on the forward window blank, the model height range (estimated by the Excel layout) that allows for at least an 8-in. *X* sweep is from 10 to 38 in. With the rail on the aft window blank, the model height range that allows for at least an 8-in. *X* sweep is from 52 to 68 in. The rail could also be mounted to span the two window blanks to cover the middle range, but this position was not used in any of the tests in the interest of time.

In the 9x7 parametric test, the RF1 rail was run in both the forward and aft window blank positions, and signature measurements of the Boom1 VS2 model were acquired at heights of 30 and 60 in. Comparisons of these signatures from *X* sweeps at Mach 1.6 and 1.8 are shown in Fig. 27. The signatures at both Mach numbers at 30 in. have much more clearly defined shock peaks than those at 60 in., and the magnitude of the overall pressure levels are higher at 30 in., as one would expect. At 60 in., the small shocks aft of the primary expansion have already coalesced.

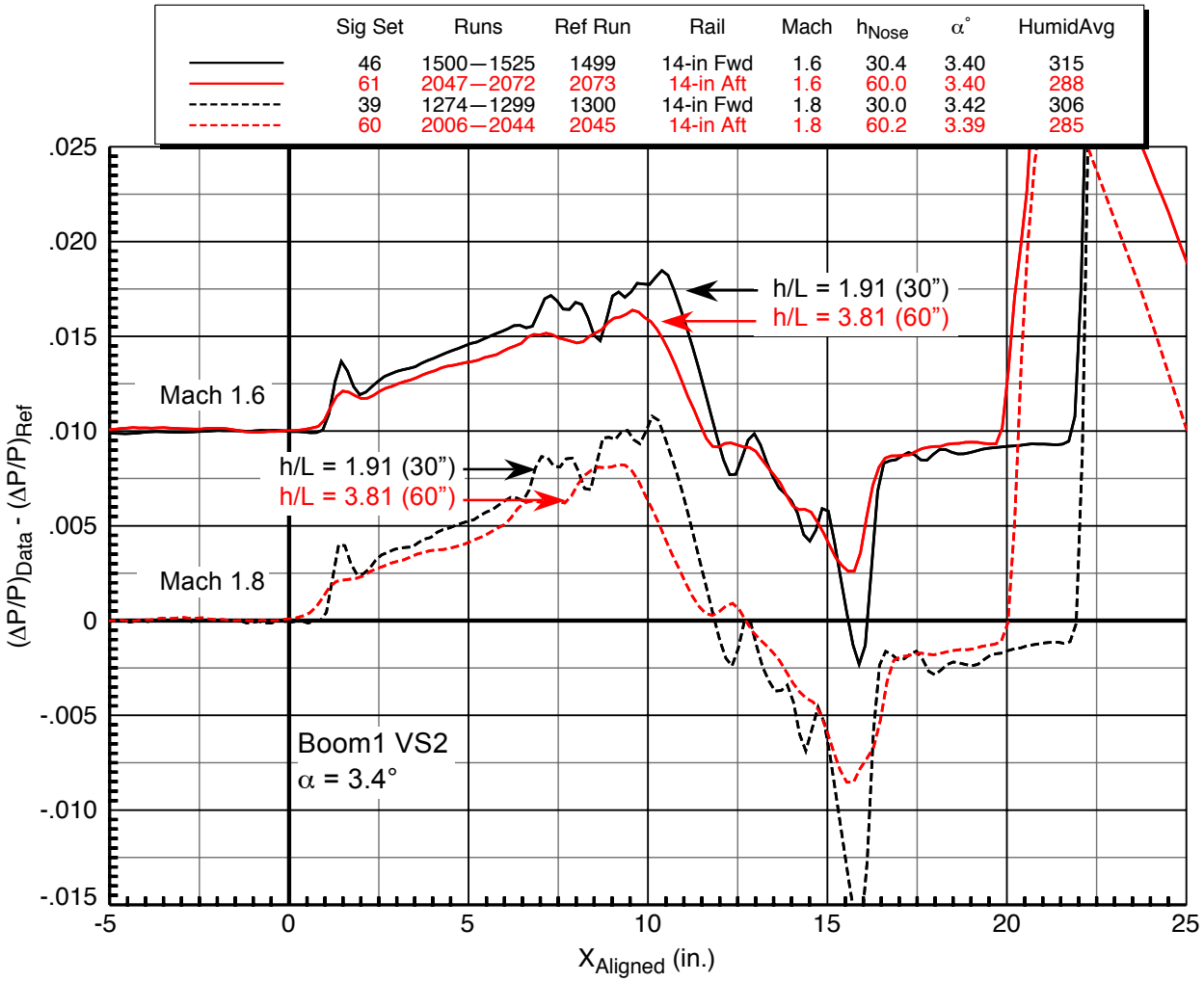

Figure 27. Effects of Boom1 VS2 model height, *X* sweeps
9x7 Parametric Test, P_T = 2297 psf

D. Rail Comparisons — 14-in. (RF1) vs. 2 in. Rails

In this section various comparisons of data from the 14-in. and 2-in. rails for the AS2 and Boom1 models are presented. Two primary differences in the effects of the rail on the data were expected between the two rails:

1) Reflection factor: The 14-in. RF1 rail was expected to not amplify the measured pressures at all, whereas the 2-in. rail was expected to cause amplifications between a factor of 1 and 2 (2 for an infinitely-wide flat plate, but lower for this 1.5-in.-wide rail).
2) Contamination of the aft part of the signatures from shock reflections off the wall: The 14-in. height of the RF1 rail was chosen to eliminate this possibility for models up to 33-in. long at a Mach 1.6 (51°) shock line angle, whereas on the 2-in. rail, the reflected shock passes back over the surface of the rail about 5 in. aft of the incident shock location at Mach 1.6, or possibly less distance aft if the lower Mach line angle closer to the tunnel wall (due to the boundary layer) is taken into account.

Flat-top rails like the 2-in. rail have been used in many sonic boom tests outside of NASA, and users of those rails have developed methods or calibration factors for correcting the data. These corrections are usually based on CFD analyses and/or experience with models of different sizes whose signatures are well known. However, in the present NASA studies discussed here, no such corrections have been generated, and the data from both rails will be presented as they were taken, with the exception of reflection factors for the 2-in. rail data computed to get the best overall match of the whole signature with the 14-in. rail data.

Figure 28 shows a comparison between the sonic boom signatures acquired with the 14-in. rail and 2-in. rail for the AS2 body of revolution in *Z* sweeps centered on h = 30 in. at Mach 1.6 and $\alpha = 0°$. The 2-in. rail data with no reflection factor correction is quite high relative to the data acquired with the 14-in. rail, as one would expect. But the aft "flat" portion of the signature, which is fairly horizontal in the 14-in. data, is sloped upward in the 2-in. data, which may be due to a reflection of the nose shock off the tunnel wall that is contaminating the aft portion of the signature.

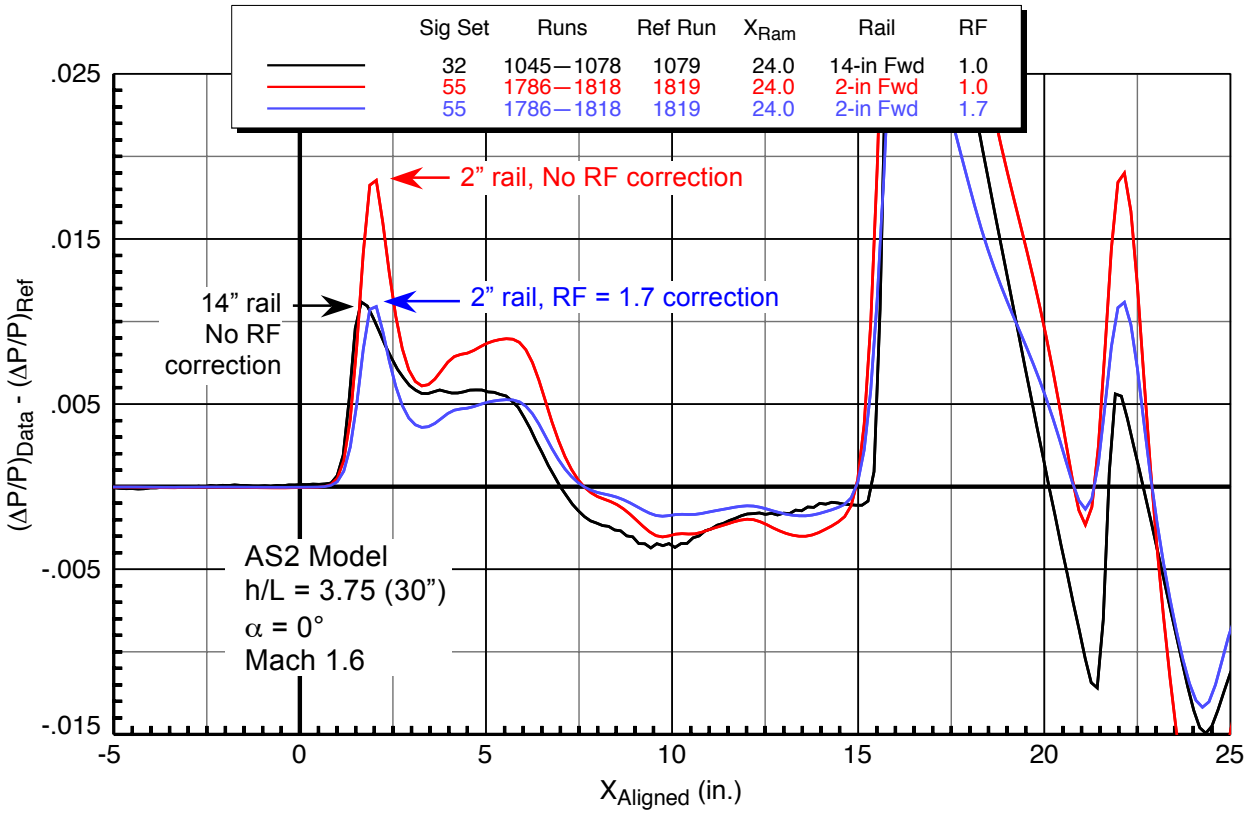

Figure 28. Rail comparisons for AS2 model, *Z* sweeps (26" to 34")
9x7 Parametric Test, M = 1.60, P_T = 2293 psf, *HumidAvg* = 301 ppm

To see what the 2-in. rail data would look like with a correction, a reflection factor of 1.7 ($\Delta P/P$ / 1.7) was applied to match the nose shock strength of the 14-in. rail—see the second sig set 55 curve, with RF 1.7. The nose

shock strength now matches that of the 14-in. rail data, but the correlation with the 14-in. data in the aft flat area is poor. From these data and other sources, it is surmised that the correction for reflection factor should not be applied evenly over the entire signature, but a thorough study of how it should be applied has not been conducted by the authors, and so the data will remain as presented herein for now.

Rail comparisons for data from the Boom1 VS2 model from both tunnels at various heights are shown in Fig's. 29 and 30. Data from the 9x7 tunnel for a *Z* sweep at a model height of 30 in. and Mach 1.6 are shown in the first figure, where, as with the AS2 data, the unadjusted signatures from the two rails show similar trends, though the 2-in. rail data shows more rounding and less definition of the pressure waves between the shocks. The adjustment of the 2-in. rail data for a reflection factor of 1.7 brings that data down to the level of the 14-in. rail data for the front half of the signature, but in the rear half (after $\Delta P/P$ crosses zero), the adjusted 2-in. rail data have significantly higher pressure levels than the 14-in. data. This could be due to the shock reflections off the wall contaminating the rear part of the signature, but as stated earlier, based strictly on the shocks following the Mach line angle, one might expect the contamination to start about 5 in. aft of the nose shock. The adjusted 2-in. rail data shows no or very little deviation from the 14-in. data at around $X = 6$, but the major differences start around $X = 11$ in..

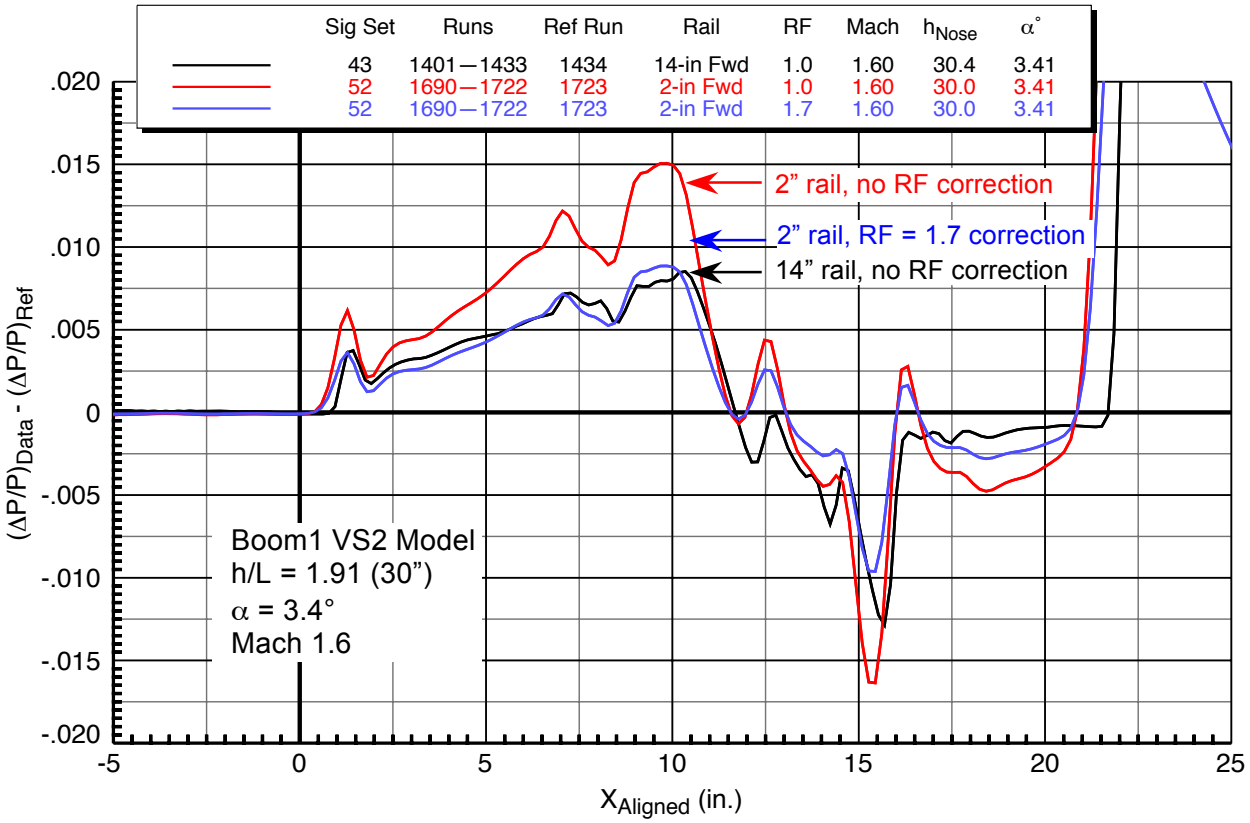

Figure 29. Rail comparisons for Boom1 VS2 model, *Z* sweeps (26" to 34")
9x7 Parametric Test, $M = 1.60$, $P_T = 2297$ psf, *HumidAvg* = 313 ppm

Rail comparisons for the same model from *X* sweeps in the 8x6 wind tunnel are shown in Fig. 30 for heights of 59 and 49 in. and at Mach numbers of 1.56 and 1.78, respectively. At $h = 49$ in. (dashed curves), the 2-in. data with RF = 1.7 applied match up fairly well with the 14-in. rail data, although the 14-in. data have numerous unexpected spikes in the signature. In solid curves at $h = 59$ in., however, there are more deviations between the curves from the two rails, so it is not clear which rail gives the better set of data from the 8x6 wind tunnel test.

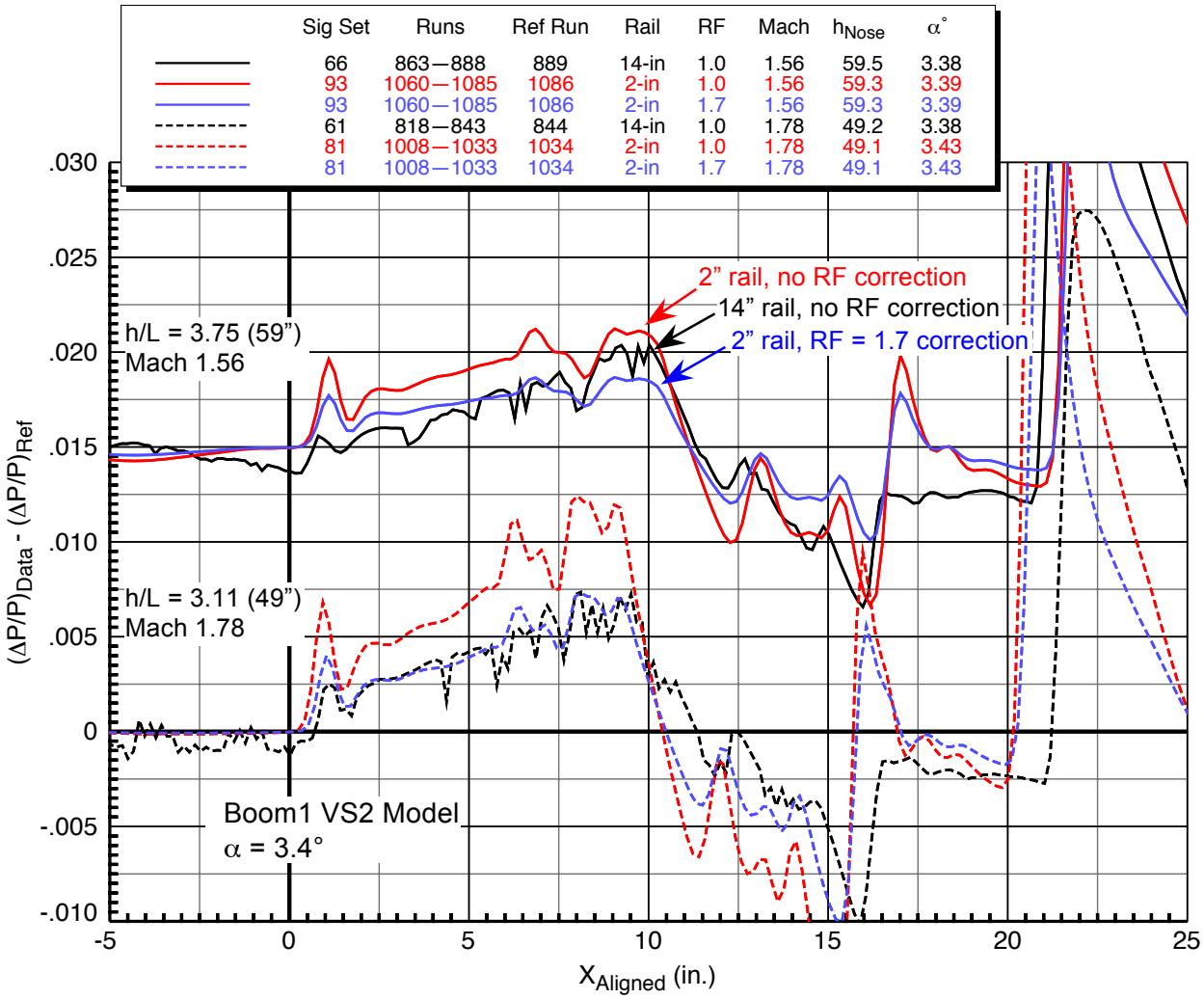

Figure 30. Rail comparisons for Boom1 VS2 model, *X* sweeps
8x6 TBC3 Test, M = 1.67, P_T = 3108 psf, *HumidAvg* = 94 ppm

E. Effect of Mounting Strut on Boom Model Signatures

The four different mounting struts, VS1 through VS4, were used with the Boom models (Boom1 or Boom2 with VS1 or VS2, and Boom3 with VS3 or VS4) in the various tests (see Fig. 11), but the VS1 strut was only used in the 9x7 TBC1 test. This test was conducted before *X* or *Z* sweeps were employed to permit spatial averaging, therefore, the Boom1 model with VS1 will not be included in the comparisons with the other three struts since the individual signature data does not have the tunnel spatial flow variations removed and thus is of poorer quality. The Boom1 model was run only with the VS2 strut in the TBC1, 9x7 parametric, and the 8x6 TBC3 tests, and the Boom3 model was run with both the VS3 and VS4 struts in the 9x7 TBC4 test—see Table 5 for the combinations of boom models and struts tested. Recall from model description section that the Boom3 model has the same aerodynamic lines as the Boom1 model aside for provisions for mounting on the new VS3 and VS4 struts, so comparing the Boom3 model with its struts with the Boom1 model with its struts is valid for illustrating strut effects. Boom1 VS2 data from the 8x6 test will not be included because such data are available from the 9x7 parametric test.

Signature comparisons for the Boom1 VS2, Boom3 VS3, and Boom3 VS4 models are made in Fig. 31 at Mach 1.6 and 1.8, all at model heights of approximately 60 in. The three signatures for each Mach number are very similar, as expected, in the forward parts up to near the maximum overpressure point, and aft of that there are differences as influenced by the struts. It seems odd though, that in the expansions just aft of the peaks in the Mach 1.6 data, the pressures from the VS3 and VS4 struts look very similar, while the pressures from VS2 are lower; it is VS2 and VS3 that are the upper swept struts, which allow the underside and back ends of the models to remain clean, so they should be more similar. The VS3 strut is longer than VS2 because it has a more forward mounting

point on the model, and thus it probably has less influence on the pressure signature below the model, resulting in a cleaner signature that is likely more representative of the real airplane signature.

The VS4 strut has a straight sting that compromises the lower aft end of the Boom3 model, but apparently the effects due to this compromise are not seen in this part of the signature at Mach 1.6. The strongest effect of the VS4 strut is in the large shock at $X = 16$ at both Mach numbers, which is from the aft-swept section of the strut that supports the sting. It was learned in the testing that this swept section was not far enough aft to keep its shock from overtaking the signature from the aft end of the model by the time the pressure field reached the rail, thus this strut was deemed unusable.

Table 5. Combinations of Boom Models and Struts Tested

Test	*Model*	*Strut*	*Strut shape*	*Spatial averaging*	*Figure*
9x7 TBC1	Boom1	VS1	Swept forward, short	No	—
9x7 TBC1	Boom1	VS2	Swept forward, mid	No	—
9x7 TBC1	Boom2	VS2	Swept forward, mid	No	—
9x7 Parametric	Boom1	VS2	Swept forward, mid	Yes	31
8x6 TBC3	Boom1	VS2	Swept forward, mid	Yes	—
9x7 TBC4	Boom3	VS3	Swept forward, long	Yes	31
9x7 TBC4	Boom3	VS4	Swept aft, straight sting	Yes	31

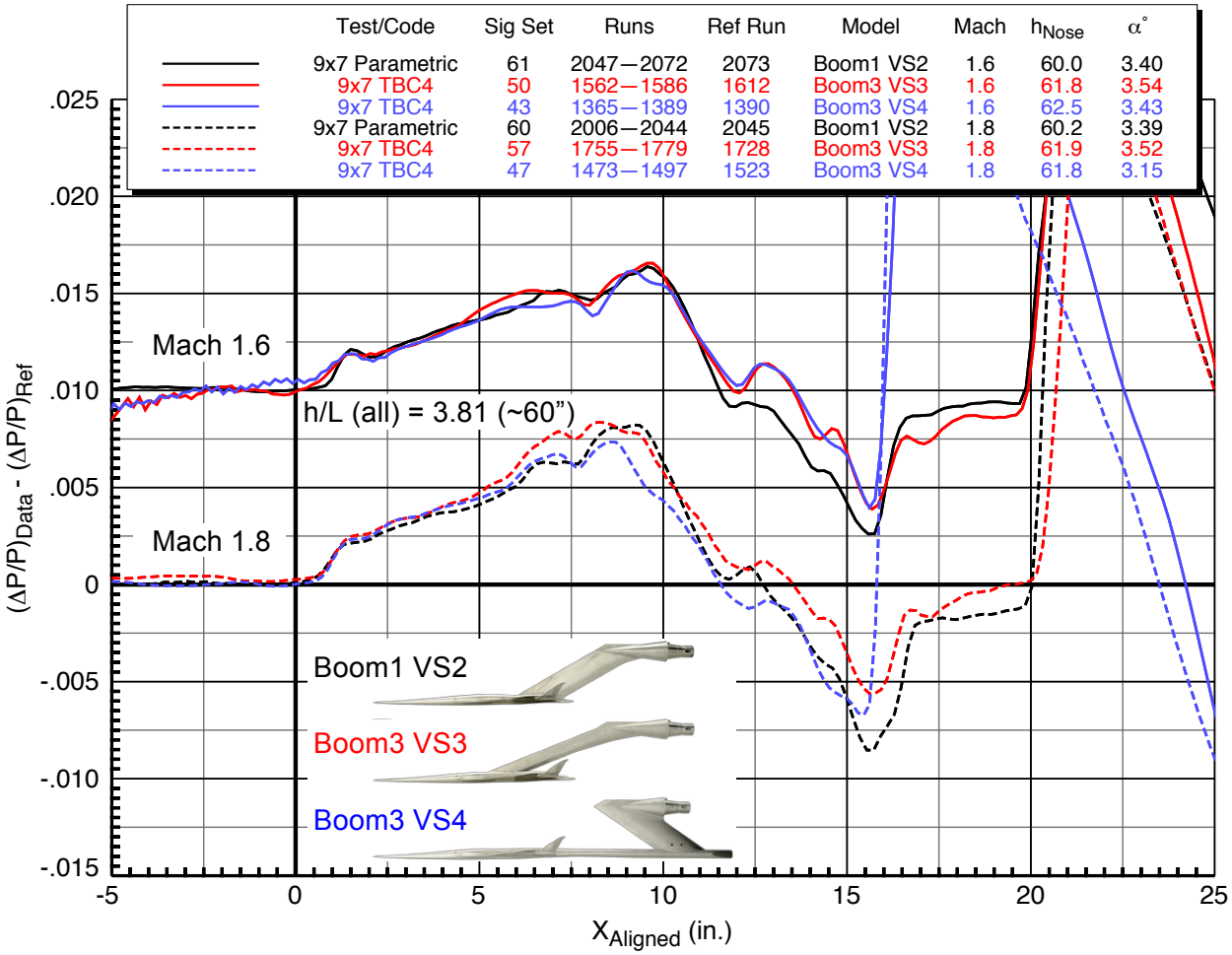

Figure 31. Boom model mounting strut effects
14-in Aft Rail, $M = 1.70$, $P_T = 2300$ psf, *HumidAvg* = 244 ppm

F. Effect of Angle of Attack

Figure 32 shows the effect of angle of attack on the sonic boom signatures of the Boom3 model from *Z* sweeps (59–65 in.) in the 9x7 TBC4 test. Angles from 2.5° to 4° are shown for the Boom3 model at Mach 1.6, and the trends of the overall pressure levels and shock peaks for the lifting parts of the model (i.e., aft of the nose shock) are consistent with the increasing lift causing stronger sonic boom signatures. Also note that the small shock at the bottom of the main expansion (X = 13) for the lowest angle of attack grows in strength and moves forward in the signature as the angle is increased.

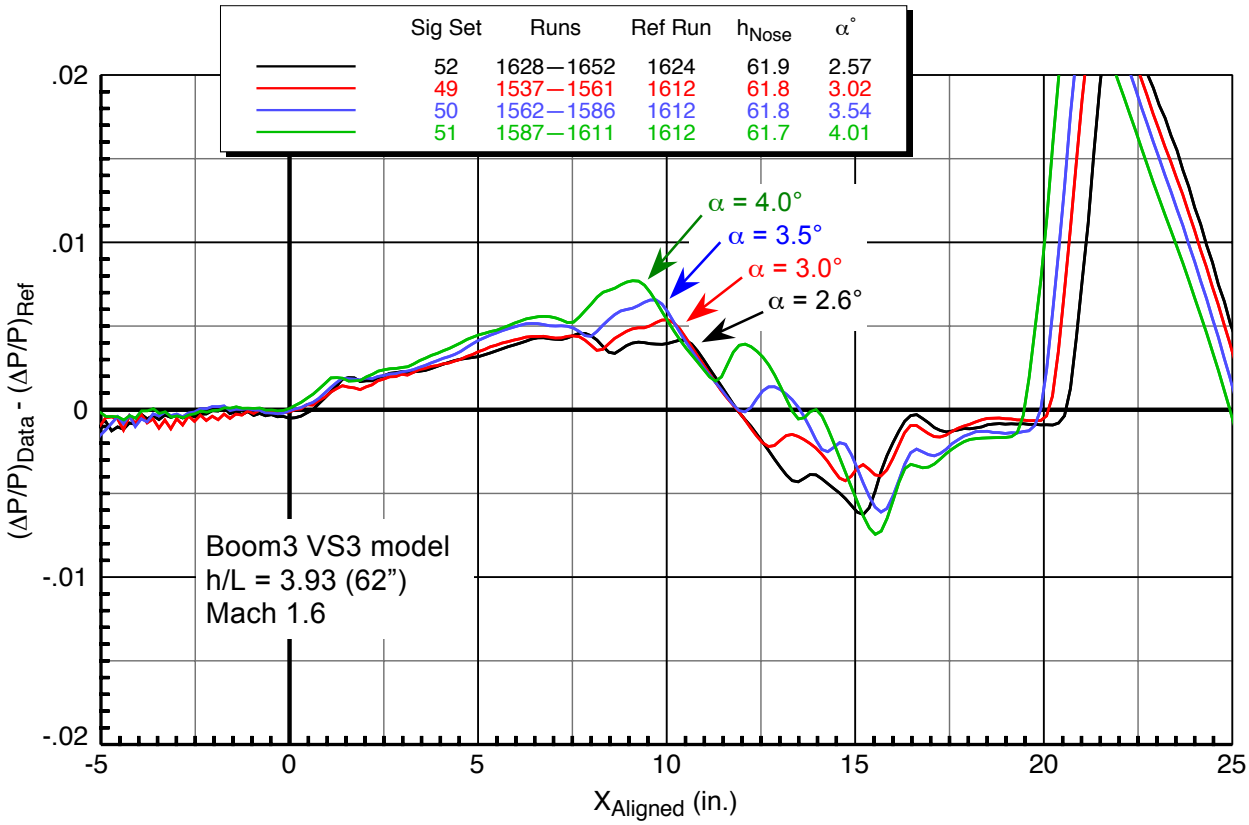

Figure 32. Effect of angle of attack for Boom3 VS3 model, *Z* sweeps (59" to 65")
9x7 TBC4 Test, 14-in Aft Rail, M = 1.60, P_T = 2300 psf, *HumidAvg* = 230 ppm

G. Effect of Off-Track Angle

The boom loudness is not only critical for the ground track under the flight path, but also off to both sides of the ground track. Signatures at off-track angles of 15°, 30°, and 45° are compared to the 0° on-track signatures for the Boom3 model in Fig. 33 at a height of 30 in. and Mach 1.6, and for the Performance model in Fig. 34 at a height of 60 in. and Mach 1.6. The 45° off-track angle signatures for both models have higher maximum pressure peaks than all the others, though only slightly higher for the Performance model. The gradients and maximum pressure drops in the main expansions generally become greater with higher off-track angles for both models, as do the magnitudes of the shocks from the components at the rear of the models. A significant difference between the sets of signatures for each model is that the nose shock and forebody pressures for the Boom3 model are very similar at all track angles, but are very uneven and inconsistent for the Performance model. The two models were designed to have the same outer mold lines at their respective scales aside from the mounting provisions along the upper fuselage of the Boom3 model and at the rear of the Performance model, so the forebody shapes should be identical. For the same physical height above the rail in the tunnel in both of these figures (~60 in.), the Performance model is at a lower *h/L* (1.39) than the Boom3 model (3.81), but this should not make a difference in the forebody pressures.

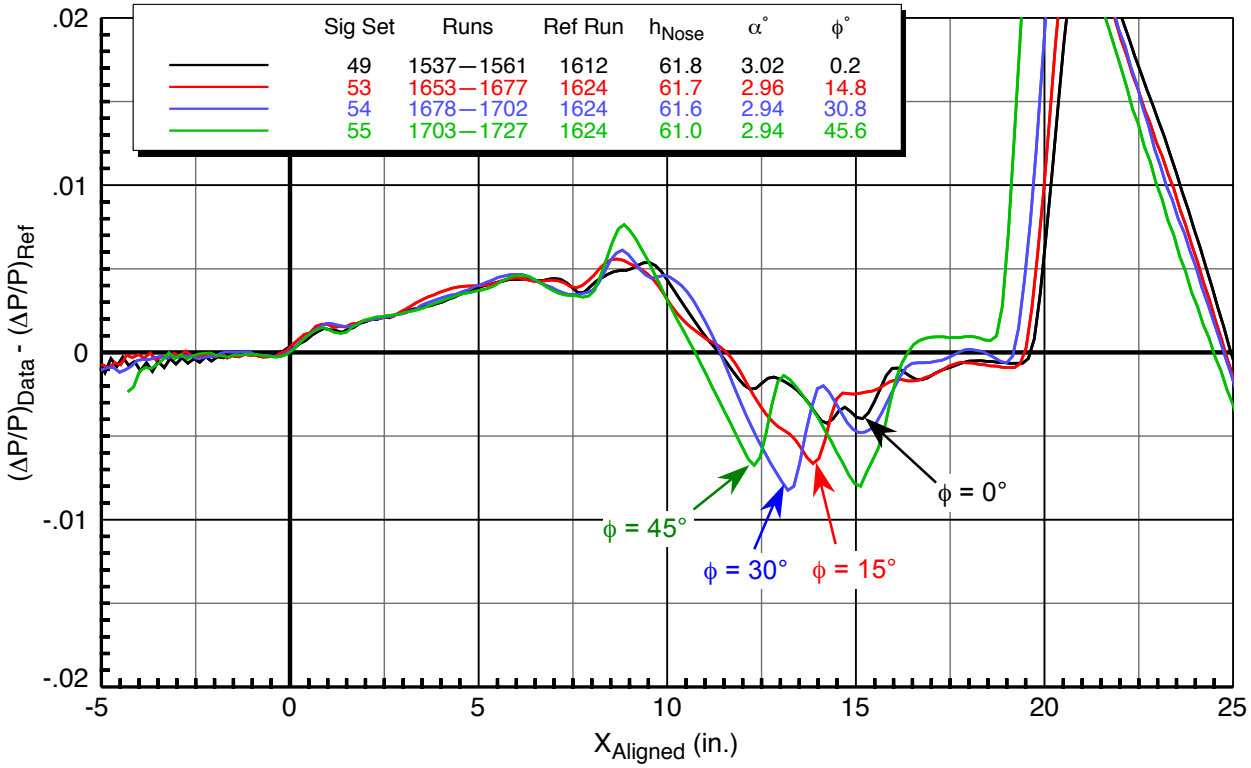

Figure 33. Effect of off-track angle for Boom3 VS3 Model, *Z* sweeps (59—65 in.)
9x7 TBC4 Test, 14-in Aft Rail, $M = 1.60$, $P_T = 2299$ psf, *HumidAvg* = 226 ppm

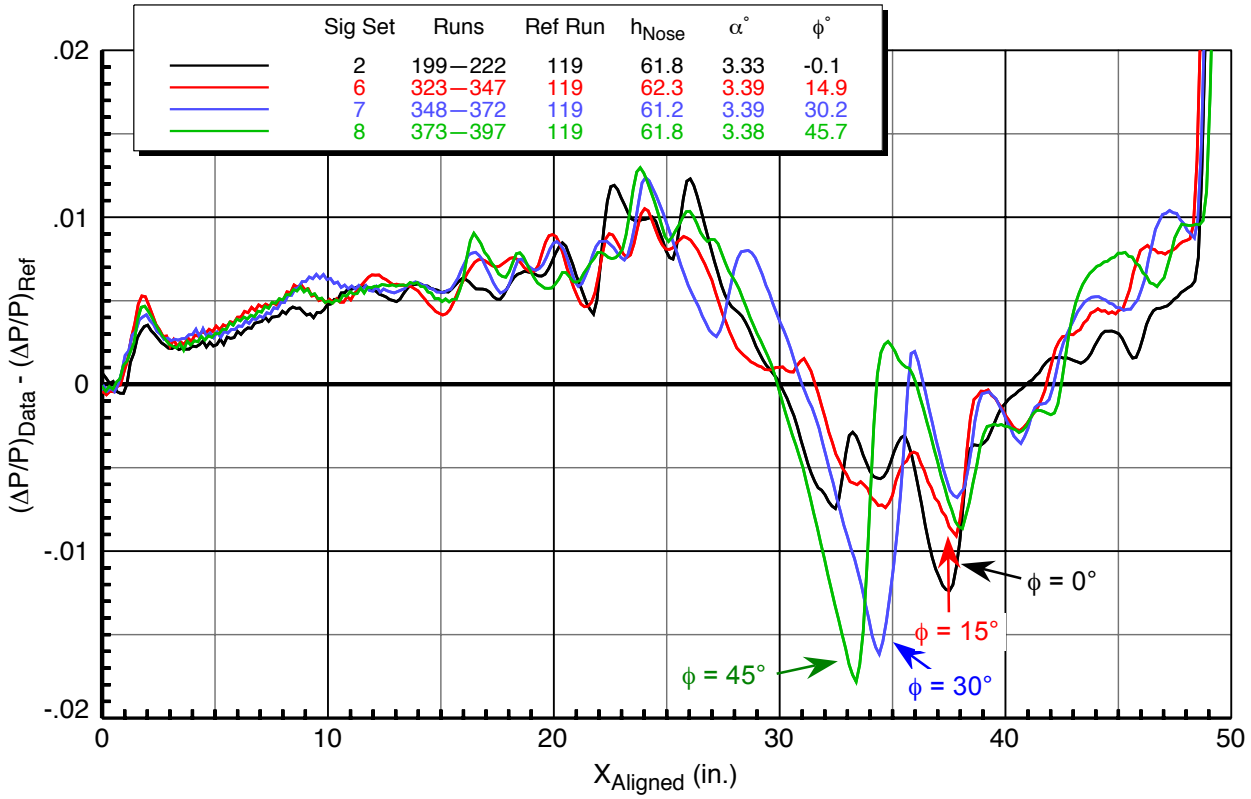

Figure 34. Effect of off-track angle for Performance Model, *Z* sweeps (59—65 in.)
9x7 TBC4 Test, 14-in Aft Rail, $M = 1.60$, $P_T = 2301$ psf, *HumidAvg* = 265 ppm

VIII. Computational Methods

Three high-fidelity NASA CFD codes where used to compute the flow around and sonic boom signatures for the Boeing models: *USM3D, OVERFLOW* and *Cart3D*. *USM3D* was the code most used in this study, and selected cases were computed using the other two codes. In this section a brief description of each of the CFD codes is given.

USM3D[31] is a tetrahedral cell-centered, finite volume Euler and Navier-Stokes (N-S) method. It provides a variety of options for solving the flow equations and several turbulence models for closure of the N-S equations. For the current study, it was used with Pointwise grid generation methods for inviscid flow simulations, and with V-Grid for laminar and turbulent (using the Spalart-Allmaras turbulence model) viscous flow simulations.

Cart3D is a high-fidelity, inviscid, unstructured-mesh analysis package for conceptual and preliminary aerodynamic design, and it was run in conjunction with the Adjoint Error Optimization (AERO) module for the current study. It allows users to perform automated CFD analyses on complex geometries.[8-10] The package includes utilities for geometry import, surface modeling, mesh generation, flow simulation and post-processing of results. The main simulation code, *FlowCart*, runs in parallel both in shared memory (OpenMP) and distributed memory (MPI) with excellent scalability. The package is highly automated so that geometry acquisition, and mesh generation can usually be performed within a few minutes on current desktop computers.

OVERFLOW (Ref Nichols, Pirzadeh) is the OVERset structured grid FLOW solver that was used by Boeing for their inviscid and viscous simulations (Ref Magee) presented in this paper. The turbulence model that was used was the Spalart-Allmaras (SA) model.

IX. Comparison of Experimental Data and Computational Simulations

Data from selected wind tunnel runs of the Boeing AS2, Boom1, Boom3, and Performance models are compared to predictions from the three CFD codes described above in this section.

A. AS2 Model

All three CFD codes were used to compute the pressure signatures for the AS2 model at distances of 30 and 60 in. below the model. As an example of an adapted grid and pressure contours from *Cart3D*, Fig. 34 shows the adjoint-adapted grid at Mach 1.6 after 13 levels of adaptation, and the sensor lines are shown in orange at 30- and 60- in. heights. The refinement pattern is driven by the features of the adjoint solution. Figure 35 shows the symmetry plane pressure contours.

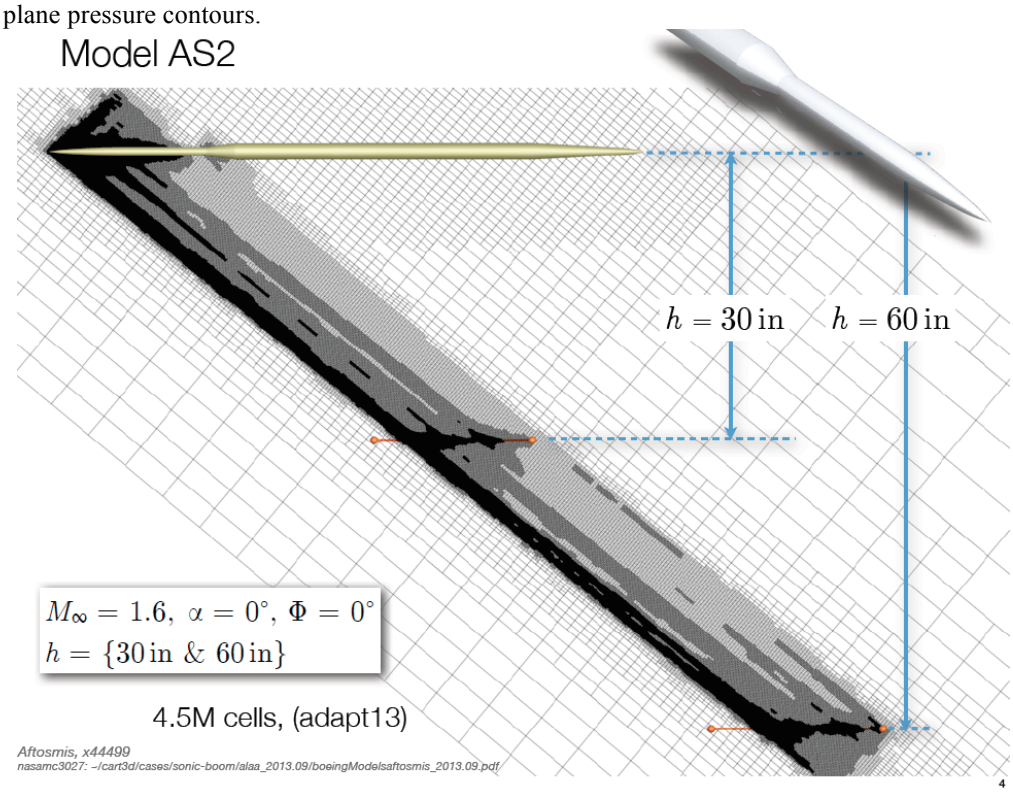

Figure 34. Boeing AS2 Body of Revolution, symmetry plane Cart3D adjoint-adapted grid

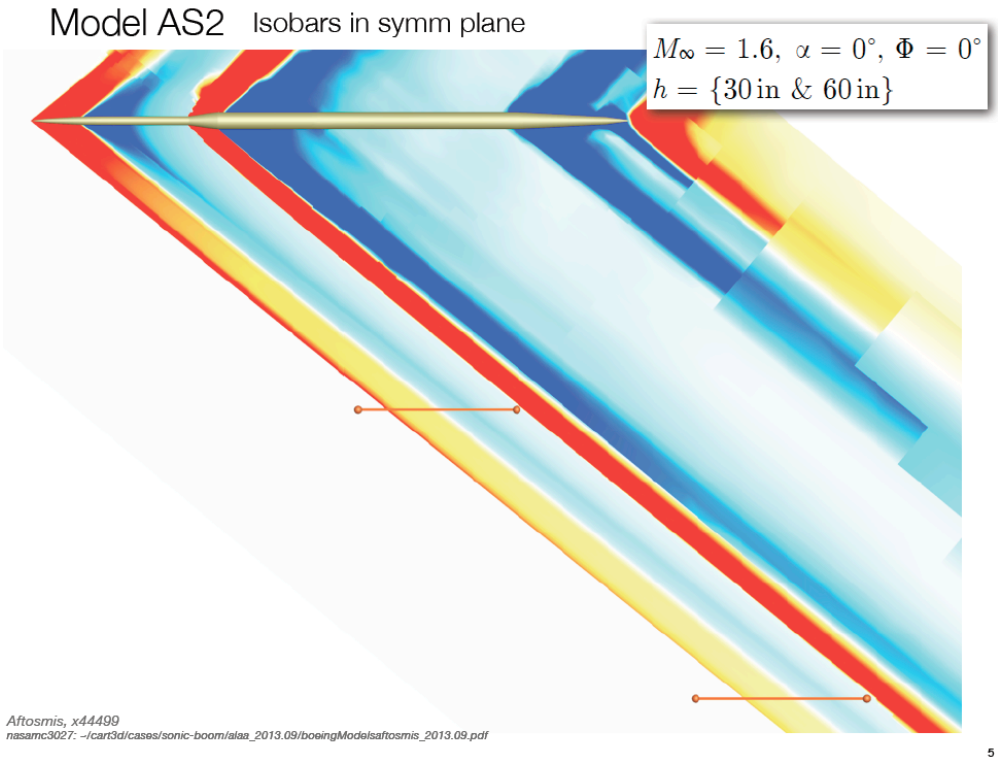

Figure 35. Symmetry plane pressure coefficient contours for Boeing AS2, *Cart3D* results

Inviscid and viscous predictions of AS2 signatures are compared with 9x7 wind tunnel data in Fig. 36 at a height of 30 in., and with 8x6 wind tunnel data in Fig. 37 at a height of 60 in. The data from the 9x7 were acquired at Mach 1.6 with the 14-in. rail, while the 8x6 data were acquired at Mach 1.56 with the 2-in. rail. The CFD predictions were run at Mach 1.6 and a Reynolds number of 4.1 million per foot, which is a little lower than the wind tunnel Reynolds number of 4.5 million per foot at $M = 1.6$ and $P_T = 2300$ psf.

The wind tunnel data in these plots are shown in the dark gray curves with circle symbols, and the predictions are shown in the colored curves without symbols. Note that the y-axis labels, $(\Delta P/P)_{Data} - (\Delta P/P)_{Ref}$, apply exclusively to the experimental data; there is no need for "reference" runs in the CFD, so the labels for the CFD cases would be just $\Delta P/P$.

Two inviscid CFD predictions, *Cart3D* and *USM3D*, and two viscous CFD predictions, *Cart3D* and *USM3D SA* (Spalart-Allmaras turbulence model) and *OVERFLOW*, are compared to AS2 model data from the 9x7 parametric test at a height of 30 in. above the rail in Fig. 36. All of the codes predict nose shock peaks between 20% and 60% higher than the experimental data peak and much faster rise times. The experimental data are from the 14-in. RF1 rail, so there is no amplification of the measured shock peak by any reflection factor. There is good agreement of all three codes with experimental data in the flat region behind the nose shock, but all of the codes over-predict the main expansion in the aft portion of the signature. The reason for this discrepancy is not known, though the same discrepancy was noted for the Lockheed Seeb body-of-revolution model.[2,14] It was surmised that the leading shock from the pressure rail striking the curved part of the AS2 model was the cause for the discrepancy, but upon further review of the 26 individual signatures in the X sweep for the 1080–1105 run series from the 9x7 parametric test, it was determined that this is not the likely cause. For the first few inches of the 16-in. X sweep, the rail nose shock does pass over the curved nose section of the AS2 model, but the model pressures in the main expansion are nearly the same as those from the latter part of the X sweep, indicating that the rail shock does not significantly influence model signature. The two inviscid and viscous CFD results in Fig. 36 match the flat portion of the signature fairly well, though the viscous *OVERFLOW* result (sig set 34) has a bit of an undershoot at the start of the shocks for the model nose ($X = 1$) and the balance adapter ($X = 15.5$).

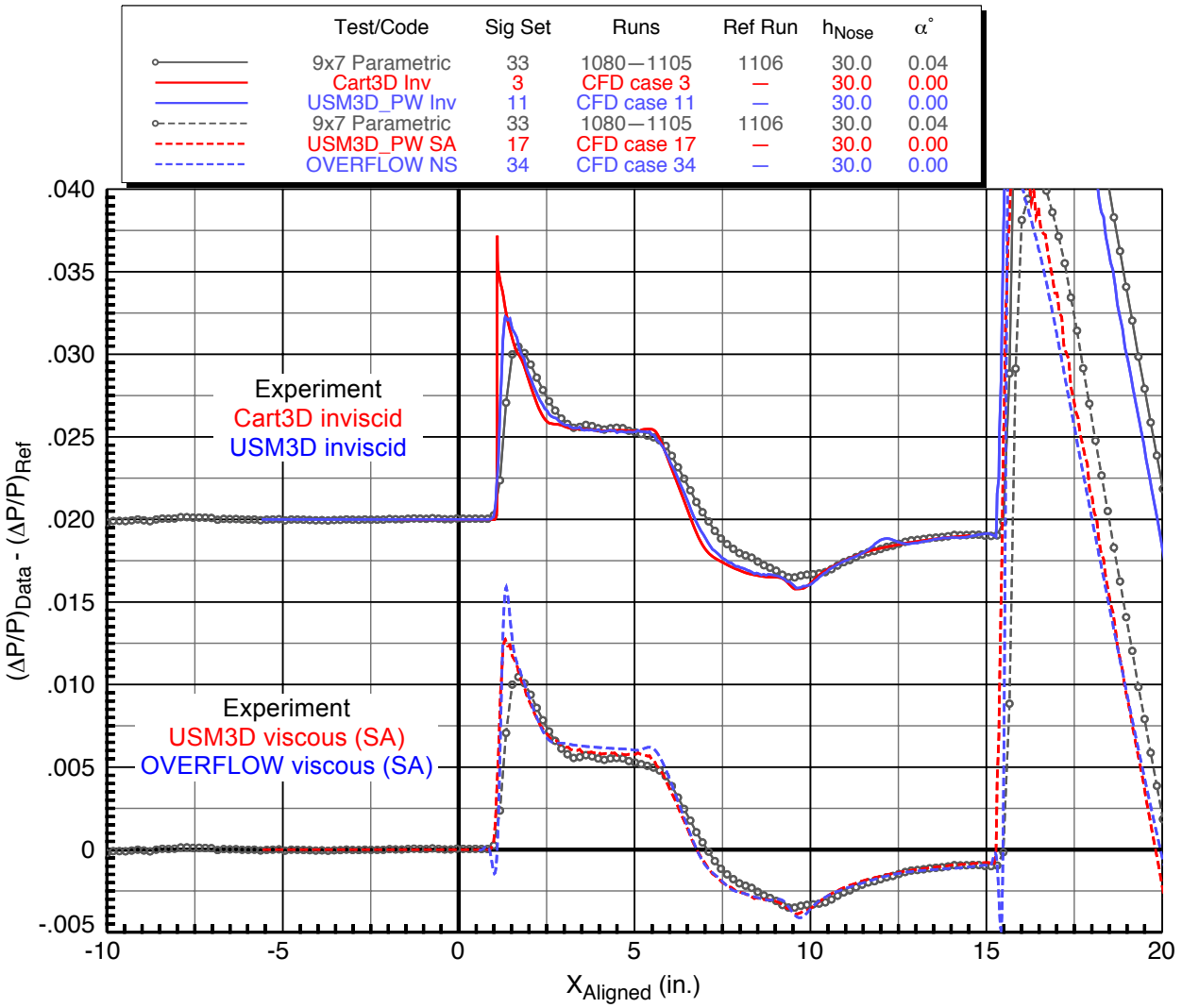

Figure 36. Experiment/CFD comparisons for AS2 Model
9x7 Parametric Test, 14-in fwd rail, M = 1.60, P_T = 2293 psf, *HumidAvg* = 306 ppm

Figure 37 below shows experiment and inviscid/viscous CFD comparisons for the AS2 model at heights of 60 in. from the 2-in. rail in the 8x6 wind tunnel. In contrast to the prior figure with the 14-in.-rail data, the nose shock peaks are substantially higher than the CFD-predicted peaks. This is consistent with the rail comparison findings in the earlier section, in which the reflection factor for the 2-in. rail abnormally amplifies the shock peaks. The experimental data in Fig. 37 also show a slight bump in the flat portion of the signature around X = 3.5. It is possible that this bump could be the reflection of the nose shock off the tunnel wall, though it is just over 2 in. aft of the nose shock in this Mach 1.56 signature, whereas a shock reflection in a Mach 1.6 flow is expected to affect the model signature a little less than 5 in. downstream of the incident shock as discussed above.

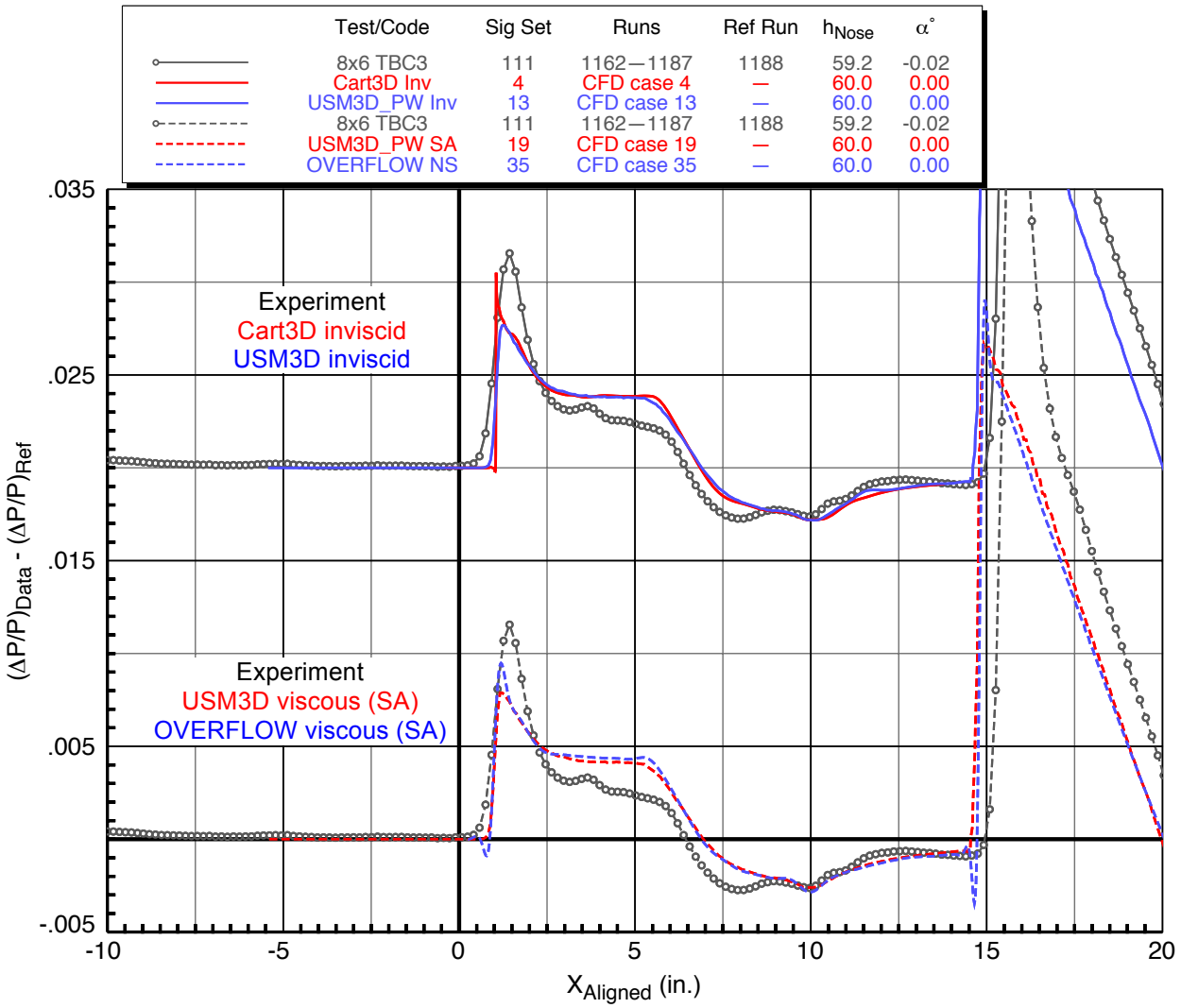

Figure 37. Experiment/CFD comparisons for AS2 Model
8x6 TBC3 Test, 2-in rail, M = 1.56 (WT), 1.60 (CFD), P_T = 2939 psf, *HumidAvg* = 66 ppm

B. Boom1 Model

The flow field around the Boom1 VS2 was computed using all three codes for a free-stream Mach number of 1.6, angle of attack of 3.4,° and Reynolds number of 4.1 million per foot. Figure 38 shows pressure coefficient contours on the surface of the Boom1 VS2 model as computed by *USM3D* with a laminar boundary layer, and Fig. 39 shows the symmetry plane pressure contours below the model for a *Cart3D* solution after 14 levels of adaption. The refinement pattern is driven by the features of the adjoint solution. As with the AS2 model predictions, the sonic boom signatures were extracted at a distances of 30 and 60 in. below the model nose for comparisons with the wind tunnel data, as indicated by the orange lines in the figure.

Inviscid *Cart3D* and *OVERFLOW* predictions for Boom1 VS2 are compared with wind tunnel data in Fig. 40 at $\alpha = 3.4°$ and $h = 30$ in. There is very good agreement between the CFD results and wind tunnel data along the flat portions of the signature, but both CFD codes predict stronger shocks at every location along the experimental data signature where there is some waviness or a rounded shock peak. The rounding is not surprising since the temporal and spatial variations in the wind tunnel flow cause individual pressure signatures in an X or Z sweep to have varying degrees of shock peak amplitudes that become somewhat washed out in the averaging. The greatest differences between the CFD and experimental data are aft of the main expansion, where the codes predict some very strong shocks from the region around the nacelles and vertical tails. The absence of a boundary layer is the cause of the discrepancy with experiment.

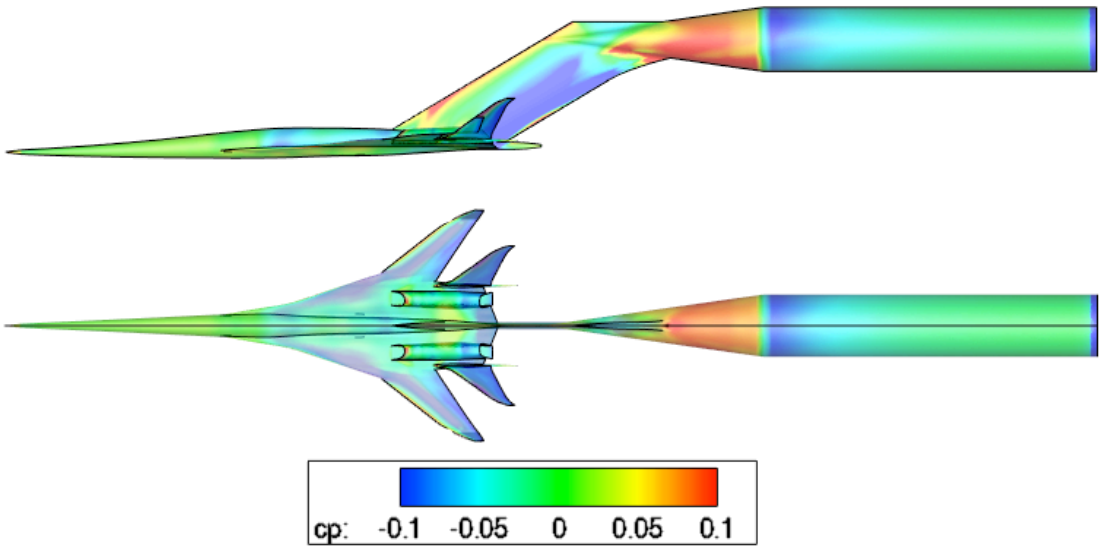

Figure 38. Pressure coefficient contours for Boom1 VS2 model, *USM3D* laminar results, $M = 1.6$, $\alpha = 3.4°$

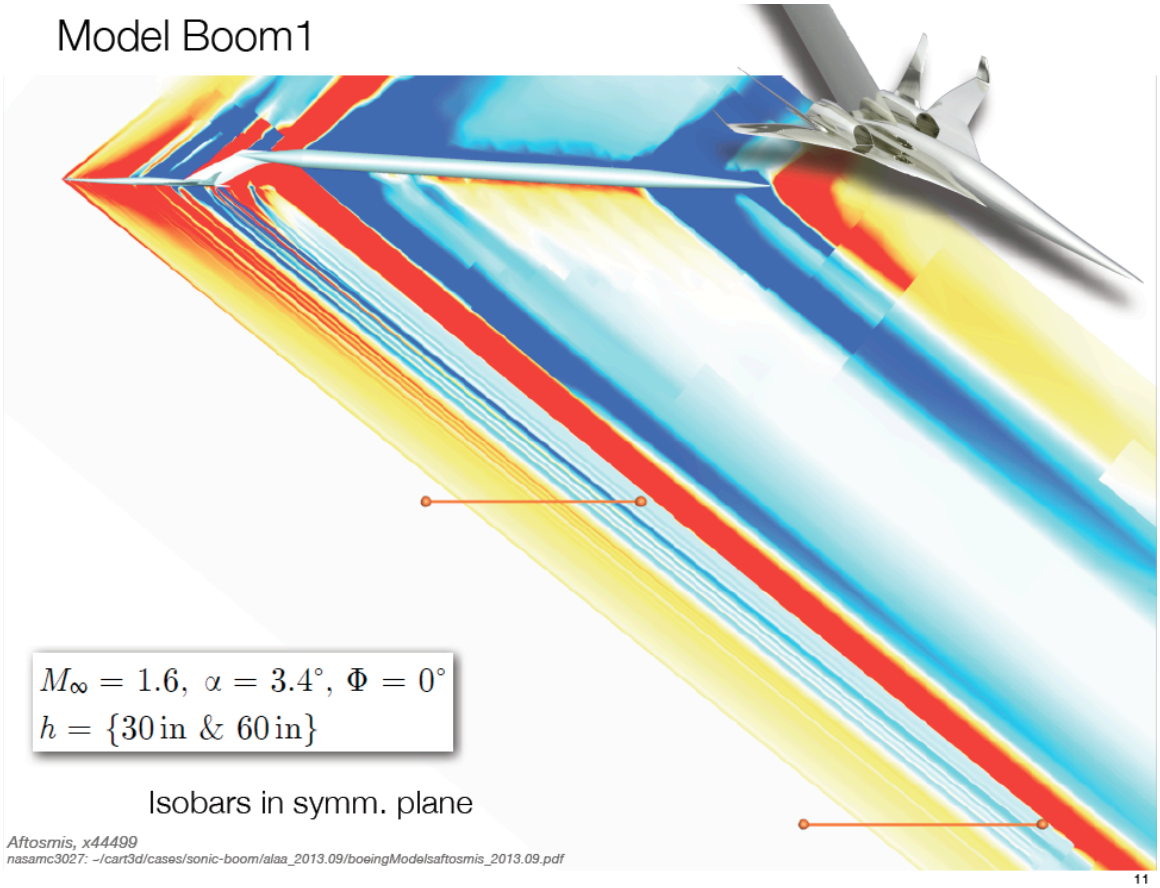

Figure 39. Symmetry plane pressure coefficient contours for Boom1 VS2 model, *Cart3D* results

Viscous *OVERFLOW* and *USM3D* laminar predictions for this model at the same conditions provide a better match with the wind tunnel data than the inviscid predictions, and the shock peaks are not nearly as amplified as for the inviscid predictions as well. Note that the *OVERFLOW* prediction captures more of the small-shock details than the *USM3D* prediction does just forward of the main expansion, but which are not seen in the experimental data.

CFD/experiment comparisons at h = 60 in. are shown in Fig. 41. One inviscid solution is given from *Cart3D* and one viscous turbulent solution is given from *USM3D* with the Spalart-Allmaras turbulence model. As with the comparisons at 30 in., the agreement is generally very good, with the shock peaks from the predictions being somewhat higher than those from the wind tunnel, especially for the inviscid solution. Note that the greatest discrepancies between the experimental and CFD data occur in the aft part of the signature, with the viscous solution being closer to the wind tunnel data than the inviscid solution.

Comparing the overall pressure level between this figure and that of the previous two figures confirms that the CFD codes did very well in capturing the effects of model height.

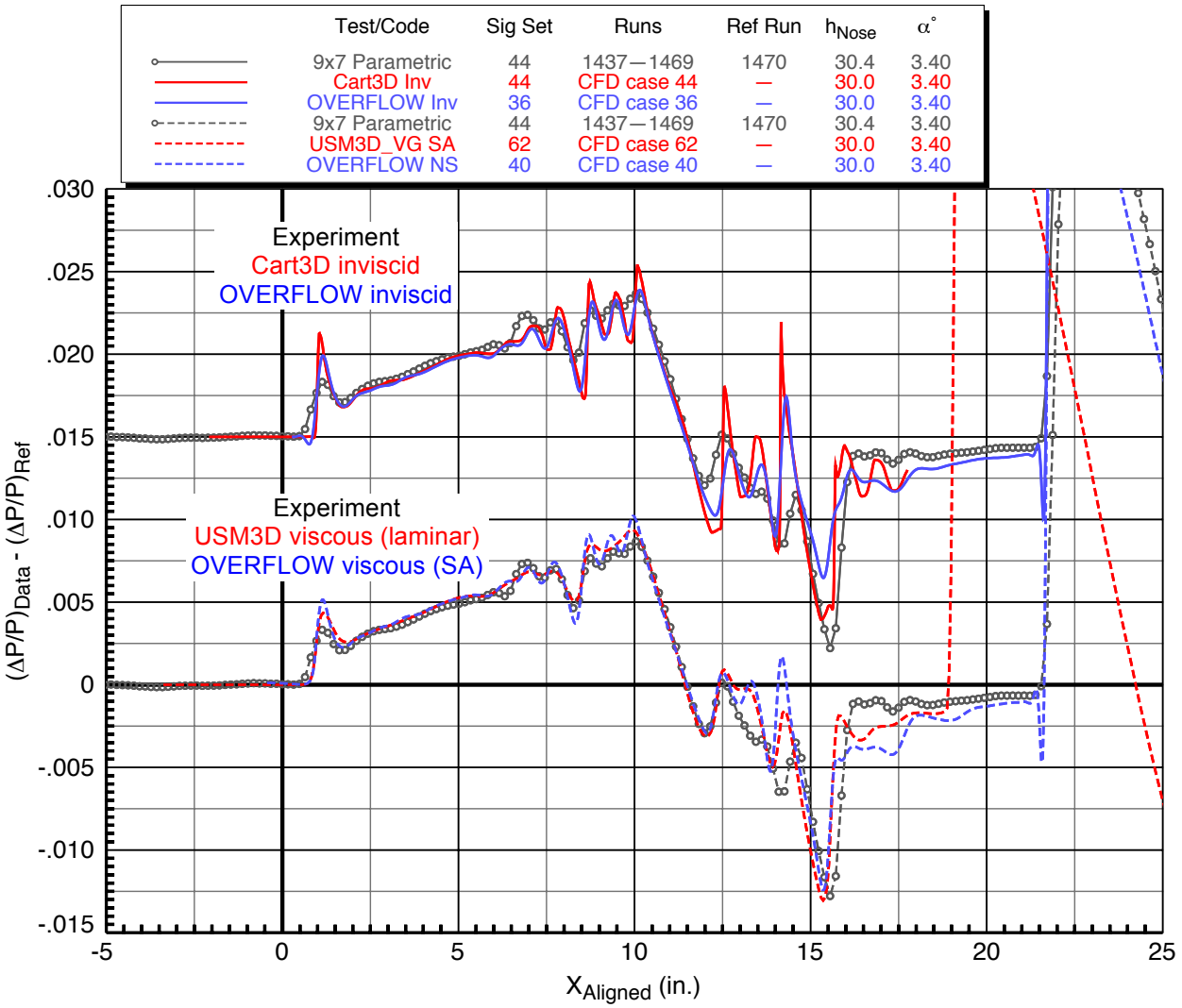

Figure 40. Experiment/CFD comparisons for Boom1 VS2 Model
9x7 Parametric Test, 14-in fwd rail, *Mach* = 1.60, P_T = 2292 psf, *HumidAvg* = 312 ppm

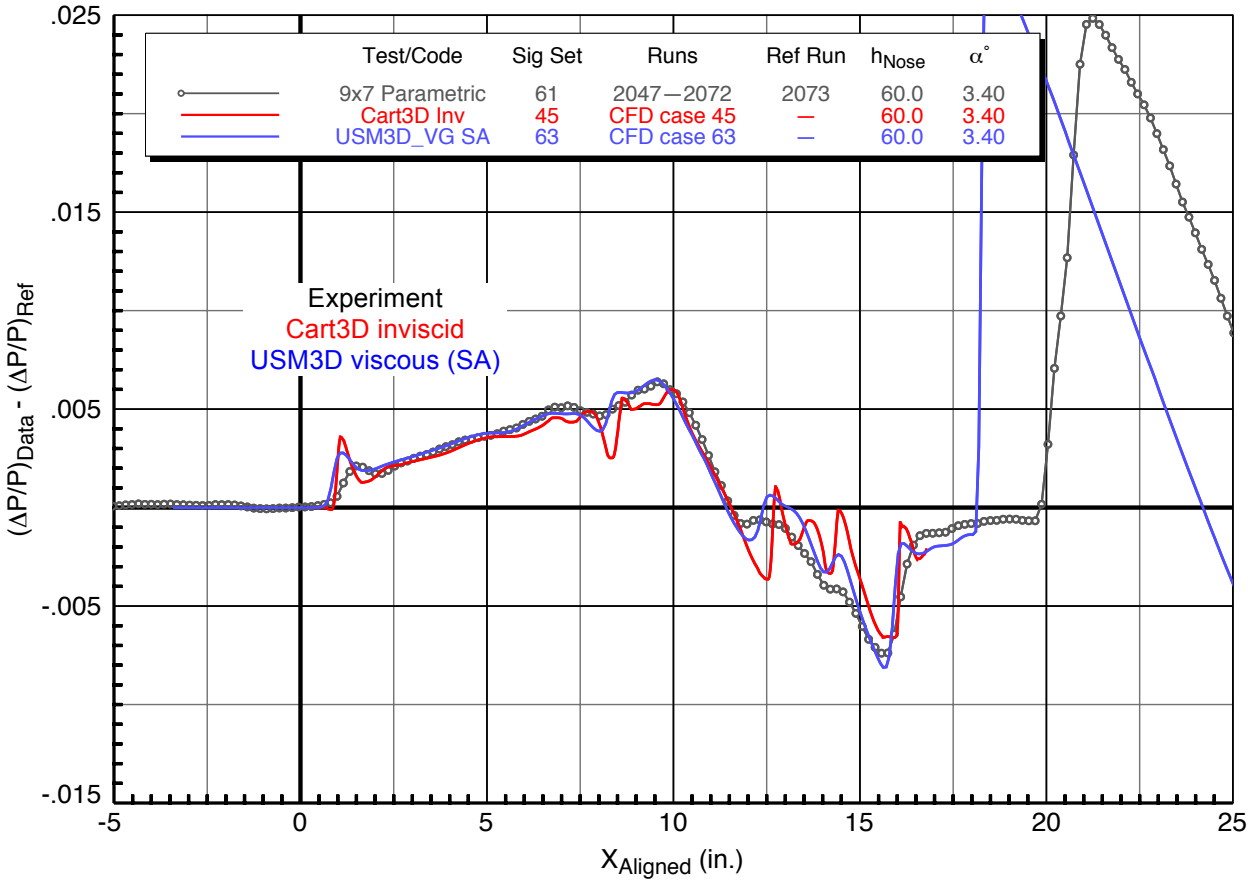

Figure 41. Experiment/CFD comparisons for Boom1 VS2 Model
9x7 Parametric Test, 14-in aft rail, *Mach* = 1.60, P_T = 2299 psf, *HumidAvg* = 288 ppm

C. Boom3 Model

Laminar and turbulent *USM3D* predictions were made for the Boom3 VS3 model at Mach 1.6, a Reynolds number of 4.1 million per foot, $\alpha = 3.1°$, and off-track angles of 15°, 30°, and 45° in addition to the on-track angle of 0°. Figure 42 shows the surface pressure contours on this model for a *USM3D* laminar solution, and the symmetry plane flow field pressure contours down to a height of 60 in. are shown in Fig. 43.

The experiment/CFD comparison plots that follow are for each of the on-track and off-track angles at a model height of 60 in., but first a plot of just the *USM3D-SA* predictions at the four track angles is given in Fig. 44 to clearly illustrate the differences in the signatures at these angles. Note that the four signatures are very similar in the forward region (as expected since the geometry here is mostly a body of revolution), with the exception that the nose shock is predominant in the $\phi = 0°$ case and becomes smaller until flat in the $\phi = 45°$ case. The reason for this could be due to the flow field grid being of finer resolution below the model than off to the sides, but this is being looked into at the time of this writing. The primary differences in the signatures occur from the lifting surfaces of the model, from the wings aft. The main expansion becomes deeper and moves forward with off-track angle, and the aft shocks become stronger. The same is generally true for the experimental data at these four track angles shown in Fig. 33, but the nose shock signature shape stays very consistent with off-track angle, as would be expected.

The four sets of curves in Fig. 45 show comparisons between the experimental data and viscous CFD results (*USM3D* laminar and turbulent SA) for this model at the conditions specified above. In general there is good agreement between the experimental and CFD results in the front part of the signatures at all track angles, though not as good for capturing the nose and wing shocks at the 45° off-track angle. In the $\phi = 0°$ case, the laminar and turbulent *USM3D* results agree with each other from the front through the main expansion, but aft of this they differ. Both *USM3D* methods predict stronger nose shocks under track, which appears smeared in the experimental data, and they also overpredict the strength of some of the aft shocks under track after the main expansion. The 15° and 30° off-track CFD predictions match the wind tunnel data very well overall, with little difference between the laminar and turbulent solutions.

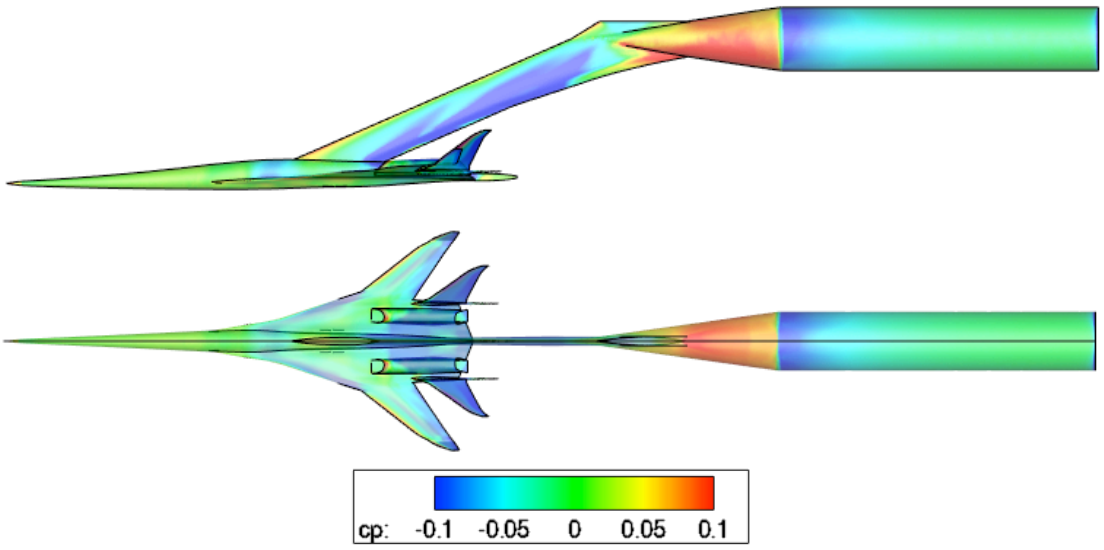

Figure 42. Pressure coefficient contours for Boom3 VS3 model, *USM3D* laminar results, $M = 1.6$, $\alpha = 3.1°$

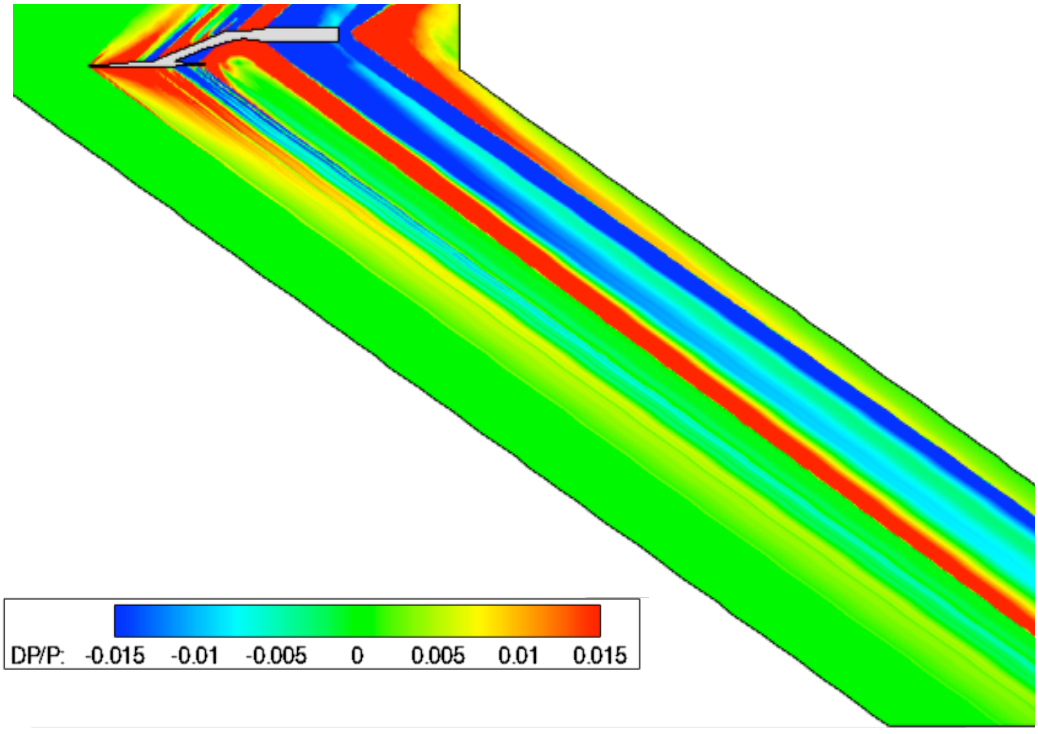

Figure 43. Symmetry plane pressure coefficient contours for Boom3 VS3 model, *USM3D* laminar results, $M = 1.6$, $\alpha = 3.1°$

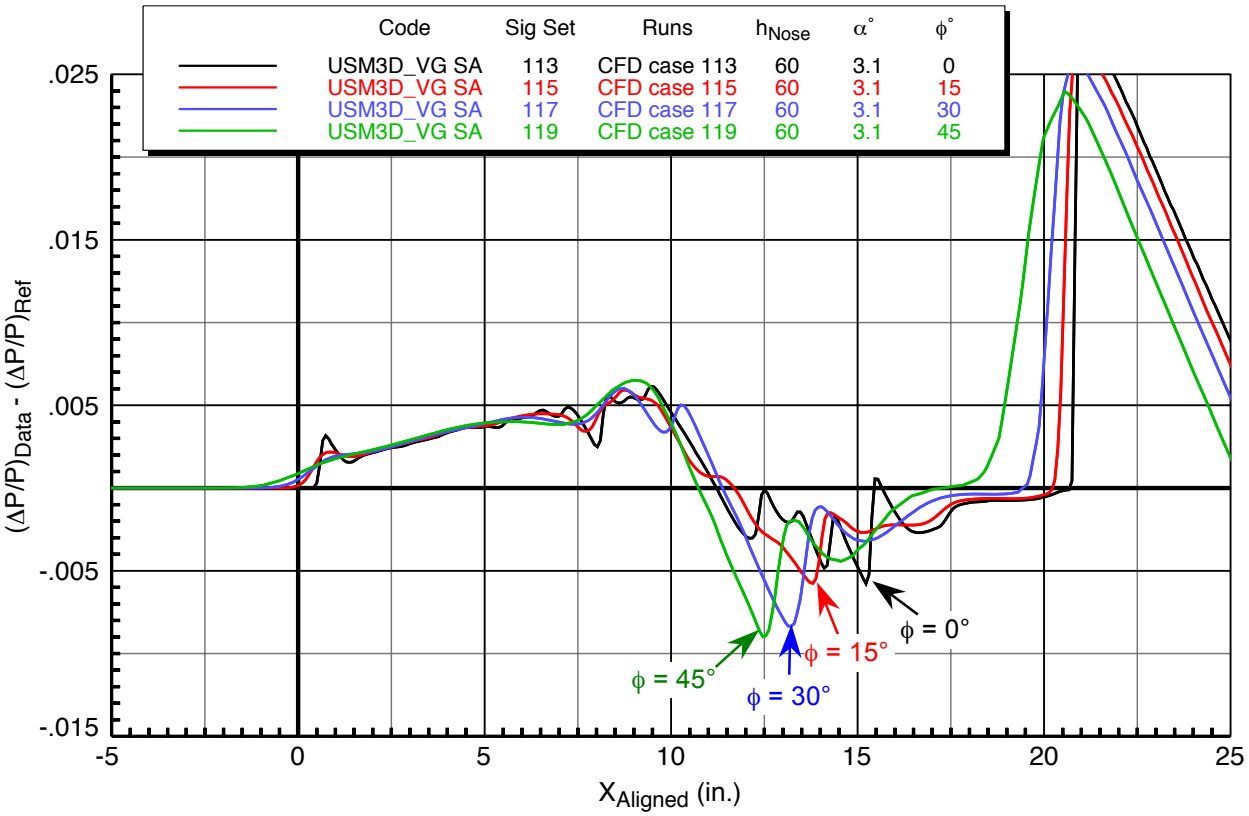

Figure 44. USM3D SA turbulent CFD predictions for effect of off-track angle for Boom3 VS3 Model
***M* = 1.60, h_{Nose} = 60 in., α = 3.10°**

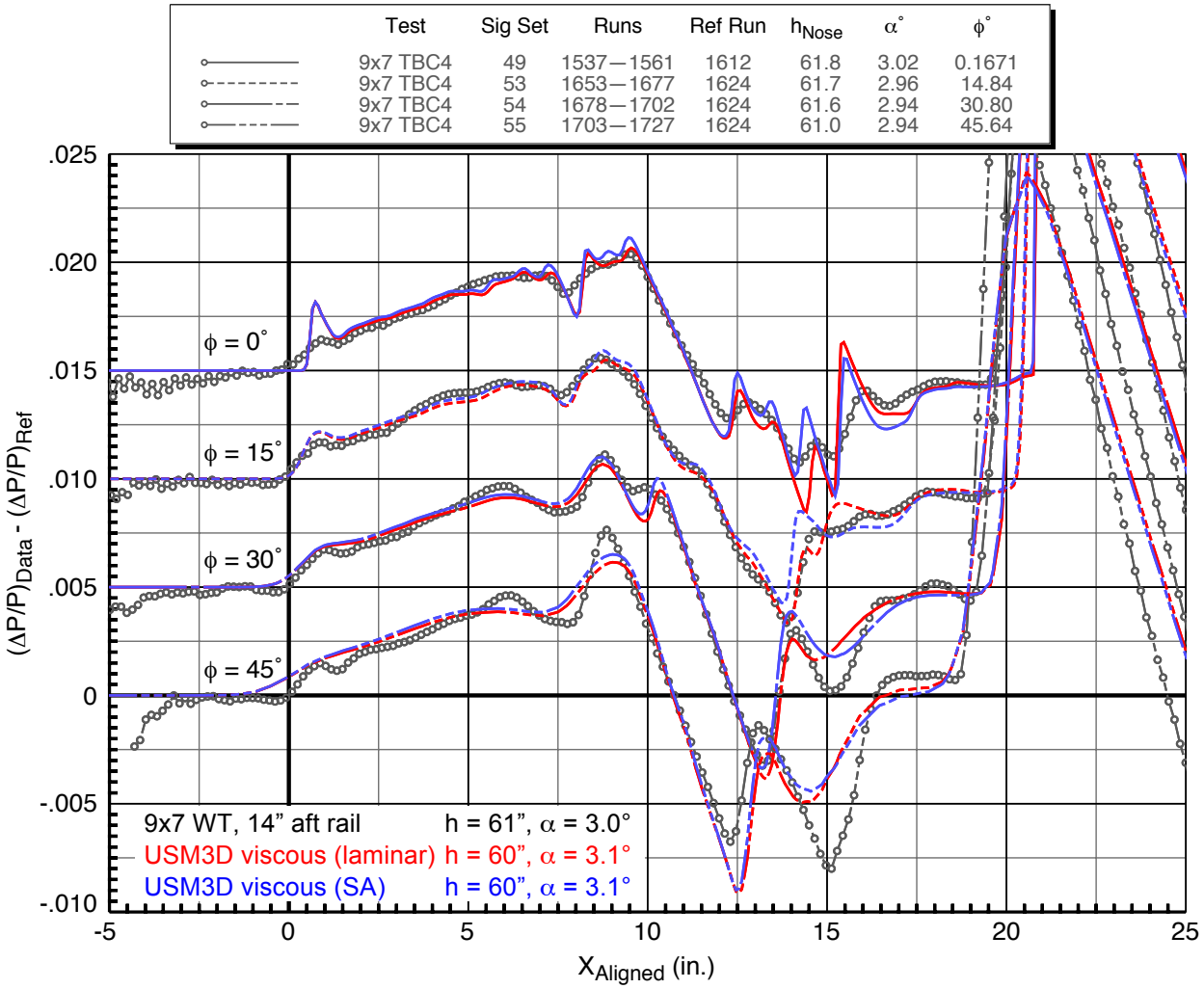

Figure 45. Experiment/CFD comparisons for Boom3 VS3 Model at various off-track angles 9x7 TBC4 Test, 14-in aft rail, M = 1.60, P_T = 2298 psf, *HumidAvg* = 223 ppm

D. Performance Model

Similar laminar and turbulent *USM3D* predictions were made for the larger Performance model as for the Boom3 VS3 model, at the same conditions of Mach 1.6, a Reynolds number of 4.1 million per foot, a height of 60 in., and for the track angles of 0°, 15°, 30°, and 45°. The angle of attack for these predictions though was 3.4° since this configuration is of the same design as the Boom1 model aside from the difference in mounting provisions. Figure 46 shows the surface pressure contours on this model for a *USM3D* turbulent solution. Note that as shown in the figure, the configuration was modeled in CFD with the sting can at the aft end and not the tailored dummy sting (refer to Fig. 8). As stated previously, the experimental data presented herein were acquired with the dummy sting, so this represents a configuration mis-match in the experiment/CFD comparisons to be presented. The dummy sting surface mesh was not available in time for preparation of those results for this paper, so the comparisons are presented as they are to show the differences/similarities in the front halves of the signatures.

A set of plots similar to those presented above for the Boom3 model showing the predicted effects of off-track angle and comparisons with experimental data are shown in Fig's. 48 and 49. The first plot, Fig. 48, shows the *USM3D-SA* predictions at the four track angles from 0° to 45°. In this case, however, unlike the Boom3 model predictions, the shape and magnitude of the nose shock at all four angles are identical, and the signatures overlap up to the start of the wing shock, as one would expect. Aft of this point, similar to Boom3, the main expansion pressures become deeper and move forward with off-track angle.

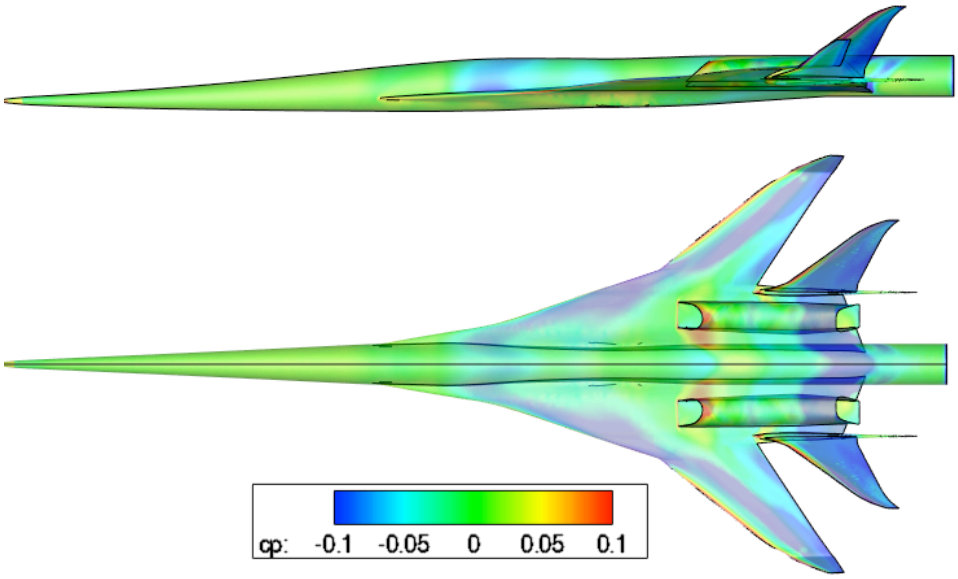

Figure 46. Pressure coefficient contours for Performance model, *USM3D SA* turbulent results, M=1.6, α=3.4°

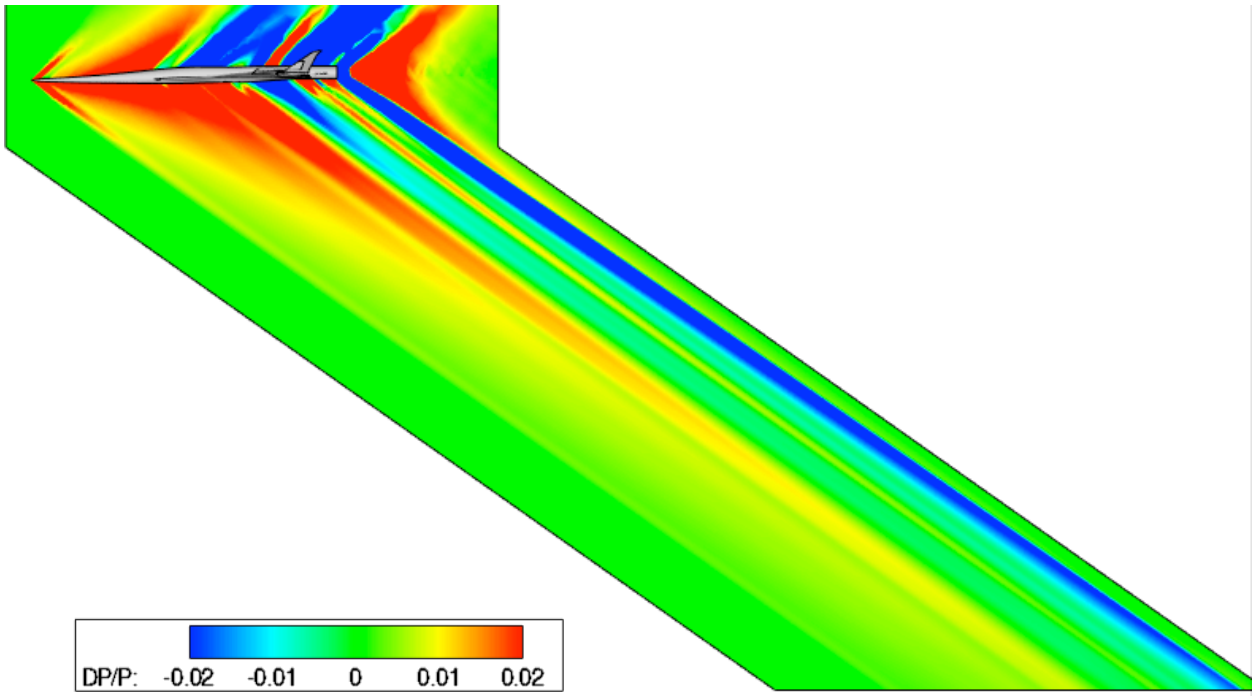

Figure 47. Symmetry plane pressure coefficient contours for Performance model, *USM3D SA* turbulent results, M=1.6, α=3.4°

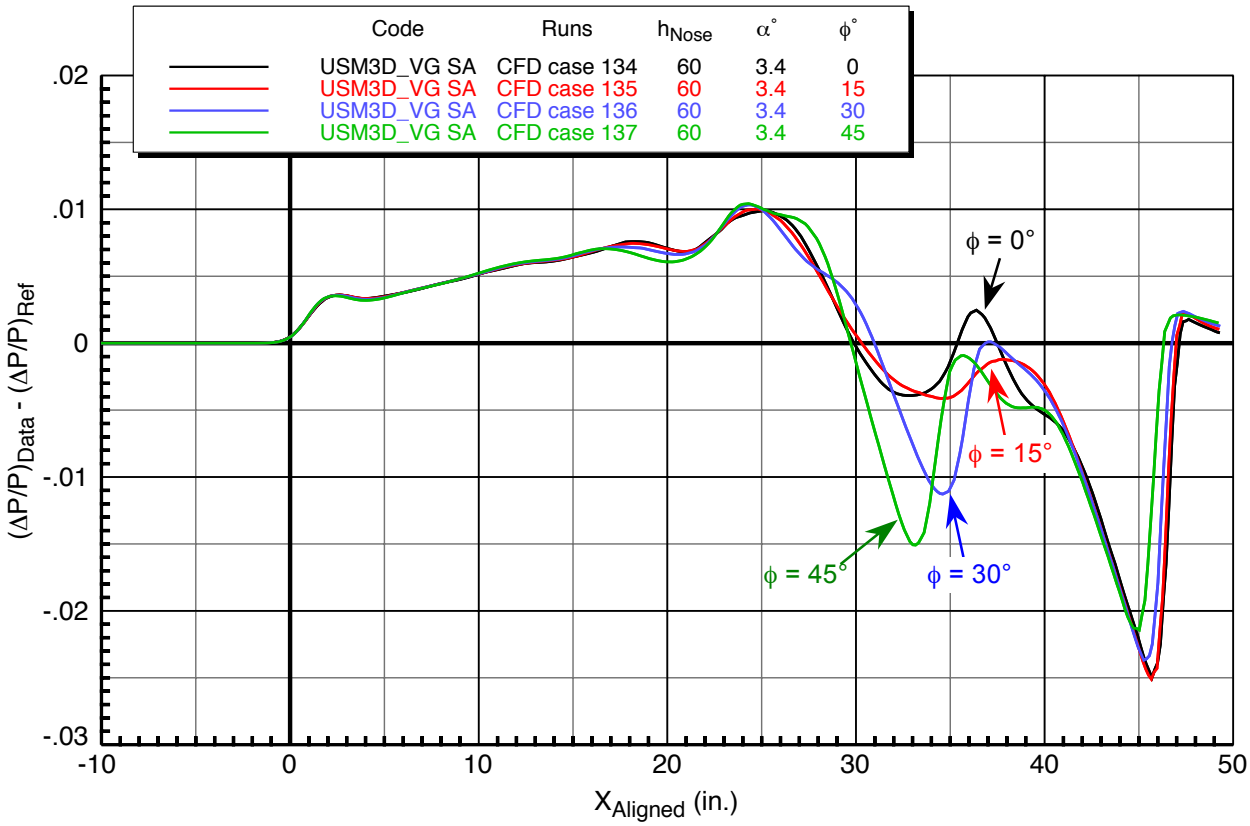

Figure 48. USM3D SA turbulent CFD predictions for effect of off-track angle for Performance Model $M = 1.60$, $h_{Nose} = 60$ in., $\alpha = 3.40^{\circ}$

Comparisons between the experimental data and CFD results (*USM3D* turbulent) for this model are presented in Fig. 49, with the caveat as stated above that the tailored dummy sting was used in the experiment and the sting can was used in the CFD. The CFD predictions did not match the experimental data in the front half of the signature (ahead of the y_0 point—where the mail expansion after the highest peak crosses the $y = 0$ line; note the 0.02 $\Delta P/P$ offsets for the upper three sets of curves) nearly as well for this model as they did for the Boom3 model. In these Performance model plots, the experimental data show a lot of definition of the small shocks along the length of the model that the CFD did not capture. There may be too much variation, however, in the measured data for this model, in that the ramp from the nose shock to the wing shock is fairly smooth in the Boom1 and Boom3 signatures, leading to some questions about the validity of the data for this model. Despite this, however, it is clear from the plots that the overall trends of the signature variations with off-track angle; in particular, matching the main expansions quite well in the 30° and 45° off-track angle cases.

The expansions and shocks aft of the y_0 point show significant disagreements between the CFD and experimental data, as expected due to the sting can vs. tailored dummy sting differences, though it is surprising to see better agreement as the off-track angle is increased.

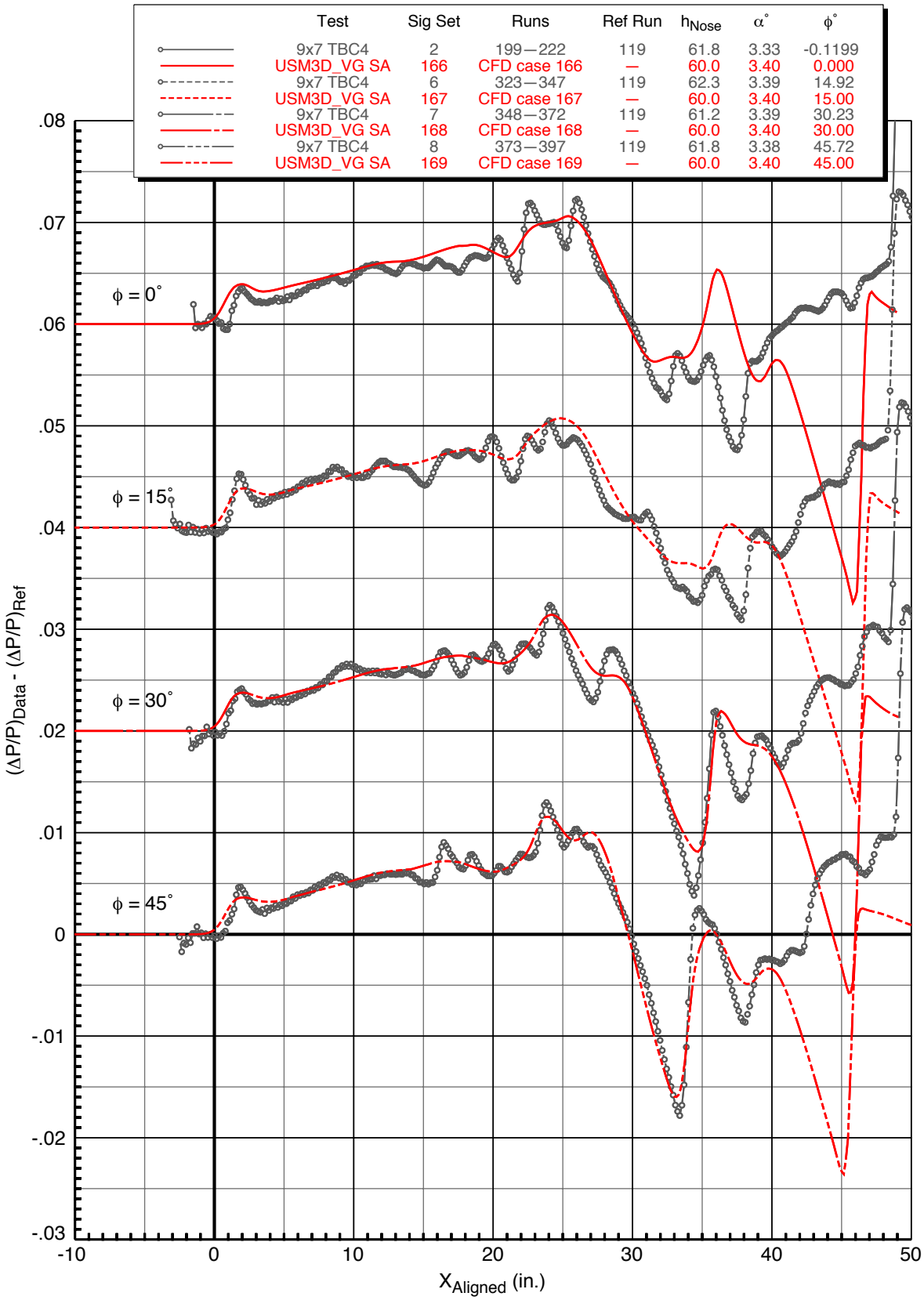

Figure 49. Experiment/CFD comparisons for Performance Model at various off-track angles
9x7 TBC4 Test, 14-in aft rail, M = 1.60, P_T = 2301 psf, *HumidAvg* = 236 ppm

X. Concluding Remarks

Near-field pressure signatures were measured and computational predictions made for three models representing Boeing's Quiet Experimental Validation Concept (QEVC) supersonic transport as well as for an axisymmetric calibration model. Experimental sonic boom pressure signatures were acquired primarily at Mach 1.6 and 1.8 in wind tunnel tests conducted during Phases I and II of a NASA Research Announcement (NRA) contract for Experimental Systems Validations for N+2 Supersonic Commercial Transport Aircraft, which was led by the NASA High Speed Project under the Fundamental Aeronautics Program.

The sonic boom test data were obtained using a 2-in. flat-top rail and a 14-in. tapered RF1 rail. Both rails captured an entire pressure signature in one data point, and successive signatures at varying positions along or above the rail were used to improve data quality through spatial averaging. The sonic boom data obtained by the rails were validated with high-fidelity numerical simulations of off-body pressures. The test results generally showed good agreement between the computational and experimental data when a variety of testing techniques including spatial averaging of a series of pressure signatures were employed. The two wind tunnels generally produced comparable data.

The spatially-averaged sonic boom test data generally showed good agreement with computational predictions. The use of the RF1 rail combined with spatial averaging of aligned signatures with different axial positions and constant altitude masked the wind tunnel distortions seen in the individual pressure signatures at most fixed model positions in the wind tunnel. The rail data were, as predicted, free from model shock reflections for the boom model. The data from these wind tunnel tests proved that accurate data with reasonable acquisition time is obtainable in the Ames 9x7 and Glenn 8x6 supersonic wind tunnels.

In summary, the wind tunnel test provided validation data that provides the confidence in the CFD methods to predict the sonic boom pressures of complex vehicles. CFD, regardless of flow solver, with an Mach aligned mesh, is able to accurately predict the sonic boom levels and the next step towards realization of civilian supersonic transportation would be the design and CFD evaluation of flight vehicles with vehicle flight demonstration testing with true atmospheric effects.

The highly accurate sonic boom pressure data from the current tests will aid in the development of improved computational and grid generation techniques for sonic boom analysis in the future by providing the data and model geometries to the aircraft industries.

XI. Acknowledgments

The authors would like to thank Linda Bangert, the Technical Lead in the High Speed Project overseeing this work, for her support and valuable input throughout the course of this work. We are grateful for the work done by the Boeing Seattle and Huntington Beach teams for their design of the QEVC concept and the wind tunnel models, for their leadership in the testing and CFD analyses. We appreciate the untiring efforts of the crews at the Ames 9- by 7-Foot Supersonic Wind Tunnel and the Glenn 8- by 6-Foot Supersonic Wind Tunnel for running the tests that provided all the experimental data herein. We are thankful for the CFD support of Mike Park and Michael Aftosmis, for adjoint-based solution adapted analyses with Cart3D, and we thank Edward Parlette, Sudheer Nayani, and Norma Farr for developing Euler and Navier-Stokes surface and volume grids.

XII. References

[1]Durston, D. A., Cliff, S. E., Wayman, T., Merret J., Elmiligui, A., and Bangert, L., "Near-Field Sonic Boom Test on Two Low-Boom Configurations Using Multiple Measurement Techniques at NASA Ames," AIAA-2011-3333, Honolulu, HI, June 2011.

[2]Cliff, S., Elmiligui, A., Aftosmis, A., Thomas, S., Morgenstern, J., and Durston, D., "Design and Evaluation of a Pressure Rail for Sonic Boom Measurements in Wind Tunnels," Seventh International Conference on Computational Fluid Dynamics (ICCFD7), ICCFD-2006, Big Island, HI, July 2012.

[3]Morgenstern, J.M., "How to Accurately Measure Low Sonic Boom or Model Surface Pressures in Supersonic Wind Tunnels," AIAA-2012-3215, 3rd Applied Aerodynamics Conference, June 2012.

[4]Magee, T. E. et al, "System-Level Experimental Validations for Supersonic Commercial Transport Aircraft Entering Service in the 2018–2020 Time Period, Phase I Final Report, NASA CR-2013-217797, 2013.

[5]Jones, W.T., Nielsen, E. J., and Park M. A., "Validation of 3D Adjoint Based Error Estimation and Mesh Adaption for Sonic Boom Prediction," *AIAA Paper 2006-1150*, 44th AIAA Aerospace Sciences Meeting and Exhibit, Reno, NV, January 2006.

[6]Lee-Rausch, E. M., Park M. A., Jones, W. T., Hammond, D. P., and Nielsen, E. J., "Application of a Parallel Adjoint-based Error Estimation and Anisotropic Grid Adaption for Three-dimensional Aerospace Configurations," *AIAA Paper 2005-4842*, 2005.

[7]Carter, Melissa B., and Deere, Karen A., "Grid Sourcing and Adaptation Study Using Unstructured Grids for Supersonic Boom Prediction," *AIAA Paper 2008-6595*, 2008.

[8]Aftosmis, M. J., and Berger, M. J., "Multilevel Error Estimation and Adaptive H-Refinement for Cartesian meshes with embedded boundaries," *AIAA Paper 2002-0863*, 40th AIAA Aerospace Sciences Meeting and Exhibit, Reno NV, Jan. 2002.

[9]Nemec, M., and Aftosmis, M., "Adjoint Error-Estimation and Adaptive Refinement for Embedded-Boundary Cartesian Meshes," *AIAA Paper 2007-4187*, 18th AIAA CFD Conference, Miami FL, June 2007.

[10]Nemec, M., Aftosmis, M., and Wintzer, M., "Adjoint-based Adaptive Mesh Refinement for Complex Geometries," *AIAA Paper 2008-0725*, Jan. 2008.

[11]Wintzer, M., Nemec, M., and Aftosmis, M. J., "Adjoint-based Adaptive Mesh Refinement for Sonic Boom Prediction," *AIAA Paper 2008-6593*, 26th AIAA Applied Aerodynamics Conference, Honolulu HI, June 2008.

[12]Choi, S., Alonso, J. J., and Van der Weide, E., "Numerical and Mesh Resolution Requirements for Accurate Sonic Boom Prediction," *AIAA Journal of Aircraft,* Vol. 46, No. 4, July-Aug. 2009

[13]Park, M. A., "Low Boom Configuration Analysis with FUN3D Adjoint Simulation Framework," AIAA-2011-3500, Honolulu, HI, June 2011.

[14]Aftosmis, M. J., Nemec, M., and Cliff, S. E., "Adjoint-based Low Boom Design with Cart3D," AIAA-2011-350, Honolulu, HI, June 2011.

[15]Louisville, A., Dervieux, A., and Alauzet, F., "Fully Anisotropic Goal-Oriented Mesh Adaptation for 3D Steady Euler Equations," Journal of Computational Physics Volume 229 Issue 8, pages 2866-2897, April, 2010.

[16]Laflin, Kelly R., Klausmeyer, Steven M., and Chaffin, Mark, "A Hybrid Computational Fluid Dynamics Procedure for Sonic Boom Prediction," *AIAA Paper 2006-3168*, 24th AIAA Applied Aerodynamics Conference, San Francisco, CA, June 2006.

[17]Haering, E., Murray, J., Purifoy, D., Graham, D., Meredith, K., Ashburn, C., and Stucky, M.,, "Airborne Shaped Sonic Boom Demonstration Pressure Measurements with Computational Fluid Dynamics Comparisons," *AIAA Paper 2005-0009*, 2005.

[18]Waithe, Kendrick A., "Application of USM3D for Sonic Boom Prediction by Utilizing a Hybrid Procedure," *AIAA Paper 2008-129*, Jan. 2008

[19]Howe, Donald C., "Hybrid Cart3D/OVERFLOW Near-Field Analysis of a Low Boom Configuration with Wind Tunnel Comparisons," *AIAA Paper-2011-3336.*

[20]Campbell, R. L., Carter, M. B., Deere, K. A. and Waithe, K. A., "Efficient Unstructured Grid Adaptation Methods for Sonic Boom Prediction," *AIAA Paper 2008-7327*, Honolulu HI, Aug. 2008.

[21]Cliff, S.E., Elmiligui, A. A.,Campbell, R. L., and Thomas, S. D., "Evaluation of Refined Tetrahedral Mesh with Projected, Stretched, and Sheared Prism Layers for Sonic Boom analysis, AIAA-2011-3338, Honolulu, HI, June 2011

[22]Cliff, S.E., Elmiligui, A., Campbell, R. L., and Thomas, S. D., "Refined Tetrahedral Meshes with Mach Cone Aligned Prisms for Sonic Boom Analysis." AIAA Journal of Aircraft.

[23]Darden, C. M., "Sonic Boom Minimization with Nose-Bluntness," NASA TP 1348, 1979.

[24]Todd E. Magee, Spencer R. Fugal, Lawrence E. Fink, Eric E. Adamson, and Stephen G. Shaw: System-Level Experimental Validations For Supersonic Commercial Transport Aircraft Entering Service in the 2018–2020 Time Period, Phase II Final Report. NASA CR unpublished.

[25]Reed, T. D., Pope, T. C., and Cooksey, J. M.: Calibration of Transonic and Supersonic Wind Tunnels. NASA CR-2920, November 1977.

[26]Soeder, Ronald H.: NASA Lewis 8- by 6-Foot Supersonic Wind Tunnel User Manual. NASA TM-105771, February 1993.

[27]George, A. R., and Seebass, R., "Sonic Boom Minimization Including Both Front and Rear Shocks," AIAA J. Vol. 9, No. 10, Oct. 1971, pp. 2091-2903.

[28]James T Heineck, Edward T. Schairer, Louise A. Walker, Laura K. Kushner: "Retroreflective Background Oriented Schlieren (RBOS)", paper 140, ISFV14 14th International Symposium on Flow Visualization June 21-24, 2010, EXCO Daegu, Korea

[29]Susan E. Cliff, Donald A. Durston, Alaa A. Elmiligui, James C. Jensen, William M. Chan: Computational and Experimental Assessment of Models for the First AIAA Sonic Boom Prediction Workshop. AIAA Paper 2014-0560, National Harbor, MD, January 2014

[30]Morgenstern, J.M., "Distortion Correction for Low Sonic Boom Measurement in Wind Tunnels," AIAA-2012-3216, 33rd Applied Aerodynamics Conference, June 2012.

[31]Frink, N. T., Pirzadeh, S. Z., Parikh, P. C., Pandya, M. J., and Bhat, M. K., "The NASA Tetrahedral Unstructured Software System," *The Aeronautical Journal*, Vol. 104, No. 1040, October 2000, pp. 491-499.

Nichols, R., Tramel, R., and Buning, P., "Solver and Turbulence Model Upgrades to OVERFLOW 2 for Unsteady and High-Speed Applications", AIAA 2006-2824, 24th AIAA Applied Aerodynamics Conference, San Francisco, California, June 2006